pillsbury

Pillsbury Winthrop Shaw Pittman LLP
1200 Seventeenth Street NW | Washington, DC 20036-3006 | tel 202.663.8000 | fax 202.663.8007

Jay E. Silberg
tel: 202.663.8063
jay.silberg@pillsburylaw.com

April 21, 2016

ATTENTION: Document Control Desk
U.S. Nuclear Regulatory Commission
Washington, DC 20555-0001

AEROTEST RADIOGRAPHY AND RESEARCH REACTOR
DOCKET NO. 50-228/LICENSE NO. R-98

RESPONSE TO REQUEST FOR ADDITIONAL INFORMATION RE: OPPORTUNITY TO SUPPLEMENT 2012 LICENSE TRANSFER APPLICATION (TAC NO. MF7221)

Ladies and Gentlemen:

Enclosed please find the response of Aerotest Operations, Inc. ("Aerotest") and Nuclear Labyrinth LLC ("Nuclear Labyrinth") to the U.S. Nuclear Regulatory Commission's Request for Additional Information Re: Opportunity to Supplement 2012 License Transfer Application (TAC No. MF7221), dated January 21, 2016, including supporting affidavits on behalf of both Aerotest and Nuclear Labyrinth.

Should you have any questions or require additional information regarding this submission, please contact Jay Silberg, counsel to Aerotest at 202-663-8063 or jay.silberg@pillsburylaw.com.

Sincerely yours,

Jay E. Silberg

Jay E. Silberg
Counsel for Aerotest Operations, Inc.

Enclosures

A020
NRR

Enclosures:

1. Response to Request to Request for Additional Information
2. Shugart, Neutronic and Thermal Hydraulic Analysis of the Geological Survey TRIGA Reactor

cc: U.S. NRC Office of Nuclear Reactor Regulation/NRLPO
U.S. NRC Region IV, Regional Administrator
NRC, NRR (Helvenston)
NRC, NRR (Adams)
NRC, OGC (Ghosh)

STATE OF MICHIGAN :
: TO WIT:
COUNTY OF OAKLAND :

I, Anthony Nellis, state that I am the President of Aerotest Operations, Inc., and that I am duly authorized to execute and file this response on behalf of Aerotest Operations, Inc. To the best of my knowledge and belief, the statements contained in this document with respect to Aerotest Operations, Inc. are true and correct.

Subscribed and sworn before me, a Notary Public in and for the State of Michigan and County of Oakland, this 21st day of April, 2016.

WITNESS my Hand and Notarial Seal:

Notary Public

My Commission Expires:

4/21/16
Date

RUTH A. [illegible]ENING
Notary Public, State of Michigan
County of Oakland
My Commission Expires Dec. 21, 2019
Acting in the County of Oakland

STATE OF UTAH :
: TO WIT:
COUNTY OF SALT LAKE COUNTY :

I, Dr. David Michael Slaughter, state that I am the Chief Executive Officer of Nuclear Labyrinth LLC, and that I am duly authorized to execute and file this response on behalf of Nuclear Labyrinth LLC. To the best of my knowledge and belief, the statements contained in this document with respect to Nuclear Labyrinth LLC are true and correct.

Subscribed and sworn before me, a Notary Public in and for the State of Utah and County of Salt Lake, this 20th day of April, 2016.

WITNESS my Hand and Notarial Seal:

Notary Public

My Commission Expires:

4-20-2016
Date

NOTARY PUBLIC
NARCISO PASILLAS
682410
COMMISSION EXPIRES
MARCH 30, 2019
STATE OF UTAH

Aerotest Radiography and Research Reactor

Docket No. 50-228

Enclosure 1

April 21, 2016

RESPONSES TO REQUEST FOR ADDITIONAL INFORMATION

1. Status of previously submitted information.

   The information previously submitted by Aerotest Operations, Inc. ("Aerotest") and Nuclear Labyrinth LLC ("Nuclear Labyrinth") (collectively "the Companies") in the 2012 License Transfer Application, responses to NRC Staff requests for additional information, and at the hearing has been reviewed by the Companies and remains, to the best of their knowledge and belief, current and up to date, except as set forth below.

2. Information regarding the current status of the damaged fuel elements at the Aerotest Radiography and Research Reactor ("ARRR").

   The Companies are aware of no information regarding the current status of the ARRR's damaged fuel elements that differs from that previously presented by the Companies to the NRC Staff.

3. Method by which Nuclear Labyrinth intends to meet the financial protection requirements of 10 CFR Part 140 after the license transfer.

   In order to avoid triggering issues relating to foreign ownership, control and domination, the Companies will discuss with the NRC Staff appropriate mechanisms that would make available $1.5 million for ARRR to meet the requirements of 10 CFR Part 140. These mechanisms could include a third party guarantee, a trust, or other appropriate mechanisms.

4. Funding of spent fuel management costs.

   In their January 10, 2013 response to NRC Staff requests for additional information, the Companies stated that spent fuel management costs would be covered by a fuel storage fee collected from customers over the 20 year license period. Following that submittal, the Companies verbally offered to NRC Staff counsel that Autoliv would provide $650,000 for spent fuel management costs prior to the license transfer. Autoliv is now committing to

provide an additional $475,000 for spent fuel management, for a total of $1,125,000. These spent fuel management funds will be placed in trust at the time of license transfer until needed for fuel management activities.

5. Decommissioning funding estimates.

As described in the Pre-filed Direct Testimony of Michael S. Anderson (Exhibit AOI100, dated June 13, 2014), the Companies had agreed that Autoliv ASP, Inc. ("Autoliv") would transfer to Nuclear Labyrinth at closing $3,376,030 to fund a decommissioning trust. Id. at A28, p. 8. This amount was based on a decommissioning plan and cost estimate prepared by EnergySolutions and submitted with the License Transfer Application. Exhibit AOI102 at Attachment 8. That cost estimate was $3,285,800 in 2011 dollars. At the request of the NRC Staff, that estimate was restated in 2012 dollars as $3,376,030. Exhibit AOI100 a A27, p. 9. Since that time, EnergySolutions has prepared a revised, updated estimate for the ARRR decommissioning cost of $3,146,060 in 2015 dollars. Notwithstanding the reduced estimate in the decommissioning cost, Autoliv will not reduce the amount that it previously committed to transfer at closing to fund a decommissioning trust.

6. Functionality of proposed design.

The NRC Staff following the license transfer hearing questioned whether the design of the proposed core for the ARRR would allow the reactor to be fully functional. See NRC Staff Rebuttal Response, NRC-054(P), July 18, 2014, pp. 23-27.

For research reactors, loading consideration include fuel placement assuring the neutronics at the experimental irradiators, flux traps, beam ports, etc. are maintained at specific conditions. Typically a research reactor will have a number of these experimental facilities at different locations in or surrounding the core. Also fuel inventory in research reactors most likely will consist of a "mixed" core which may consist of fuel elements with different uranium loading, (8.5, 12, 20, 30, etc. % by weight), cladding (SS or Al), U-235 burn-up, and age. The proper fuel element placement takes all these circumstances into consideration to ensure safe operation while assuring research conditions are achieved. The placement of fuel elements in the ARRR proposed core included such an evaluation.

This evaluation was part of Nuclear Labyrinth's due-diligence process. The evaluation examined uranium loading (8.5, 12),

cladding (SS or Al), U-235 burn-up, age, damage, application of fitness of duty criteria, handling methods, and other characteristics. Dr. Slaughter viewed the physical conditions and characteristics of each of the elements during the 2012 inspection recorded on DVD. He also examined the historical written records for the description of the individual elements from past inspections. He tracked each element from its introduction into the core, its location and movement to estimate it annual burnup. Dr. Slaughter then correlated those findings to the annual U-235 burnup reported to the Nuclear Materials Management and Safeguards System by Aerotest. He studied the environmental conditions, location, movement, time and temperature of the elements, to relate those parameters to fuel chemistry processes, especially with respect to the elements that were damaged. This was done to better understand the reasons for failure so elements in similar circumstances can be identified. (A few elements that did not show damage were eliminated from future use through this process.) Where necessary, discussions with Aerotest staff were held to clarify the information.

Dr. Slaughter did not write a report or correlate his findings in a single document. The sole purpose of the process was to convince that there was sufficient fuel to sustain operation of the reactor. The MCNP5 calculations benefited from this work in that its input files contain the specific burn-up of the retained elements. The historical information on the control rods was also incorporated in the model.

A detailed fuel loading and condition evaluation was performed by Dr. Slaughter to ensure a functioning asset capable of performing the anticipated mission. This analysis was specific to determine if there was sufficient fuel inventory to operate at licensed power of 250 Kw and for sustained operation at power of 160 Kw for the license period. The results of the investigation were provided in a response to question 5b (Exhibit NRC-026) which asked "Estimate the number of fuel elements that need replaced in the future and the associated costs". The response stated, "Currently, based on a fully reflective core design, we do not expect to need new fuel elements. However, fuel evaluations are ongoing and core calculations supporting the new core design will not be completed until the end of March [2014]." The MCNP5 calculations were completed and the results added additional support to the above response given in RAI 5b. The number and condition of useable fuel inventory (summarized in Exhibit AOI300) support the statement that no additional fuel is required during the license period using the fuel in the proposed core and 20 in reserve. The

final portion of the response to question 5b did not occur due to the NRC prohibition on ARRR operation.

The MCNP5 TRIGA reactor input deck (code)'s used in Dr. Slaughter's analysis employed the individual description and location of fuel elements and control rods to ensure a more accurate simulation of the neutronics distributed in the ARRR core. The input file also contains the extensive description of the ARRR core structure, pool, unique irradiation fixtures, etc. The basic MCNP5 TRIGA reactor was commissioned by the Department of Energy (NEUP) to assist in the relicensing research reactors. Professor Jeffery King, Interim Head of Nuclear Science and Engineering program, Colorado School of Mines lead the investigators in this endeavor. The United States Geological Survey TRIGA Reactor ("GSTR") was used to validate the code. It is important to note that the physical description of many of the dimensions and materials used for the core structure of the GSTR are the same as that found in the ARRR. These findings were found by comparison of GSTR and ARRR's architectural/engineering drawings. This is typical of TRIGA reactors of similar type and generation.

The neutronic characterization of the GSTR required that the MCNP model detailed in the input deck be validated against the current core operating conditions, demonstrating the model's ability to represent the current configuration of the GSTR. This validation involved three tests: a control-rod calibration based on experimentally derived control rod worth curves from the GSTR, a critical position and multiplication factor prediction comparison, and a flux characterization across the GSTR core. The results are included in Shugart, "Neutronic and Thermal Hydraulic Analysis of the Geological Survey TRIGA Reactor" (2013), a copy of which is provided with these responses.

Changes specific to the ARRR facility are incorporated in the model (detailed in the input file) which include control rod location and elimination of the transient rod, pool diameter individual fuel description and auxiliary fixtures (i.e., reflector, flux traps) . The changes warranted a benchmark activity similar to the one described above. Unfortunately the ARRR is not operational so historical conditions were simulated and records of experimentally derived control rod worth curves from the ARRR, a critical position and multiplication factor prediction were used for comparison. (Flux measurements across the ARRR core were not available).

The NRC Staff's rebuttal testimony of Alexander Adams stated that "the Staff has not conducted a confirmatory code run of Dr. Slaughter's proposed ARRR core and the Companies have not provided the Staff with the necessary data to evaluate the MCNP5 inputs and outputs illustrated in Exhibit AOI207. In order to evaluate Exhibit AOI207, the Staff would need to examine, for example, the engineering drawings of the core to determine the relationship of core components and details of material composition to determine what components are made of. Therefore, I cannot comment on Dr. Slaughter's assessment in detail. Generally, though, from a nuclear design perspective, the proposed core design appears to be reasonable given the fuel element constraints that exist."

Mr. Adams did state that the NRC Staff operated "similar" codes and the results indicated a different conclusion than that reached by Dr. Slaughter. He did not however provide an example of a MCNP5 input file and results supporting his statement. It is clear that the "similar" codes he referred to did not benefit from the specific facility and fuel detail. With the lack of relevant facility and fuel information, the MCNP5 code used in Mr. Adams analysis would have difficulty benchmarking his code to the ARRR experimental measurements.

A discussion of thermal-hydraulic behavior was not included by Dr. Slaughter or requested by the NRC staff through the RAI process. The extensive experimental data obtained by General Atomics, the TRIGA reactor designer and manufacturer, on the thermal hydraulic behavior associated with core structure, fuel design and fuel loading has been used and remains the basis to ensure the temperature safety limit is not breached for the ARRR's fuel elements. For the ARRR, there is no change in license power, core structure, operation, TRIGA fuel pin design, and fuel loading (8.5 and 12 percent by weight uranium loading, 20 percent enriched). Therefore, one can safely predict that the thermal-hydraulic behavior will not significantly change. Thus, the current safety limits in the ARRR license will apply. As for the recent modeling of thermal hydraulic behavior associated with relicensing, in general those licensees have confirmed their safety limits (established by General Atomics' earlier experimental data) to be acceptable. The accuracy of the models in representing the occurring thermal hydraulic phenomena remains an issue with differing results and uncertainties between the methods.

NEUTRONIC AND THERMAL HYDRAULIC ANALYSIS OF THE GEOLOGICAL SURVEY TRIGA REACTOR

by

Nicolas Shugart

A Thesis submitted to the Faculty and the Board of Trustees of the Colorado School of Mines in partial fulfillment of the requirements for the degree of Master of Science (Nuclear Engineering)

Golden, Colorado

Date _____

Signed: _____
Nicolas Shugart

Signed: _____
Dr. Jeffrey King
Thesis Advisor

Golden, Colorado

Date _____

Signed: _____
Dr. Jeffrey King
Assistant Professor and Interim Head
Nuclear Science and Engineering Program

ABSTRACT

The United States Geological Survey TRIGA Reactor (GSTR) is a 1 MW reactor located in Lakewood, Colorado. In support of the GSTR's relicensing efforts, this project developed and validated a Monte Carlo N-Particle Version 5 (MCNP5) model of the GSTR reactor. The model provided estimates of the excess reactivity, power distribution and the fuel temperature, water temperature, void, and power reactivity coefficients for the current and limiting core. The MCNP5 model predicts a limiting core excess reactivity of $6.48 with a peak rod power of 22.2 kW. The fuel and void reactivity coefficients for the limiting core are strongly negative, and the core water reactivity coefficient is slightly positive, consistent with other TRIGA analyses. The average fuel temperature reactivity coefficient of the full power limiting core is -0.0135 $/K while the average core void coefficient is -0.069 $/K from 0-20 % void. The core water temperature reactivity coefficient is +0.012 $/K. Following the neutronics analysis, the project developed RELAP5 and PARET-ANL models of the GSTR hot-rod fuel channel under steady state and transient conditions. The GSTR limiting core, determined as part of this analysis, provides a worst case operating scenario for the reactor. During steady state operations, the hot rod of the limiting core has a peak fuel temperature of 829 K and a minimum departure from nucleate boiling ratio of 2.16. After a $3.00 pulse reactivity insertion the fuel reaches a peak temperature is 1070 K. Examining the model results several seconds after a pulse reveals flow instabilities that result from weaknesses in the current two-channel model.

TABLE OF CONTENTS

LIST OF FIGURES

LIST OF TABLES

LIST OF SYMBOLS

A - initial activity following irradiation in the GSTR (Bq).

A_{flow} - Flow area of the channel (m)

A_{au} - atomic weight of gold (g)

D_e - equivalent hydraulic diameter (m)r

En - average coolant enthalpy (J/kg)

E - energy produced (MWH)

E_{Sm149} - fission yield of samarium-149 (atoms/fission)

F - MCNP tally result (atoms/b-cm)

f - friction factor

G - mass flow rate (kg/s)

g - acceleration due to gravity (m/s^2)

h - enthalpy

i – numeric index

k - MCNP reactivity calculation result

k_{eff} - effective multiplication factor in a reactor

l - particle track length (m)

M - number of active cycles

M_{Au} - mass of the gold foil (g)

$M_{U\text{-}235}$ - mass of Uraniuim-236 burned (g)

m - individual cycle number

n - node index

N - arbitrary number, Chapter 2

N - number of rods in core, Chapter 3

N_a - Avagrado's number

OD - Outer Diameter of fuel element (m)

P - reactor power (W)

Pr - pressure (Pa)

Pi - pitch (m)

P_{rod} - power in a rod (kW)

$P(v,T)$ - distribution of the target velocities in the experiment(m/s)

PF - peaking factor

q - heat source per unit volume (J/m^3)

R - relative error

$\dot{R}$- reaction rate (1/s)

R_{fuel} - thermal resistivity of the fuel ($(m^2K)/W$)

R_{clad} - thermal resistivity of the cladding($(m^2K)/W$)

S - approximation of standard deviation

SPR - source particle rate (N/s)

t - time

T - duration of the irridation (s)

TR - MCNP tally result from the model

T_{cl} - the centerline temperature of the fuel rod (K)

$T_{1/2}$ - half-life of gold-198 (s)

U - internal energy (J)

$\acute{v}$ - velocity of the target (m/s)

v - velocity of incident particles (m/s)

x - quantity of interest from an MCNP calculation

$\bar{x}$- average value of x

$\overline{x^2}$ - average value of x squared

z - axial coordinate (positive direction is upwards)

α - fitting coefficient used in RELAP calculations

β - fitting coefficient used in RELAP calculations

B_{eff} - effective delayed neutron fraction

δ - energy per fission (MeV)

γ - fitting coefficient used in RELAP calculations

ρ - density (kg/m^3)

ρ - reactivity ($)

ν - number of neutrons per fission

σ - microscopic cross-section of an stationary nuclei (b)

σ_{abs} - adsorption cross section of samarium 149 (b).

σ_f - fission cross section of uraniu 235 (b)

Σ_{tot} - total neutron cross-section (b)

φ - fitting coefficient used in RELAP calculations

ξ- random number between 0-1

ACKNOWLEDGMENTS

This project, which has taken the better part of two years of my life, is an interesting stepping-stone in my academic career, and has been an amazing learning opportunity in both life and nuclear engineering. I would never have been able to achieve this without the support of my adviser, Dr. Jeffrey King, and his belief in my own potential, even when I sometimes doubted it myself. I would like to thank you Dr. King, not for making this enjoyable, or fun, because it wasn't, but for making this perhaps one of the greatest learning opportunities I will ever receive, and I look forward to completing my Doctorate with you. Some things in life should not be fun, but they should be right, or at least provide a reasonable result within the uncertainty bounds of the problem, and this was a lesson you taught me over the past three years. Even if occasionally your drive for perfection seemed to conflict with my desire for progress I realize now that sometimes it just has to be right.

I would also like to thank my friends and co-workers whose help and support keep me going, and whose ideas helped me in many of the more difficult parts of this analysis, even if it was just as someone to bounce ideas off of. Specifically I would like to thank Jeremy Washington for his help on MCNP5, Weston Collins for his assistance brainstorming the thermal-hydraulic problems, and Jason Sexauer, Daniel Suhr, Savannah Fitzwater, Sarah Morgan, Jared Hughes and Brady Nun for their support over the past two years.

Finally, I would like to thank my committee for their support, especially Dr. Olson without whose help the PARET model would ever have come into existence.

CHAPTER 1
INTRODUCTION

The United States Geological Survey (USGS) constructed the Geological Survey TRIGA Reactor (GEST) to perform neutron irradiation experiments in support of their mission to provide relevant scientific information about the planet (United States Geological Survey, 2008). The GSTR provides neutron activation and radioisotope production capabilities for the USGS and also supports the Colorado School of Mines (CSM), providing CSM's new Nuclear Science and Engineering Program with access to the facility for research and teaching purposes.

The NRC granted the original GSTR facility a license after construction finished in February of 1969; however, this license expired on February 24, 2009. As part of the license renewal process, the NRC required that the GSTR's original safety analysis be updated to reflect the current operating conditions, legal requirements, and analysis methods. This project developed a suite of computational models to give the GSTR access to the modern analysis tools needed for relicensing. These tools will also assist in the development of future experiments at the GSTR. The new computational tools include neutronic, steady state thermal-hydraulic, and transient thermal-hydraulic operation models of the GSTR. This project used the Monte Carlo N-Particle (MCNP) code (X-5 Monte Carlo Team, 2003) to construct the neutronics model, the Reactor Excursion and Leak Analysis Program (RELAP) (Information Systems Laboratories, Inc., 2010b) to develop the thermal-hydraulics model, and the Program for the Analysis of Reactor Transients (PARET) code (Woodruff and Smith, 2001) to confirm the thermal-hydraulics models.

Previous work at CSM developed an initial version of the MCNP model of the GSTR. While mostly complete, the model had not been validated and needed to be updated to reflect the limiting core analyses requested by the NRC. Therefore, the first goal of the present project was to update and validate the existing MCNP model of the GSTR. Validation consists of testing the model's ability to match experimental data collected by the GSTR staff, including neutron flux profiles, control rod worth curves, critical rod positions, and core excess and shutdown reactivity values. This validation effort is a critical step in the GSTR's re-licensing effort, as the validated MCNP model determines many of the parameters requested by the NRC.

The steady-state thermal-hydraulic model was constructed based on previous re-licensing models created for other TRIGA reactors (Marcum and Woods and Reese, 2011; Marcum, 2008; Oregon State University Radiation Center , 2010). This model represents the hot-channel within the GSTR core, and allows the steady-state heat flux from the hot rod, as well as the cladding, fuel, and channel water temperatures, to be predicted under steady-state operating conditions.

A transient reactor model evaluates the reactor during operational transients, power pulses, and off-normal conditions. The MCNP model's predictions for the thermal feedback coefficients from the reactor will inform a point-kinetics model to represent the bulk activity of the reactor core. The model represents the core average behavior, and the results are scaled using the power factor to represent individual rods, or areas of the GSTR core.

In order to support the GSTR's relicensing effort, this thesis includes several distinct objectives:

1) complete and validate the MCNP model of the GSTR and demonstrate the model's ability to predict reactor conditions,

2) analyze the GSTR's limiting core configuration,
3) construct and validate a RELAP steady-state model of the hot fuel channel,
4) predict the departure from nucleate boiling ratio (DNBR) for the hot rod under steady state operating conditions for the limiting core configuration,
5) construct and validate PARET and RELAP models for transient conditions in the core, and
6) predict the transient behavior of the reactor under the limiting core configuration.

While the geometry and material definitions in the original MCNP model of the GSTR were mostly complete (aside from error checking), the model needed proper validation to ensure that it accurately predicts the behaviors of the current GSTR core. Objective one focused on demonstrating this through several methods. The integral control-rod worth curves for the model have been matched to experimental data from the GSTR. The computed control rod critical positions match the experimentally determined positions to within the model's uncertainty and a safety factor to compensate for measurement and error. The model predictions satisfy the GSTR Technical Specifications during operation and shutdown conditions, including limits on the excess and shutdown reactivity margins. The model also predicts reasonably accurate foil activation rates and axial fluxes in the GSTR central thimble irradiation facility. Matching the model's predictions to experimental results from the GSTR provides assurance that the model can support the analyses requested by the NRC.

The second objective ensures that the GSTR is able to function safely under the worst-case set of operating conditions. The purpose of the limiting core is to set a bounding condition on core configurations that can be run without endangering the public. A good limiting core should push the limits of the current GSTR safety guidelines. Under these conditions, if the

GSTR can still operate safely, then, in theory, any less challenging core configurations will also be safe. To ensure this is true, the limiting core's critical conditions must meet all of the limits established in the GSTR's technical specifications. The limiting core calculations identify the hot rod and provide a detailed power profile for the fuel within this rod. The MCNP model also calculates the fuel temperature reactivity coefficient, moderator temperature reactivity coefficient, and void reactivity coefficient for the limiting core.

The reactor must safely remove the heat generated during normal operation without causing fuel damage. The RELAP model developed in objective three demonstrates this. Like the MCNP model, the RELAP model requires validation to ensure that the results given by the model are accurate. Initially this validation examined the recorded temperatures from the reactor's thermocouples; however, the uncertainty in this data was too large to provide meaningful validation. Instead, a comparison to similar TRIGA reactor models ensured that, from a safety perspective, the model's predictions are consistent, and meet the needs of the relicensing analysis.

The NRC requires that the departure from nucleate boiling ratio (DNBR) for the GSTR be calculated as part of the re-licensing process. Departure from nucleate boiling is a condition where a thin film of vapor covers a fuel element, significantly decreasing the ability of that element to transfer heat to the coolant. In these conditions, the fuel element's temperature increases rapidly as the heat generated by the rod cannot escape. Objective four uses the RELAP model to calculate the DNBR for the hot rod channel. Since the hot rod channel is a limiting case for the GSTR, the hot channel DNBR also serves as the worst DNBR within the GSTR.

Objective five focuses on developing a model for the transient behavior of the GSTR. RELAP contains a point-kinetics model that, when applied to a two-channel RELAP model, allows the steady-state model to approximate the transient behavior of the reactor. This model, however needs some form of validation, which comes from analyzing the differences between the RELAP model and a similar model developed using PARET. The PARET code simulates the transient behavior of test reactors, and uses a coupled point kinetics and thermal-hydraulic model to predict the transient conditions within a reactor core simular to RELAP (Woodruff and Smith, 2001; Adoo et al., 2011; Woodruff et al., 1996). This allows PARET to provide a second case to compare to the results of the RELAP model to, as the proposed limiting core is unique from any core currently or historically used at the GSTR.

Objective six ensures that the limiting core will operate safely under transient conditions. Similar to the MCNP analysis, the RELAP and PARET analyses verify the safe operating bounds of the GSTR during transient conditions with the limiting core.

The next chapter describes TRIGA reactors and the GSTR in detail, as well as the methodology for the selection of each of the analysis codes, and details on how each code functions. Chapter 3 then describes the neutronic analysis, including the MCNP reactor model, in detail. Chapter 4 describes the RELAP and PARET models, and the thermal-hydraulic analysis preformed for the GSTR. All of the results are summarized in Chapter 5, while Chapter 6 lists possible future work. Appendix A contains the MCNP 5 model of the GSTR operating core. Appendix B contains the RELAP steady-state model, Appendix C contains the RELAP two-channel transient model, and Appendix D has the PARET model.

CHAPTER 2
BACKGROUND

This project focuses on simulating the behavior of the U.S. geological Survey TRIGA Reactor (GSTR) with three different computer codes: MCNP5, RELAP5 and PARET-ANL. Each code focuses on a specific aspect of the reactor's operation. Since TRIGA reactors are research, not power, reactors, this analysis is different from that for a commercial power plant, as a TRIGA reactor requires fewer features to ensure the safety of the public compared to larger commercial reactors. This chapter includes a description of the unique features of TRIGA reactors, as well as the background of the three codes used in this project.

2.1. TRIGA Reactors

General Atomics designed the Training Research and Isotope - General Atomics (TRIGA) reactor in the 1960's to serve as a rugged research and training reactor suitable for training future nuclear engineers without any major risk of endangering students or the public (Fouquet, Razvi, and Whittemore, 2003). TRIGA reactors are the most numerous form of research reactor, with 66 facilities currently in operation (General Atomics, 2011a). TRIGA reactors are designed with strong negative thermal feedbacks, making the reactor highly resistant to core damage even in extreme situations (Fouquet, Razvi, and Whittemore, 2003). These features are common to every TRIGA reactor, even though the specific details of the core geometry or core dimensions change from reactor to reactor (Nuclear Installation Safety Division, 2004a).

A TRIGA reactor operates through controlled nuclear fission in a manner identical to large energy production reactors. TRIGA reactors, however, require much less infrastructure to

operate safely. Most TRIGA reactors, including the GSTR, are housed at the bottom of large pools that provide both shielding and the primary method of cooling for the reactor (Nuclear Installation Safety Division, 2004b). The GSTR consists of a reactor core housing the fuel elements in a circular grid surrounded by a graphite reflector. Figure 2.1 shows an image of the GSTR in operation.

As Figure 2.1 shows, a TRIGA core tends to be compact, leading to a high rate of neutron leakage from the core. While this leakage is an integral part of the TRIGA reactor's inherent safety, it also allows for neutron irradiation without having to significantly re-design the core (Nuclear Installation Safety Division, 2004a).

TRIGA reactors incorporate inherent safety features, where natural forces, as opposed to engineered or operator-controlled mechanics, ensure the safety of the reactor and public in an

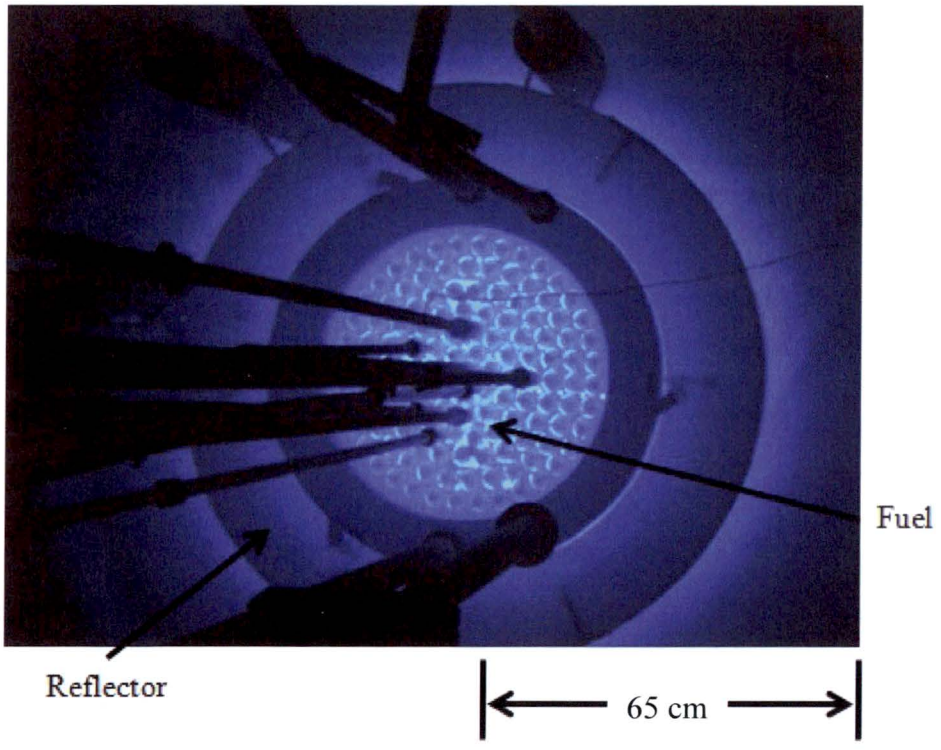

Figure 2.1. GSTR core during operation.

emergency situation (Fouquet, Razvi, and Whittemore, 2003). Edward Teller proposed the design to create a reactor that would shut down without any human interaction and without fuel damage if the control rods were completely removed from the reactor core (General Atomics, 2011b). The TRIGA reactor's uranium-zirconium-hydride fuel provides the majority of this safety (Nuclear Installation Safety Division, 2004a).

TRIGA reactor fuel has an inherently large negative temperature reactivity coefficient (Simnad, 1981). The largest contributor to this effect comes from the inclusion of hydrogen within the fuel to moderate the neutrons. Because the hydrogen included in the fuel heats with the fuel, a "warm neutron effect" reduces the moderating ability of the fuel as reactor power increases (General Atomics, 2011b). As the hydrogen in the fuel heats up, its ability to moderate neutron energy (and thus increase the effective fission cross section of the uranium within the fuel) decreases, while the excess energy within each hydrogen atom becomes available to be transferred to passing neutrons, hardening the neutron spectrum (Clifford, Hopkins, and West, 1966). This encourages neutrons to leave the fuel and enter the surrounding water, increasing the role of neutron capture outside of the fuel, and reducing overall reactivity (Haake and Krase, 1967). At the same time, the harder (faster) neutron spectrum encourages parasitic neutron capture within the U-238 present in the fuel, further reducing the number of fissions (Nuclear Installation Safety Division , 2004b). Finally, neutrons that escape into the water will be thermalized, but will have some difficulty returning into the fuel through the cladding materials once at thermal energies (Nuclear Installation Safety Division, 2004b). This effectively increases the net loss of neutrons from the core. These three factors contribute to provide the prompt negative temperature feedback inherent in TRIGA fuel (Nuclear Installation Safety Division, 2004a).

TRIGA reactors differ from commercial power reactors in a number of key areas that cause unique situations during re-licensing. Research reactors are typically much smaller than commercial power reactors. The GSTR's power output of 1 MW_{th} is approximately $1/3000^{th}$ that of a typical commercial nuclear power plant (which typically produces 1 GW_e). The lower power output of a TRIGA reactor requires less safety and operational infrastructure compared to commercial power reactors (Nuclear Installation Safety Division, 2004b). From a thermal-hydraulics standpoint, the much lower power output requires less extensive cooling systems than commercial power reactors (Nuclear Installation Safety Division, 2004b). The small size of a TRIGA reactor allows the reactor to reach a cold shutdown state within minutes of a SCRAM, as the power output of the decay products can be completely removed through natural convection in the reactor pool (Nuclear Installation Safety Division, 2004b).

Uranium-zirconium-hydride fuel also allows TRIGA reactors to "pulse." In pulsed operations, one control rod is rapidly removed from the core, adding a large amount of reactivity to the reactor (Nuclear Installation Safety Division, 2004b). The fuel reacts to the temperature increase caused by the sudden increase in power by providing a large amount of negative reactivity, which limits the rate of the nuclear reaction and prevents fuel damage. During the brief duration of the pulse, the reactor can operate at a power level of several gigawatts, allowing for safe experiments requiring large, short duration, neutron fluxes.

2.1.1. TRIGA Fuel Rods

General Atomics developed several different TRIGA fuel rod configurations (Tomsio, 1986) (Table and Figures 2.2a and 2.2b). The GSTR uses three different fuel rod types, one which is clad in aluminum (Figure 2.2a), and two of which are clad in stainless steel (Figure 2b). All three types use a uranium-zirconium hydride fuel enriched to less than 20 wt.% uranium-235

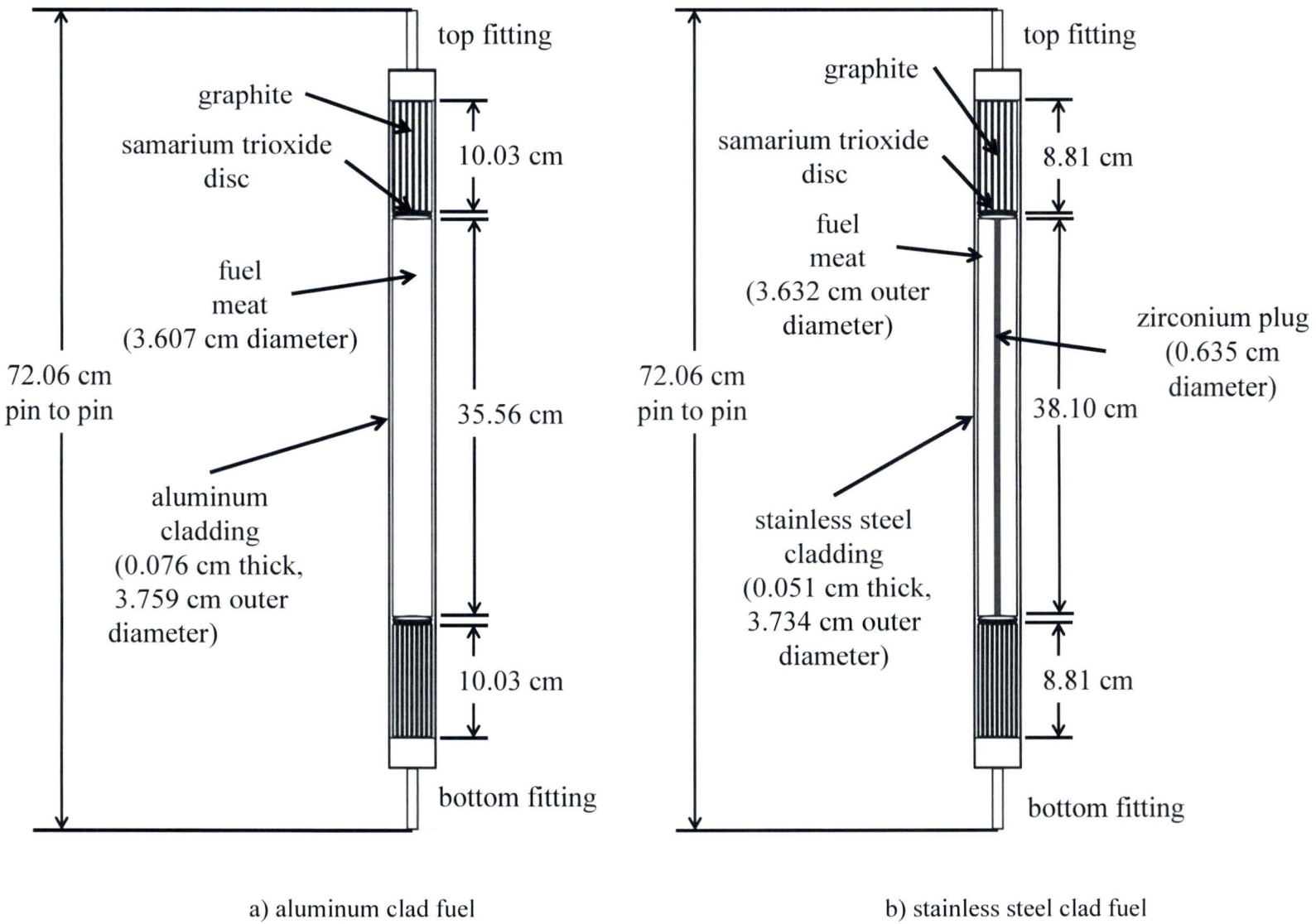

a) aluminum clad fuel

b) stainless steel clad fuel

Figure 2.2. Schematics of the TRIGA fuel types used in the GSTR.

(Simnad, 1981). Both fuel types have a length of 72.06 cm (Figures 2.2a and 2.2b) (Tomsio, 1986). The aluminum clad fuel has an outer diameter of 3.76 cm (Figure 2a) while the stainless steel clad fuel has an outer diameter of 3.73 cm (Figure 2b). Internally, the fuel is sandwiched between two graphite plugs above and below the fuel meat to reduce neutron leakage out of the top and bottom of the fuel rod (Figures 2a and 2b). Early TRIGA fuel rods included disks of samarium to act as a burnable neutron absorber; however, General Atomics stopped manufacturing these elements after 1964 (Tomsio, 1986). The present analysis ignores the effects of the burnable absorber, as all of the fuel at the GSTR is old enough that the burnable absorber has been depleted.

Table 2.1 shows the basic properties of the fuel types currently in the GSTR. All of the fuel in the GSTR is enriched to < 20 wt.% uranium-235, although the amount of uranium within the fuel meat (by weight percent) differs 8 wt.% to 12 wt.% based on the fuel rod design from. General Atomics also developed a fuel rod clad with Incoloy (Tomsio, 1986); however, the GSTR has never used this type of element.

The aluminum-clad fuel is the oldest TRIGA reactor fuel manufactured by General Atomics (Day, 2004). The fuel meat within an aluminum-clad rod contains 8 wt.% uranium, and is 35.56 cm tall (Figure 2.2a). The GSTR still uses several aluminum-clad fuel rods, which are

Table 2.1. GSTR Fuel types and basic information.

Fuel Type	Enrichment (%)	Cladding Material	Weight Percent Uranium in Fuel Meat (%)
8 % aluminum - clad	< 20	aluminum	8
8.5% stainless steel- clad	< 20	stainless steel	8.5
12 % stainless steel - clad	< 20	stainless steel	12

limited to the outer fuel rings in response to concerns over the lower melting temperature of aluminum (Day, 2004).

The stainless-steel clad fuel within the GSTR is a mixture of 8.5 wt.% and 12 wt.% fuel. The fuel in all stainless steel clad fuel element is 38.10cm long. A zirconium plug is located in the middle of the fuel meat (see Figure 2b) as a consequence of the manufacturing techniques used in manufacturing the U/ZrH fuel (Tomsio, 1986).

The dimensions of TRIGA fuel pins are not consistent and vary from reactor to reactor and batch to batch. The dimensions in Figures 2.2a and 2.2b form the basis for all of the fuel modeling efforts in this thesis.

2.2. Geological Survey TRIGA Reactor

The Geological Survey TRIGA Reactor (GSTR) is a 1 MW_{th} TRIGA Mark I reactor housed at the Denver Federal Center located in Lakewood, Colorado. The reactor core is contained in a water-filled pool 2.13 m wide and 7.62 m deep. Figure 2.1 shows the reactor core of the GSTR. The reactor core is 26.51 cm in radius from the inside of the lazy susan and 64.77 cm inches tall with 126 fuel locations located around a central thimble. A graphite reflector surrounds the core and is designed to reduce neutron leakage out the sides of the reactor (see Figure 2.1). These fuel locations are split into six concentric fuel rings labeled B through G. Four control rods are located in the C- and D-Rings of the core. Outside of the core, a radial graphite reflector limits radial neutron leakage (the fuel itself is designed to minimize axial leakage). The reflector also houses a lazy susan irradiation facility in a groove fixed within the graphite reflector, as shown in Figure 1.

There are four control rods within the GSTR (see Figure 2.3 a, 2.3b and 2.3c). Three are fuel-followed boron-enriched graphite control rods (Figure 2.3a), while the forth is a void-followed pulse rod (Figure 2.3b). The rod drives above the reactor raise the rods during normal operation. All four rods incorporate an electro-magnetic SCRAM feature. During a SCRAM, the electro-magnet that binds the control rods to their drives deactivates, allowing gravity to pull the rod back into the core. As part of the GSTR technical specifications, the core must shutdown (become subcritical) with three of the four rods inserted to allow for the possibility of a rod becoming stuck. The GSTR's fuel followed control rods are referred to as the shim 1, shim 2,

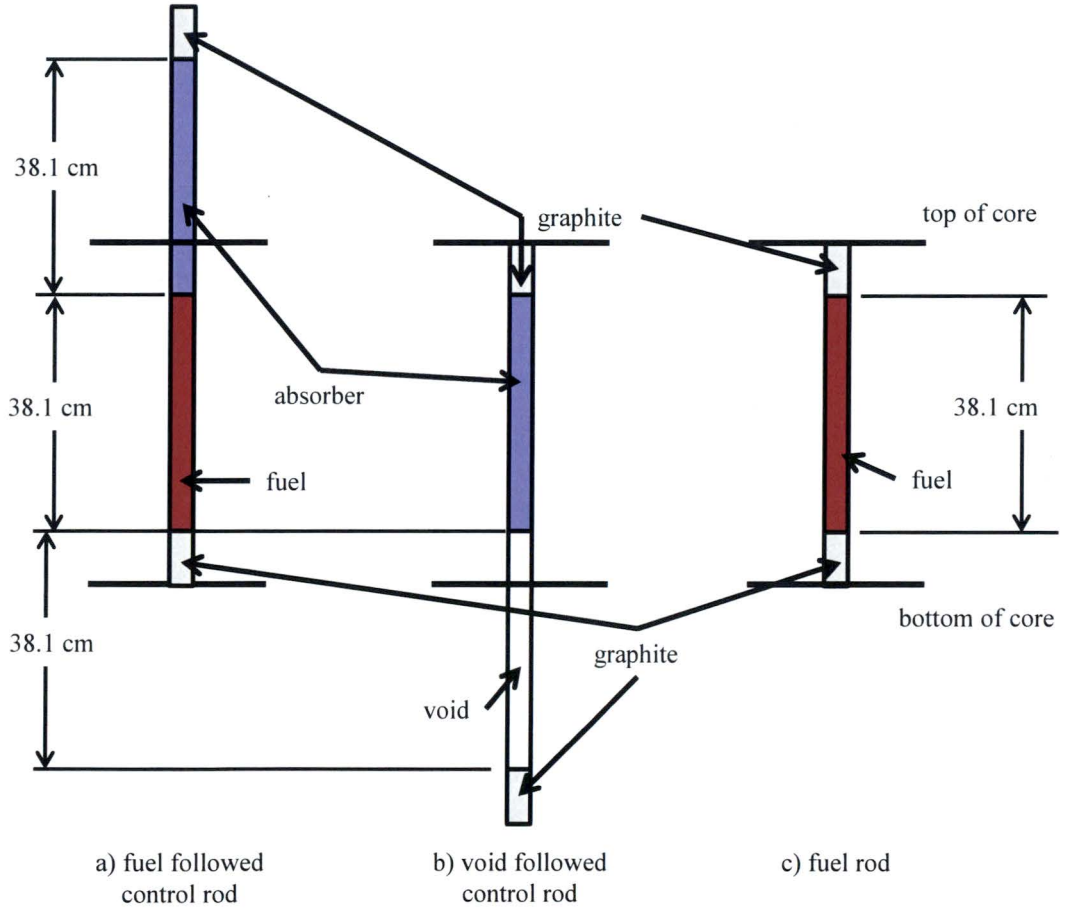

Figure 2.3. The different control rod types used in the GSTR compared to a fuel rod.

and regulating rods. These rods contain a fuel element following the boron enriched graphite (see Figure 2.3a), which reduces the impact of removing the control rod on the core flux profile. The final control rod, the transient rod, is void followed, (see Figure 2.3b), and uses an electro-pneumatic rod drive instead of the mechanical system used by the other three control rods. This system can quickly eject the transient rod from the core to initiate a pulse operation. Otherwise, the transient rod serves the same function as the other three rods; however, the pneumatic drive is not as sensitive as the mechanical rod drives. The void follower reduces the total reactivity worth of the transient rod.

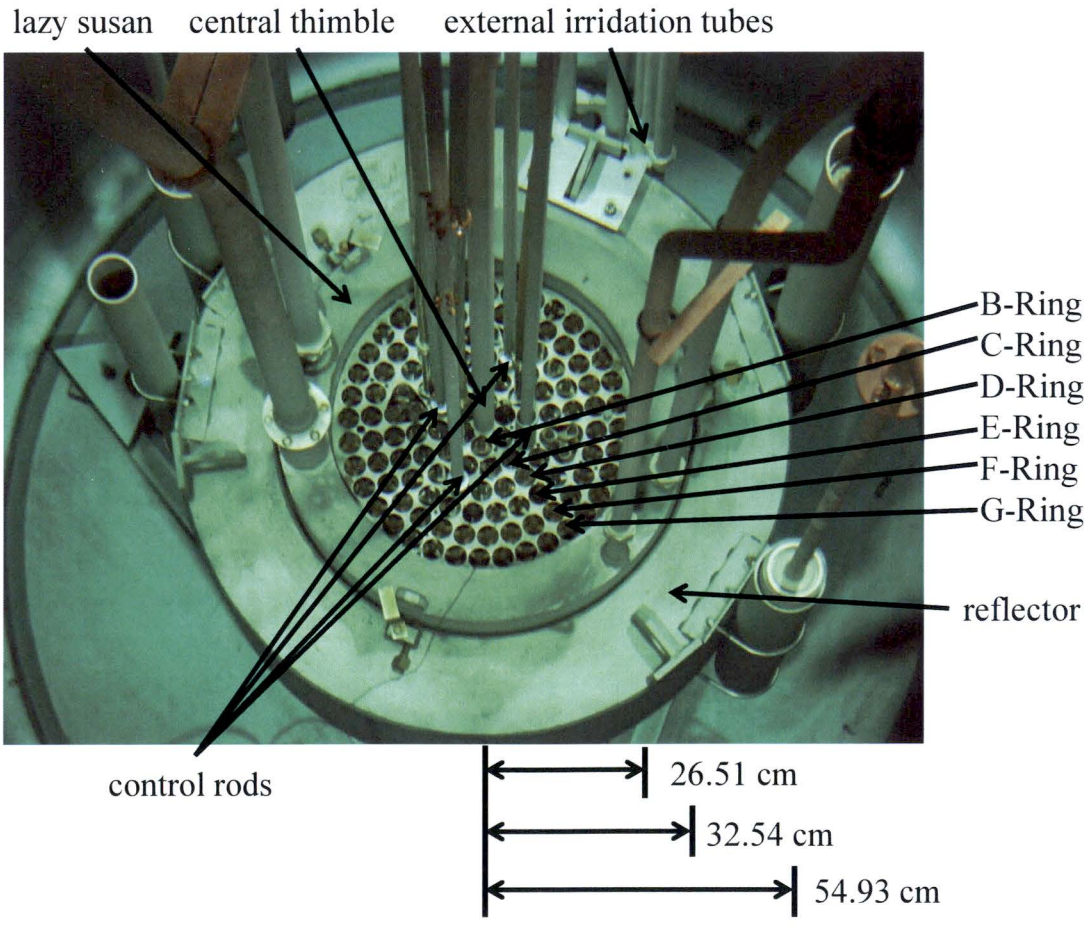

Figure 2.4. The GSTR Core with the different experimental facilities shown

There are three primary experimental facilities within the GSTR - the central thimble located within the reactor core, and the lazy susan and external irradiation tubes located outside of the core (see Figure 2.4). Located in the middle of the core, the central thimble provides a high-flux irradiation location. Normally, the central thimble is water filled, but can be evacuated to provide a beam tube for radiography.

The lazy susan sits outside of the core in an insert placed in the GSTR's graphite reflector (see Figures 2.1 and 2.4). A pneumatic system allows the forty sample locations within the lazy susan to be remotely loaded and unloaded and a mechanical drive rotates the lazy susan around the core. Originally designed for isotope production, the GSTR currently uses the lazy susan for sample irradiation.

Two irradiation tubes sit outside of the reflector. A reactor operator must manually insert samples into the tubes from outside of the reactor tank by lowering or raising the sample into the reactor by hand.

2.3. Code Selection

Within the last 14 years, multiple TRIGA reactors have sought re-licensing, or have sought alterations to their licenses to alter their capabilities (Marcum, 2008; Jensen and Newell, 1998). As a result of their age and large number, many TRIGA reactor facilities have developed independent tools to support relicensing analysis (Merroun et al., 2009; Mesquita, 2007; Miller and Feltus, 2000; Huda and Rahman, 2004; Housiadas, 2002). In the case of the GSTR, a partially completed MCNP5 neutronics model already existed from previous work at CSM. Given the difficulty in constructing an accurate model from scratch, this project finishes and validates the partially completed model. This model is described in detail in Chapter 3.

While several custom codes for thermal-hydraulics have been developed or were in the process of being validated (Merroun et al., 2009; Mesquita, 2007; Miller and Feltus, 2000; Housiadas, 2002; Kazeminejad, 2008), most of these codes were not focused on a re-licensing scenarios, or were only in the early stages of validation.

A survey of existing thermal-hydraulics codes indicated that the RELAP package has been in use for safety analysis for decades and for research reactors as early as the late 1990's (Jensen and Newell, 1998). RELAP is designed specifically for nuclear applications, and used extensively inside and outside of the United States (Marcum, 2008; Jensen and Newell, 1998; Mesquita, 2007; Anderson, 2010; Ferreri, 1995; Binh el at., 2007; Antariksawan et al., 2005; Maria, 2010; Marcum, Woods and Reese, 2009). Aside from RELAP, the newer TRACE code (which combines RELAP and several other thermal-hydraulics codes, and is intended to eventually replace RELAP) is also used in some applications (Cheng et al., 2009; Takasuo, 2006). The present project selected RELAP based on the codes history of use for research reactors modeling.

The work done by Oregon State University (OSU) in re-licensing their TRIGA reactor provided a basis for the GSTR analysis. The OSU analysis combined MCNP and RELAP results to produce the relicensing data requested by the NRC. A detailed description of the OSU RELAP model (Marcum, 2008) provided the basis for this project's RELAP model.

PARET-ANL combines point-kinetics with a thermal-hydraulic model to provide capabilities similar to RELAP (Woodruff et al., 1996; Hamidouche et al., 2004). The code is optimized for research-sized reactors, unlike RELAP, which is primarily designed for large commercial power reactors (Adoo et al., 2011; Woodruff, 1982; Jonah, 2011). Previous

validation work has also used PARET (Huda and Rahman, 2004). This background led the project to using PARET to provide a comparison to the RELAP calculations.

2.4. Monte Carlo N-Particle

Monte Carlo N-Particle (MCNP) is a Monte Carlo particle transport code extensively used in the nuclear research field for its ability to simulate a wide range of particle transport scenarios including reactor design, shielding, and dosimetry problems (Hendricks et al., 2000; X-5 Monte Carlo Team, 2003a). MCNP5 is the most recent release of MCNP and uses a combination of random numbers paired with different tables and functions to simulate the probabilistic behavior of a random particle traveling within different materials. MCNP can simulate neutrons, electrons and photons (X-5 Monte Carlo Team, 2003a). The Los Alamos National Laboratory develops MCNP5 and its variants. All of the neutronic calculations for the GSTR relicensing effort are based MCNP5 version 1.60.

An MCNP input file is referred to as a "deck" (a legacy term from when actual decks of cards provided the program inputs) that contain the geometric, material, and input parameters for the problem, including the particle source and any detectors for particle fluxes or reaction rates the user wishes to define. The code begins by creating a particle either from a user-defined source or through a calculated fission source profile (in the case of a criticality calculation). Which material the particle is currently in determines the distance that particle travels before an interaction occurs with one of the atoms in the material (as defined by material cards and the appropriate cross-section library). MCNP calculates this distance by (Carter and Cashwell, 1975):

$$l = -\frac{1}{\Sigma_{tot}} ln(1-\xi) = -\frac{1}{\Sigma_{tot}} ln(\xi). \qquad (2.1)$$

After traveling this length, an interaction occurs based on the material the particle is within. If there are multiple nuclides in the region, another random number determines which nuclide the particle interacts with. At this point the particle will either have been removed from the simulation (as a result of some form of capture reaction), or a new energy, direction and speed are determined, and the process begins again (Carter and Cashwell, 1975).

A general weakness of Monte Carlo codes, including MCNP5, comes from the code's inability to generate general information not specified in the input deck. A user sets conditions within the deck to track, and when a particle triggers one of these conditions (a fission reaction, or entering a specific portion of the geometry for existence) that data is recorded for the output file (X-5 Monte Carlo Team, 2003b). After the program has finished the run (from either user settings, or a manual interrupt) the results are placed in the output file based on the user's conditions specified in the input file (X-5 Monte Carlo Team, 2003b).

As MCNP is designed as a generic particle transport problem solver, the simulation can run in two ways. The primary method uses a generic source that can function using any of the particles found in MCNP (X-5 Monte Carlo Team, 2003b). With this source, the geometry, distribution, and energy of the particles can be set in the input deck. Particles are created by the code based on the source definition, and run through the described process until they are absorbed or killed (a setting can also stop MCNP from continuing to track the particle if it exists for too long), at which point the source creates another particle (X-5 Monte Carlo Team, 2003b). This continues until a pre-set limit is reached, either time or number of particles (X-5 Monte Carlo Team, 2003a).

The criticality, or k-code, mode only functions with neutrons (X-5 Monte Carlo Team, 2003b). In this mode, MCNP treats fission reactions as captures that set the location for the next generation of neutrons in the simulation (X-5 Monte Carlo Team, 2003a). Unlike the basic source definition, which simply runs until a set time or number of particles has been reached, a k-code calculation uses many iterations of several (usually over 10,000) particles each. The first several iterations (defined by the user) determine the shape of the source distribution based on the locations of the fission events (Brewer, 2009). Once MCNP determines the source distribution for a given cycle, multiplication factor for that cycle is determined by comparing the number of fission neutrons created with the number of neutrons that began the cycle (Brewer, 2009). This ratio determines multiplication factor and many iterations are needed to minimize the uncertainty in the calculation (Brewer, 2009). All the neutronic simulations run in support of the GSTR re-licensing effort use the k-code method.

MCNP is also capable of tracking particle flux, current, energy disposition and interactions within an area of interest through the use of tallies (X-5 Monte Carlo Team, 2003a). These tallies can be set to cover a surface, volume, or a single point within the geometry of the problem. All tallies are normalized to be per starting particle (X-5 Monte Carlo Team, 2003a). MCNP is also capable of approximating reactions using a flux calculation with ENDF reactions (X-5 Monte Carlo Team, 2003a). Reaction rates in MCNP use (X-5 Monte Carlo Team, 2003a; Lewis, 2008):

$$C = \int \Phi(E) f(E) dE. \tag{2.2}$$

The statistical uncertainty of a monte carlo answer is proportional to the number of particles tracked in the simulation through the Strong Law of Large Numbers (Artstein and Vitale, 1975), but an inherent problem is that if another situation comes up, another simulation must be run (X-5 Monte Carlo Team, 2003a). Generally speaking, in each iteration, the relative error (R) for some measured quantity is calculated as (Carter and Cashwell, 1975):

$$R = \frac{1}{\bar{x}}\sqrt{\frac{\overline{x^2}-\bar{x}^2}{M-1}}, \tag{2.3}$$

where:

$$\bar{x} = \frac{1}{M}\sum_m x_m \ \ and \ \overline{x^2} = \frac{1}{M}\sum_m x_m^2. \tag{2.4}$$

MCNP uses these values to generate the covariance and correlation for the problem (X-5 Monte Carlo Team, 2003a).

A Monte Carlo simulation calculates precision using the Strong Law of Large Numbers (Artstein and Vitale, 1975). Under this law, the average value will approach the expected value as the number of attempts to find that value approaches infinity (Artstein and Vitale, 1975). Since an infinite number of runs cannot be done, MCNP calculates the precision of any value given as a function of the number of attempts run. In short, while any individual particle (or even batch of particles) may not represent the physical situation, a sufficiently large number may provide a reasonable approximation for the physical system. MCNP measures this precision through a standard deviation calculation (X-5 Monte Carlo Team, 2003a):

$$S^2 = \frac{\sum_{i=1}^{N}(x_i - \bar{x})^2}{N-1} \cong \overline{x^2} - \bar{x}^2 \tag{2.5}$$

2.4.1. Temperature Adjustments in MCNP

The MCNP5 distribution includes the makxsf utility which allows for manipulation of cross-section libraries, Doppler-broadening of existing cross sections, and interpolation between existing sets of thermal scattering (S(α,β)) data (Brown, 2006). Like MCNP5, makxsf reads an input file to allow the user to access the functions of the makxsf code. A user can copy cross-section data from existing libraries (datasets) into a new library. New cross-sections can be Doppler-broadened based on a lower-temperature dataset. Should the dataset also contain probability tables for unresolved resonances, makxsf can interpolate the tables if a higher-temperature dataset is provided (Brown, 2006), otherwise the lower-temperature probability table is simply copied over to the new library. Finally S(α,β) data interpolation is also possible if both a lower and higher temperature S(α,β) datasets are available (Brown, 2006).

Doppler broadening with makxsf incorporates several portions of the NJOY and DOPPLER codes (Brown, 2006; Muir and MacFarlane, 1994). NJOY is a code designed to process nuclear cross-sections and contains the BROADR subroutine, which is also included in makxsf and DOPPLER (Muir and MacFarlane, 1994). BROADR alters neutron cross-sections through a temperature-velocity relationship to find a temperature and velocity where the cross sections match according to (Muir and MacFarlane, 1994):

$$\rho v\bar{\sigma}(V,T) = \int d\acute{v}\, \rho\, |v - \acute{v}|\, \sigma(|v - \acute{v}|)\, P(\acute{v},T). \tag{2.6}$$

The DOPPLER code expands this method to work on the ACE (A Compact ENDF) format cross-section data, as opposed to the raw ENDF (Evaluated Nuclear Data File) data which NJOY starts with (Brown, 2006). The makxsf code uses DOPPLER for probability tables as well, through a simple interpolation between two data points (Brown, 2006).

2.4.2. MCNP ENDF Libraries and Zirconium Cross-Sections

The impact of cross-section selection on the neutronic modeling of a TRIGA reactor is non-trivial. Several reports have discussed the effects different cross-section libraries have on the predicted multiplication factor calculated for TRIGA reactors via Monte Carlo methods (Bess, Marshall, and Maddock, 2011; Snoj, Trkov, and Ravnik, 2007; Snoj, Zerovnik, and Trkov, 2011). The findings of these reports point to inaccuracies in the most recent zirconium cross-section libraries that only become apparent in fuel types that use a large amount of zirconium within the fuel meat, such as TRIGA fuel rods (Snoj, Trkov, and Ravnik, 2007; Snoj, Zerovnik, and Trkov, 2011). The ENDF/B-VII.0 libraries typically predict higher k_{eff} values for TRIGA benchmark models when compared to both the ENDF/B-VI.6 and JEFF 3.1 neutron cross-section libraries (Snoj, Zerovnik, and Trkov, 2011). Further analyses of the individual isotopes within the ENDF/B-VII.0 library, as well as tests using the $S(\alpha,\beta)$ data within each library found that the ENDF/B-VII.0 $S(\alpha,\beta)$ data gave the greatest contribution to the difference between the ENDF/B-VII.0, ENDF/B-VI.6 and JEFF 3.1 libraries (Snoj, Zerovnik, and Trkov, 2011). These differences between ENDF/B-VII.0 and ENDF/B-VI.6 are many times the calculated standard deviation of the benchmark model (Snoj, Trkov, and Ravnik, 2007). More detailed experiments found that the ENDF/B-VII.0 libraries increase the thermal neutron flux, leading to a larger multiplication factor (Snoj, Zerovnik, and Trkov, 2011). Unfortunately,

further experiments need to be done to determine the correct treatment for zirconium within neutron cross section libraries, and are outside the scope of this project.

2.5. Reactor Excursion and Leak Analysis Program

The Reactor Excursion and Leak Analysis Program (RELAP) is a computational fluid dynamics (CFD) suite developed for the Nuclear Regulatory Commission to provide a regulatory thermo-hydraulic code for use in reactor applications (D'Auria and Galassi, 1998). RELAP uses a finite-difference algorithm to determine the thermo-hydraulic properties of a user-defined geometry, and has the capability to represent both steady state and transient conditions (D'Auria and Galassi, 1998).

Unlike several more modern codes, RELAP uses a one-dimensional two-fluid model to represent a two-phase system comprised of water, possibly some non-condensable components in the steam phase, or soluble components in the liquid phase (Ranson and Hicks, 1984). This allows the code to represent complex thermal-hydraulic systems (such as nuclear reactor cooling systems) while being computationally less intensive than a full three-dimensional model. A series of eight equations solve eight variables (pressure, phasic specific internal energies (for both liquid and gas phases), vapor volume faction, phasic velocities (both liquid and gas), non-condensable quality, and boron density) within the thermal-hydraulic system (Information Systems Laboratories, Inc., 2010a).

Geometry is provided to the code as a string of numeric lines in a text file. Each line of code is referred to as a card, while an entire input file is referred to as a deck (Informations Systems Laboratories, Inc., 2010b). RELAP has a number of pre-defined geometry types that can describe the geometry of a system. Each geometry represents a different hydraulic

component in a light-water reactor's cooling system (Informations Systems Laboratories, Inc., 2010b). Special hydraulic components, referred to as time dependent volumes, represent boundary conditions within the system as their hydraulic properties (i.e. temperature, pressure, fluid velocity, etc.) are user defined and not affected by the RELAP computation (Informations Systems Laboratories, Inc., 2010b). Solid components, such as pipe walls and fuel rods, are represented as heat structures (Informations Systems Laboratories, Inc., 2010b).

Heat structures use a one-dimensional heat-transfer approximation to represent heat flow through a solid medium. The heat structure can have either a rectangular or a cylindrical geometry. A series of nodes represent the solid materials in a heat structure as seen in Figure 2.5. Aside from the nodes for a one-dimensional analysis, multiple sets of nodes can be connected axially (although heat does not transfer from one set of nodes to another) to represent more complex structures (Figure 2.5) (Information Systems Laboratories, Inc., 2010a). Multiple axial nodes are required when connecting a single heat structure to multiple hydraulic components (such as those in a pipe). Each heat structure can only connect to a single hydraulic

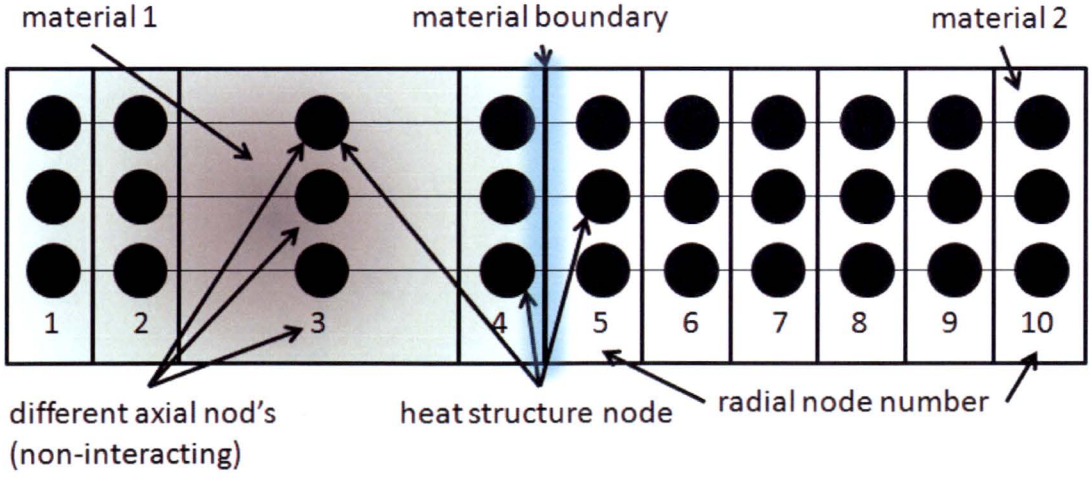

Figure 2.5. Example of a heat structure in RELAP with 10 nodes in two different materials with non-uniform mesh lengths.

component, and multiple materials can be represented within a single heat structure as long as the thermal data (thermal conductivity and volumetric heat capacity) for each material is provided by the user (Figure 2.5) (Information Systems Laboratories, Inc., 2010a). RELAP allows for this thermal data to be input through tables, equations, or as a constant value (Information Systems Laboratories, Inc., 2010a).

RELAP calculates the temperature and heat flux at each node of a heat structure. A heat generation term can also be applied to a node, or distributed throughout a heat structure to represent internal heat generation (such as within a heating coil or fuel rod) (Information Systems Laboratories, Inc., 2010b). Every heat structure has two boundary conditions (Riemke, Davis, and Schultz, 2008). These can be set to hydraulic volumes (to represent an interface between the heat structure and fluid), constant power fluxes, constant temperatures, insulated boundaries, or reflecting boundaries (representing the center of a cylinder) (Riemke, Davis, and Schultz, 2008).

RELAP uses several convergence criteria to determine if a model has converged when running a steady-state problem (Information Systems Laboratories, Inc., 2010a). The steady-state condition for RELAP monitors the change in the thermodynamic density, internal energy, and pressure to monitor the change in the system as a whole (Information Systems Laboratories, Inc., 2010a). Thus, once these three variables reach a constant value (with respect to time), the system has reached steady state (Information Systems Laboratories, Inc., 2010a). Within the code this is represented as (Information Systems Laboratories, Inc., 2010a):

$$\left(\frac{d(\rho\, h)}{dt}\right)_i^n = \frac{(\rho_i^{n+1}\, U_i^{n+1} + P_i^{n+1}) - (\rho_i^n\, U_i^n + P_i^n)}{\Delta t^n}. \tag{2.7}$$

However, this function is not well behaved with respect to time, as large fluctuations in the value of the derivative can occur, making a direct measurement difficult (Information Systems Laboratories, Inc., 2010 a). To compensate, RELAP uses a fitting function that is well behaved and can be solved over a number of time steps to determine steady state (Information Systems Laboratories, Inc., 2010a):

$$\left[\left(\frac{d}{dt}(\rho\, h)\right)^2\right]^n = e^{\alpha+\beta t^n+\gamma(t^n)^2+\varphi(t^n)^3}, (t_o \leq t^n \leq t). \tag{2.8}$$

2.6. Program for the Analysis of Reactor Transients

The Program for the Analysis of Reactor Transients (PARET-ANL) provides a simple but accurate model for reactor transients through a combined point-kinetics and thermal-hydraulic model (Woodruff and Smith, 2001). PARET was initially designed to analyze the SPERT-III experiments (Woodruff, 1982), and has since become a general use thermal-hydraulic code optimized for research reactors, espically those with plate-type fuel (Woodruff, 1984; Woodruff and Smith, 2001).

Like RELAP, PARET uses one-dimensional approximations for the thermal-hydraulic calculations (Adoo et al., 2011). Unlike RELAP, PARET is not capable of modeling general thermal-hydraulic geometries, and instead models a reactor core and the coolant channels within the core (Adoo et al., 2011; Woodruff and Smith, 2001). PARET-ANL can currently model a core of 1 to 50 fuel channels. This greatly simplifies input deck construction compared to RELAP.

PARET uses a momentum-integrated model to solve for the fluid conditions in coolant channels, based on the following governing equations (Adoo et al., 2011):

$$\frac{\partial \bar{\rho}}{\partial t} = -\frac{\partial G}{\partial z}, \tag{2.9}$$

$$\frac{\partial G}{\partial t} + \frac{\partial}{\partial z}\left(\frac{G^2}{\rho'}\right) = -\frac{\partial P}{\partial z} - \left(\frac{f}{\rho}\right)\left(\frac{|G|G}{2\,D_e}\right) - \bar{\rho}g, \tag{2.10}$$

$$\rho'' \frac{\partial E}{\partial t} + G\frac{\partial E}{\partial z} = q. \tag{2.11}$$

These equations examine the relationship between the average density ($\bar{\rho}$), mass flow rate (G) pressure (P), and heat source in a unit volume (q) (Woodruff, 1982). Each channel is independent of the other channels. A standard six-group point-kinetics model calculates the transient power generation within the simulated fuel elements (Woodruff and Smith, 2001).

PARET represents solid volumes using a series of axial and radial nodes. PARET can model up to three materials within a fuel rod, representing the fuel, cladding and another material (e.g. gap gasses) (Woodruff and Smith, 2001). All node points are assumed to be in the center of the region. Radial nodes are assumed to be of equal length starting from the centerline of the fuel element, and extending to the outer edge of the cladding (Woodruff and Smith, 2001). The user defines axial node lengths; these must conform to the total length of the rod once added together. Only 20 axial sections may be defined for any fuel element, and PARET only considers the active axial length of a fuel rod (i.e. the length of the fuel) (Woodruff and Smith, 2001).

The next chapter describes the neutronics model used in this project, as well as the validation and analysis calculations performed by the MCNP model.

CHAPTER 3
NEUTRONICS ANALYSIS

This chapter looks at the neutronic analysis performed by this project. The initial sections provide background information on the analysis and the GSTR reactor. Following this is a detailed description of the GSTR MCNP model, and the different core layouts examined in the project. The remainder of this chapter shows the results of the calculations performed by the MCNP models. This includes both the validation work on the GSTR, and the neutronic analysis of the GSTR limiting core.

3.1. Introduction

The Geological Survey TRIGA Reactor (GSTR) is a 1 MW_{th} Testing Research Isotope – General Atomics (TRIGA) Mark I reactor located at the Denver Federal Center in Lakewood Colorado. As part of the relicensing process, the United States Nuclear Regulatory Commission (NRC) requires an update to the reactor's safety analysis report and technical specifications to document the current operating conditions of the reactor. A Monte Carlo N-Particle (MCNP) (X-5 Monte Carlo Team, 2003a and 2003b) model of the reactor provides the basis for the neutronics analysis needed to update the safety analysis report and technical specifications. This analysis is broken into two stages. First, validating the MCNP model with data from the current GSTR core. Then, evaluating a limiting core to determine the core's excess and shutdown reactivity margins, reactivity feedback coefficients, and power distribution.

The next section provides a detailed description of the GSTR, followed by a description of the MCNP model in Section 3.3. Section 3.4. describes the validation of the model against the

current operating GSTR core and Section 3.5. presents the neutronics analysis conducted with the model for the limiting GSTR core.

3.2. Description of the Geological Survey TRIGA Reactor

The reactor core of the Geological Survey TRIGA Reactor (GSTR) is contained in a water-filled pool 2.13 meters wide and 7.62 meters deep. Figure 3.1 shows the reactor core of the GSTR. The reactor core is 26.51 cm in radius from the inside of the lazy susan and 66.81 cm tall with 126 fuel locations located around a central thimble (see Figure 3.1). These fuel locations are split into six concentric fuel rings labeled B through G. Four control rods are

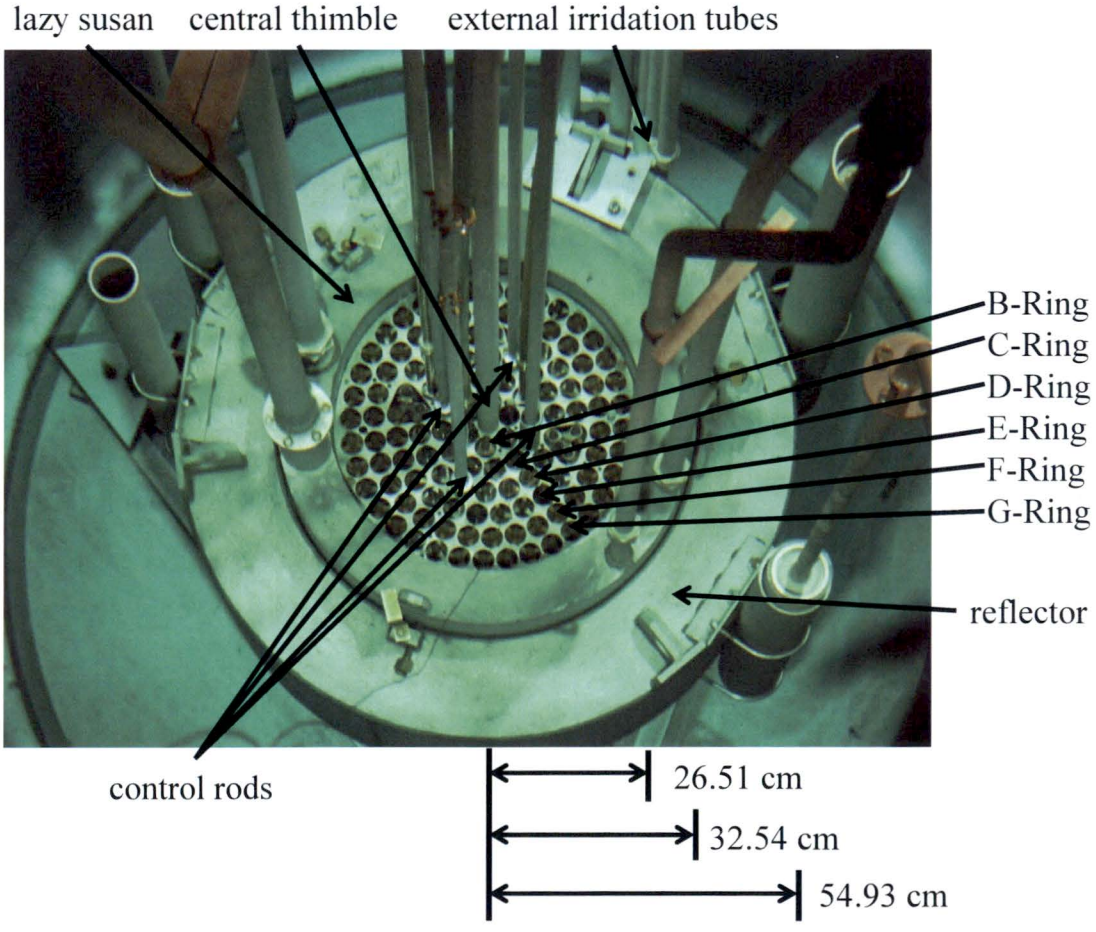

Figure 3.1. The GSTR core, highlighting the reflector, control rods, and fuel.

located in the C and D-Rings of the core (see Figure 3.1). A radial graphite reflector serves to limit radial neutron leakage (the fuel rods contain inserts to limit axial leakage, see Figures 3.2a and 3.2b). The reflector also houses a lazy susan irradiation facility in a groove fixed within the graphite reflector, as shown in Figure 3.1.

General Atomics developed several different TRIGA fuel rod configurations (Tomsio, 1986). Table 3.1 describes the three fuel rod types considered in the GSTR relicensing analysis: one of which is clad in aluminum (Figure 3.2a), and two of which are clad in stainless steel (Figure 3.2b). All three types contain a uranium-zirconium hydride fuel enriched to less than 20 wt.% U-235 (General Atomics, 2011). Both fuel rod types have a length of 72.06 cm (Tomsio, 1986). Early TRIGA fuel rods included disks of samarium to act as a burnable neutron absorber; however, General Atomics stopped manufacturing these elements after 1964 (Tomsio, 1986). The present analysis ignores the effects of the burnable absorber, as all of the fuel at the GSTR is old enough that the burnable absorber has been depleted.

The aluminum-clad fuel rods are the oldest TRIGA reactor fuel manufactured by General Atomics (Day, 2004). The fuel within an aluminum-clad rod contains 8 wt.% uranium, and is 35.56 cm tall and 3.759 cm in outer diameter (Figure 3.2a). The GSTR still uses several aluminum-clad fuel rods, which are limited to the F and G rings in response to concerns over the

Table 3.1. GSTR fuel types.

Fuel Type	Enrichment (wt.%)	Cladding Material	Uranium in Fuel Meat (wt.%)
8 % aluminum clad	< 20	aluminum	8
8.5% stainless steel clad	< 20	stainless steel	8.5
12 % stainless steel clad	< 20	stainless steel	12

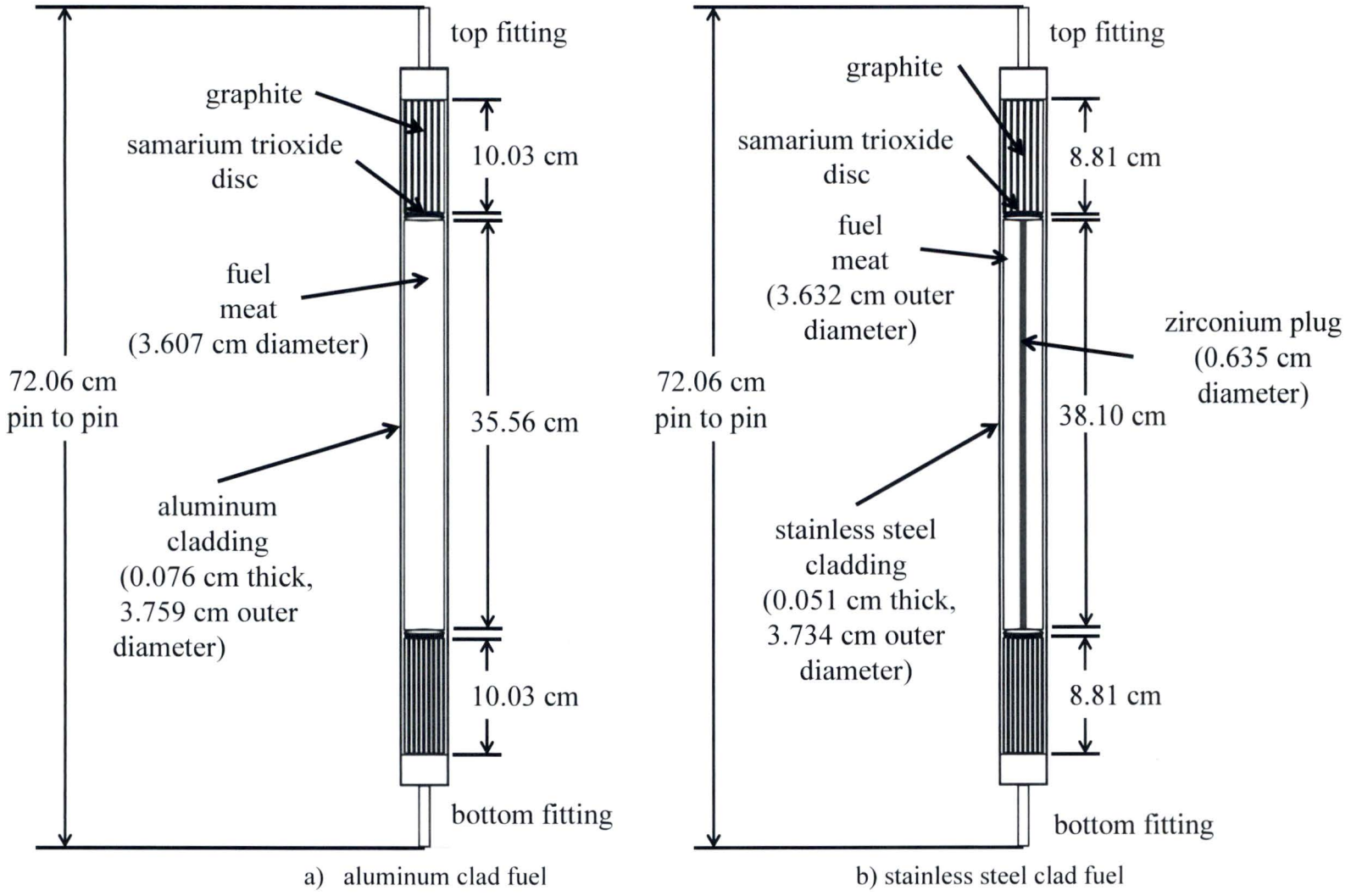

Figure 3.2. Schematics of the TRIGA fuel types used in the GSTR.

lower melting temperature of aluminum (Day, 2004).

The stainless-steel clad fuel rods within the GSTR are a mixture of 8.5 wt.% and 12 wt.% fuel. The fuel in all of the stainless steel clad fuel elements is 38.1 cm long and 3.73 cm in outer diameter (Figure 3.2b). A zirconium plug is located in the middle of the fuel meat, as a consequence of the techniques used in manufacturing the U/ZrH fuel (see Figure 3.2b) (Tomsio, 1986). The dimensions of TRIGA fuel pins are not consistent and vary from reactor to reactor and batch to batch. The dimensions in Figures 3.2a and 3.2b represent a best estimate and form the basis for all of the fuel modeling efforts in this analysis.

There are four control rods within the GSTR (Figure 3.1). Three are fuel-followed borated graphite control rods (Figure 3.3a), while the forth is a void-followed borated graphite pulse rod (Figure 3.3b). The rod drives above the reactor raise the rods during normal operation. All four rods incorporate an electro-magnetic SCRAM feature. During a SCRAM, the electro-magnet that binds the control rods to their drives deactivates, allowing gravity to pull the rods back into the core. As part of the GSTR technical specifications, the core must shutdown (become subcritical) with three of the four rods inserted in order to allow for the possibility of a rod becoming stuck. The GSTR's fuel followed control rods are referred to as the shim 1, shim 2, and regulating rods. These rods contain a fuel element of similar dimensions to the stainless steel clad fuel elements (Figures 3.3b and 3.3c) following the borated graphite, which reduces the impact of removing the control rod on the core flux profile. The final control rod, the transient rod, is void followed, and uses an electro-pneumatic rod drive instead of the mechanical system used by the other three control rods. This system can quickly eject the transient rod from the core to initiate a power pulse. Otherwise, the transient rod serves the same function as the

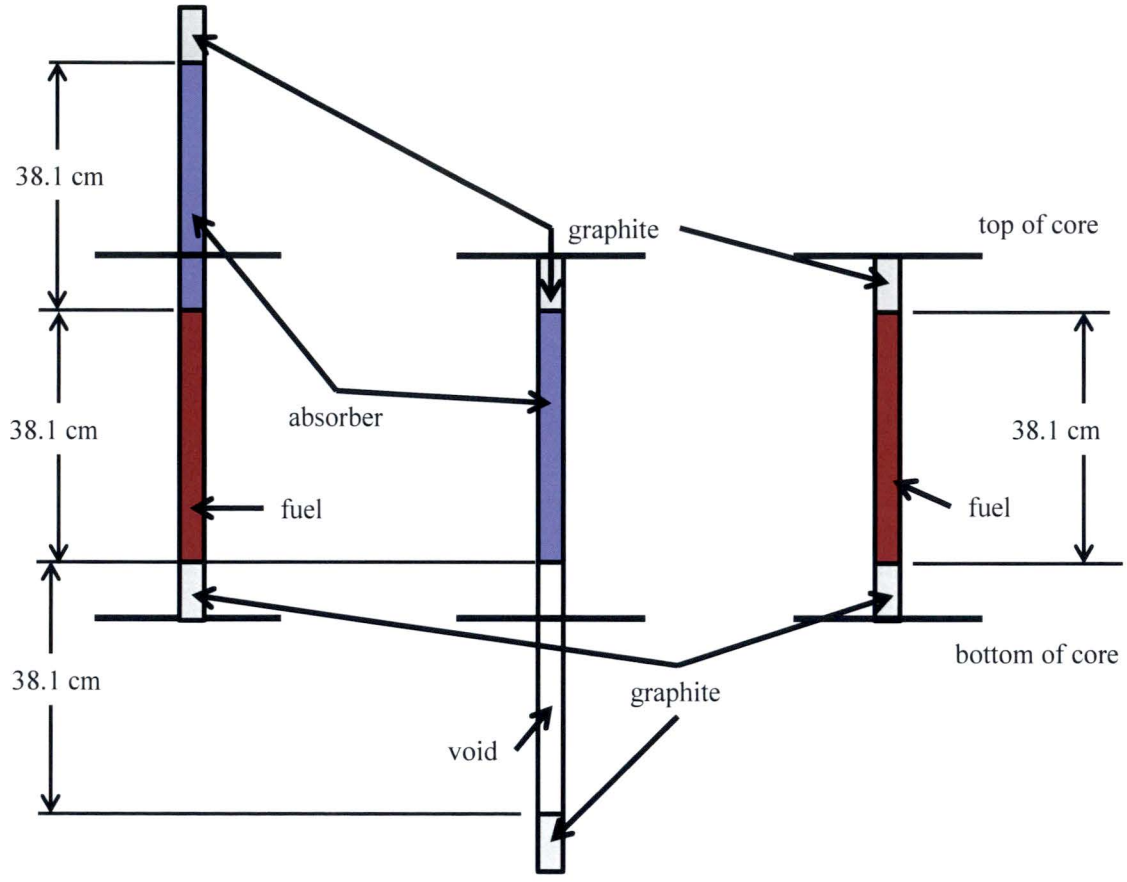

Figure 3.3. Diagram of the two control rod types used in the GSTR, showing how the fuel and void followers line up to a regular fuel element.

other three rods, except that the pneumatic drive is not as sensitive as the mechanical rod drives. The void follower reduces the total reactivity worth of the transient rod.

Three primary experimental facilities are available within the GSTR: the central thimble located, the lazy susan, and the external irradiation tubes (see Figure 3.1). Located in the middle of the core, the central thimble provides a high-flux irradiation location. Normally, the central thimble is water filled, but can be evacuated to provide a beam tube for radiography. The lazy susan sits outside of the core in an insert placed in the GSTR's graphite reflector (see Figure

3.1). A pneumatic system allows the forty sample locations within the lazy susan to be remotely loaded and unloaded and a mechanical drive rotates the lazy susan around the core. The GSTR currently uses the lazy susan (originally designed for isotope production) for sample irradiation. The two external irradiation tubes sit outside of the reflector. A reactor operator must manually insert samples into the tubes from outside of the reactor tank by lowering or raising the sample into the reactor by hand.

3.3. Description of the GSTR Core Model

Figures 3.4a and 3.4b provide radial and axial views of the reactor core model, respectively, and show all of the important aspects of the model's geometry. The model's geometric description is based on blueprints and other archival data from the GSTR. Within the model, the core consists of the fuel rods, the top and bottom grid plates, and the control rods, surrounded by a graphite reflector (Figures 3.4a and 3.4b). The lazy susan is outside of the fuel within a groove set into the reflector (Figure 3.4b). To save modeling and computation time, the lazy susan consists of a uniform mixture of aluminum and air, roughly equal to the homogenized composition of the actual lazy susan.

Material definitions within the model are based on archival records from the GSTR that indicate the type and composition of the different material regions in the GSTR. The stainless steel in the model is type 304L while the aluminum is alloy 6061. Within the model, the fuel and control rods have uniform compositions; the axial geometry of the control rods is defined in more detail to better replicate experimental data (see Section 3.4.).

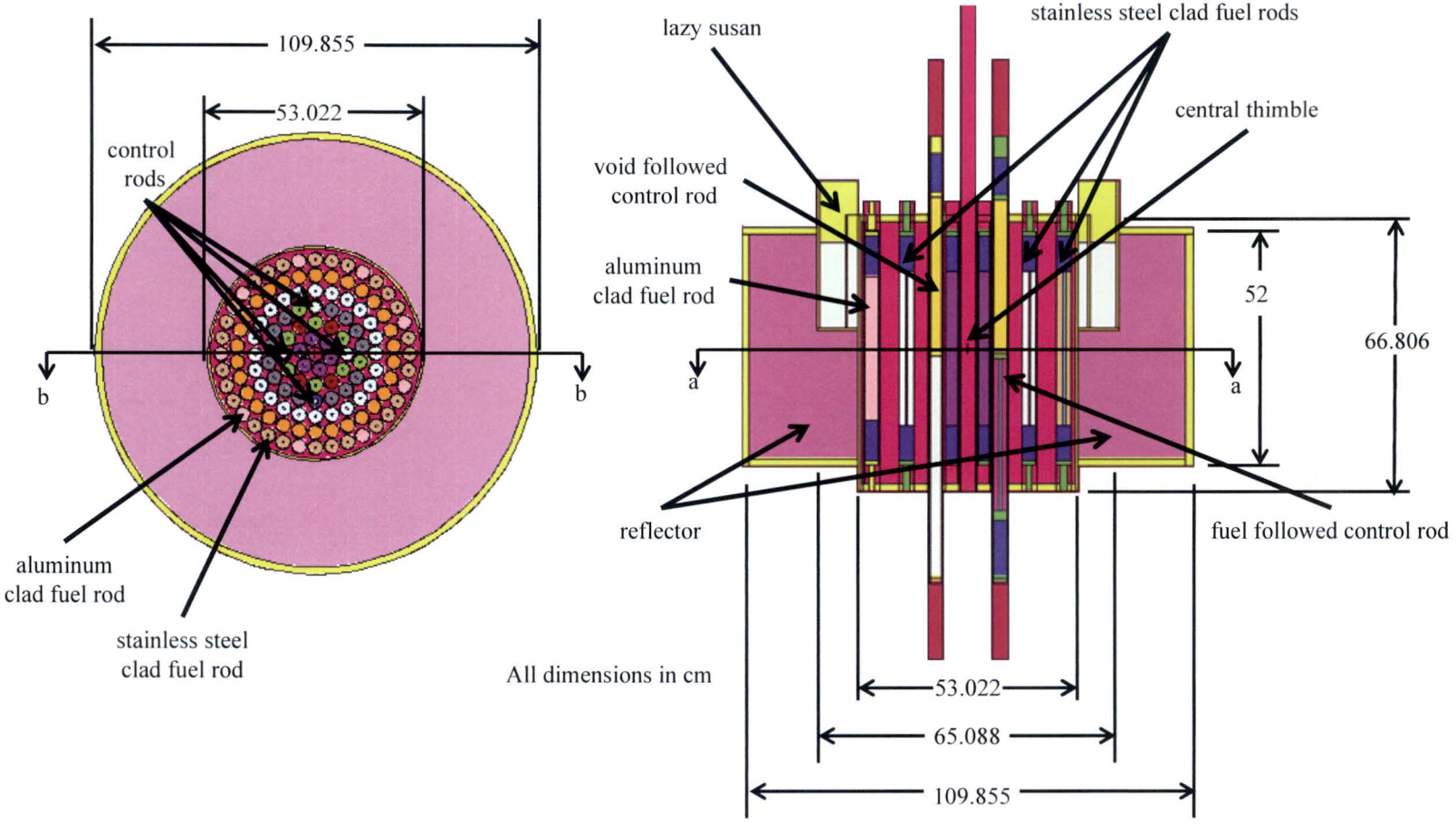

a) radial view a-a b) axial view b-b

Figure 3.4. Radial and axial views of the MCNP model of the GSTR core in the current operating configuration.

Figure 10 shows the current operating core layout of the GSTR. The layout contains 125 fuel elements (including the fuel followers in the control rods), with the control rods located in the C- and D-Rings of the reactor. Twelve stainless steel clad fuel elements of 12 wt.% uranium are in the C- and D-Rings of the core interspaced with 8.5 wt.% uranium stainless steel clad fuel elements. The F-Ring is comprised entirely of aluminum-clad fuel, while roughly half of the outermost G ring is aluminum-clad fuel. The remainder of the core is filled with 8.5 wt.% stainless steel clad fuel (see Figure 10).

The model runs with 1000 active cycles following 15 inactive cycles with 50,000 neutrons per cycle. This provides an average 1σ uncertainty of ~$0.01 based on a MCNP

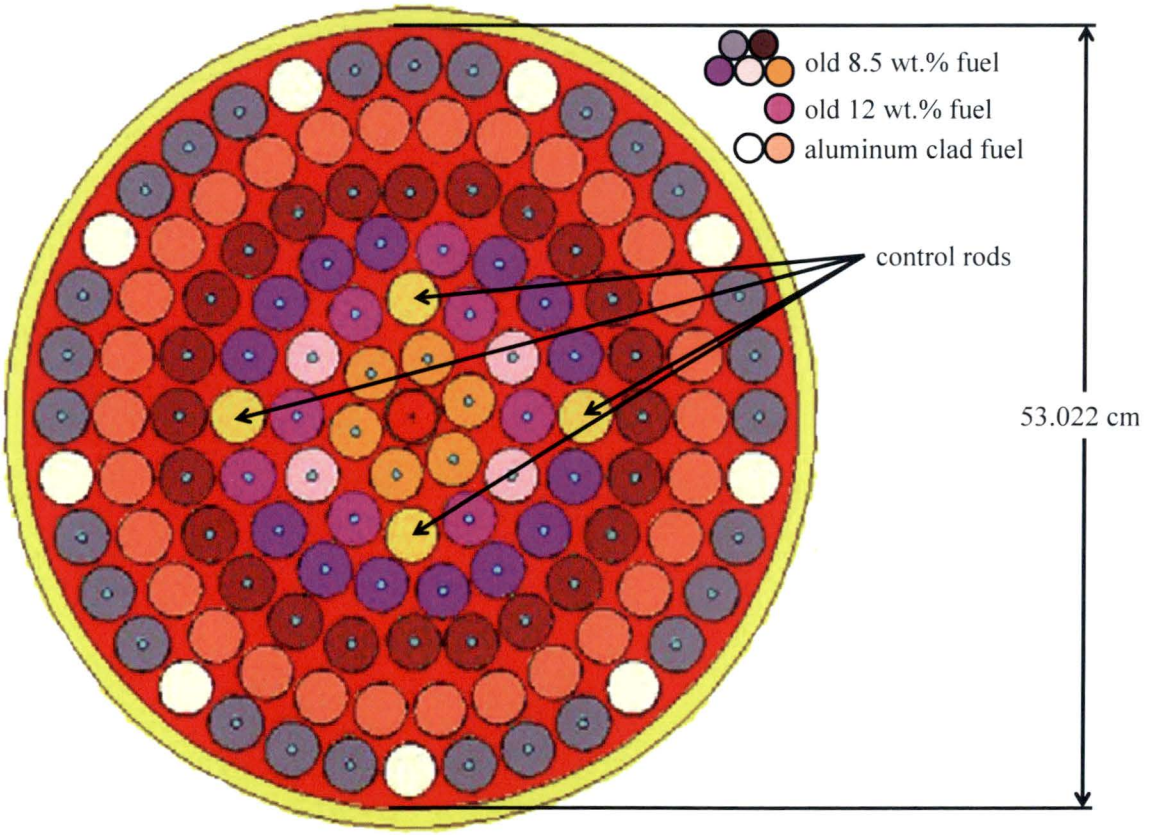

Figure 3.5. Fuel layout in the current GSTR operating core.

calculated β_{eff} of 0.00728. The reactor model utilizes the ENDF/B-VII.0 libraries. All uncertainties presented in this paper represent 3σ estimates. The makxsf utility, distributed with MCNP5, Doppler broadened the neutron library data and interpolated the S(α,β) temperature data where needed to construct the full power core (see Section 3.3.3.).

All reactivities in this chapter are given as:

$$\rho = \frac{k-1}{\beta_{eff}}. \tag{3.1}$$

The MCNP model calculates the effective delayed neutron fraction and neutron generation time using the adjoint-weighted point kinetics parameter calculation method available in release 1.60 of MCNP5 (Kiedrowski et al., 2012). The predicted effective delayed neutron fraction and neutron generation time for the model are $7.28\text{x}10^{-3}\pm9.0\text{x}10^{-5}$ and $4.28\text{x}10^{-5}\pm2.1\text{x}10^{-7}$, respectively.

3.3.1. Fuel Depletion Analysis

The GSTR staff uses an equation derived in-house and approved by the NRC to calculate the amount of uranium-235 consumed in grams as a function of the amount of energy produced by the core:

$$M_{U-235} = E \times 0.05158. \tag{3.2}$$

To evaluate the amount of unranium-235 consumed in each fuel rod, a per-rod power factor (*PF*) adjustment changes the equation to:

$$\mathrm{M_{U-235}} = \frac{\mathrm{E} \times 0.05158 \times \mathrm{PF}}{\mathrm{N}}. \tag{3.3}$$

An analytical approach estimated the effective burnup of each type of fuel in each ring within the GSTR core. While a complete inventory history exists for all of the new fuel acquired by the GSTR, a complete history is not available for the second-hand fuel added to the reactor over the reactor's lifetime. This uncertainty regarding fuel history makes it unlikely that a more detailed analysis using detailed burnup codes such as MCNPX or ORIGEN (Pelowitz, 2008; Beddingfield and Swinhoe, 2004) would yield better results than the simple analytical approach described in this sub-section.

Currently, the GSTR contains 125 fuel rods, including the fuel followers in three of the control-rods. The MCNP model of the GSTR calculated peaking factors for fuel rods in the core, averaged by fuel type and location. For instance, in the C-Ring, the fuel rods containing 12 wt.% uranium and 8.5 wt.% uranium fuel were considered separately. With the peaking factors calculated, Equation 3.3 calculates the uranium consumed in each fuel type while a separate methodology (described below) calculated the amount of fission products produced within the fuel.

Based on the revised material definitions, MCNP recalculated the peaking factors. If the newly calculated peaking factors differed from the previous ones, the burnup was recalculated with the new peaking factors, which in turn produced new fuel material definitions to calculate a new set of peaking factors. This process continued until the peaking factors converged, at which point the fuel composition was assumed to adequately represent the actual conditions within the core.

Figure 3.6 shows the composition of an 8.5 wt.% E-ring fuel before and following 25 at.% depletion of uranium-235 using the above method. The fission product yields from the

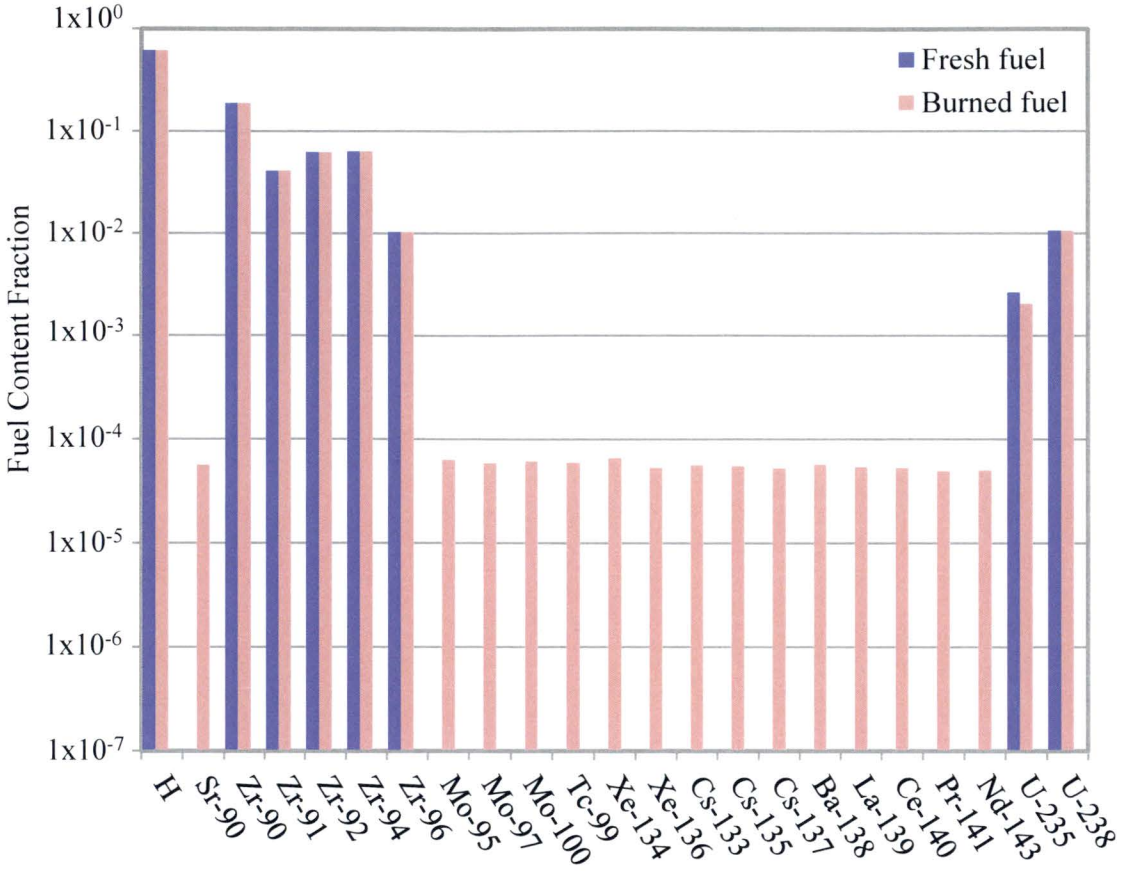

Figure 3.6. Composition of an 8.5 wt.% E-Ring fuel element before and after 25 atom % uranium 235 depletion.

depleted uranium-235 atoms are calculated using tables released by the Los Alamos National Laboratory (England and Rider, 1994). The analytic depletion methodology considers the ten most frequent light and eleven most frequent heavy fission products (plus samarium-149) of uranium-235 (see Table 3.2). Each uranium-235 atom was replaced by a single heavy and a single light fission product based on the yields in Table 3.2. Samarium-149 has a large neutron capture cross-section and exists at equilibrium concentrations in any thermal reactor (Lewis, 2008). To compensate, the burnup methodology alters the yield of the heavy fission products to compensate for the equilibrium concentration of samarium-149, shown in Equation 3.4:

Table 3.2. Isotopes considered in the depletion analysis.

Light Products		Heavy Products	
Isotope	Yield (%)	Isotope	Yield (%)
Mo-95	10.53	Xe-134	10.93
Zr-94	10.48	Ba-138	9.44
Zr-93	10.29	Cs-133	9.34
Zr-96	10.27	Cs-135	9.12
Mo-100	10.19	La-139	8.94
Tc-99	9.90	Xe-136	8.80
Zr-9	9.76	Ce-140	8.67
Mo-97	9.76	Cs-137	8.63
Zr-91	9.45	Nd-143	8.31
Sr-90	9.37	Pr-141	8.16
		Ce-142	8.16
		Sm-149	1.51

$$N_{Sm149} = \frac{E_{Sm-149} \times \sigma_{f-U235} \times N_{U235}}{\sigma_{abs}}. \quad (3.4)$$

The yields of the remaining non-saturating nuclides are renormalized such that the total yield of each group (heavy or light) is unity.

3.3.2. Description of the Limiting Core

A thorough analysis of the GSTR's limiting core configuration is key to the reactor's relicensing application. A limiting core represents the most compact critical assembly available to the operators, and usually consists entirely of fresh fuel. It is unlikely that the GSTR will be able to acquire a full core of fresh fuel in the future, and thus, the limiting core consists of a combination of fresh fuel and partially depleted fuel currently in the GSTR inventory.

The limiting core provides a safety envelope for the operating conditions of the reactor. The limiting core must safely operate under federal guidelines, and will provide both the

regulators and the operators an upper bound on the acceptable operating conditions for the core under the new license. The limiting core also provides a basis for several limits in the GSTR's technical specifications. These include the limits on the core's excess reactivity, shutdown reactivity, and transient rod worth, as well as a new limit on the minimum number of fuel elements in the reactor core.

Three guidelines informed the selection of the limiting core for the GSTR relicensing analysis: a large power peak towards the core center resulting from fresh 12 wt.% uranium stainless steel clad fuel surrounded by depleted 8.5 wt.% stainless steel clad uranium fuel, a core excess reactivity close to but not exceeding $7.00, and minimizing the number of fuel elements

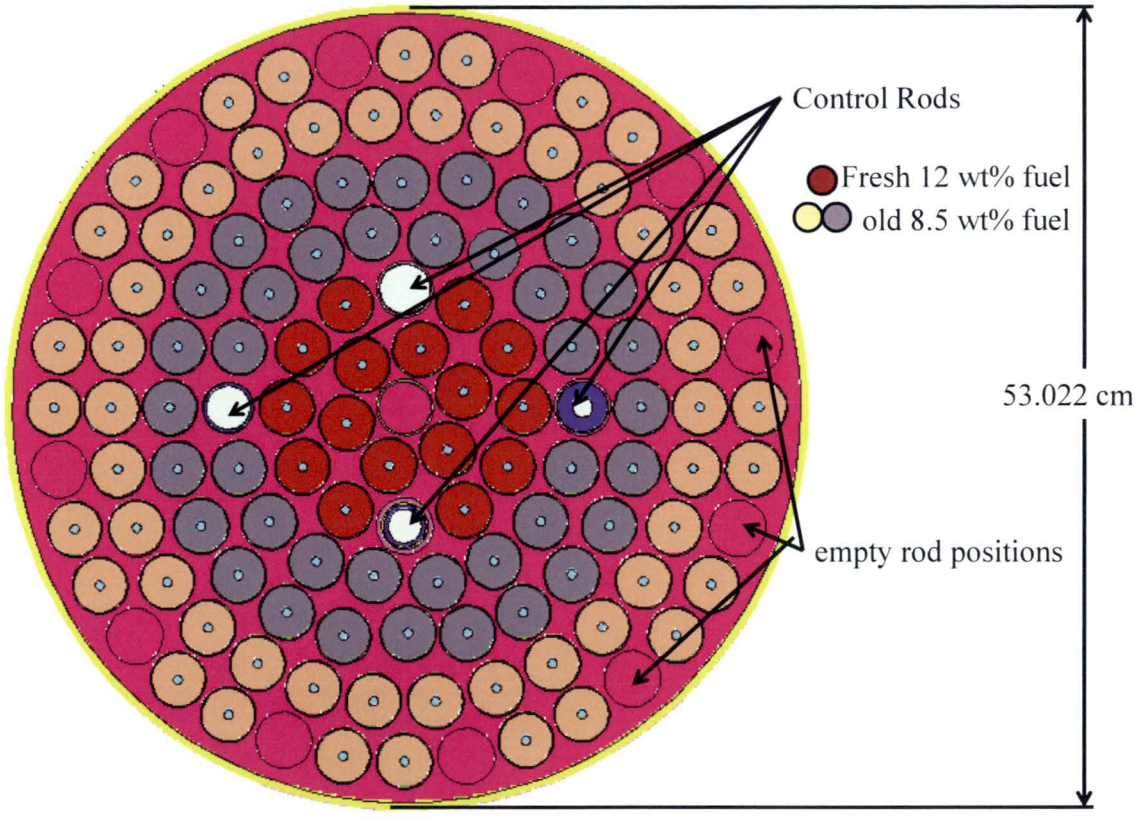

Figure 3.7. Radial view of the GSTR limiting core

able to meet the first set two conditions. Increasing the peaking in the center involves removing fissile material from the outside of the core, which lowers the overall reactivity of the reactor. Therefore, the limiting core results in a highly peaked hot-rod, which yields a higher risk of fuel damage to that element, as opposed to a less peaked, but more reactive core. To meet these criteria, an analysis of several cores containing from 80 to 110 elements found that a 110-element core reached a central peak power of 22.2 kW, with a maximum excess reactivity of \$6.48. Figure 3.7 illustrates this core, which serves as the basis for the re-licensing analysis for the GSTR.

3.3.3. Full-Power Model

While licensed to operate at 1 MW, the GSTR usually operates at a measured power closer to 915 kW in order to provide a margin of safety. For the relicensing analysis, the high power trip threshold of 1.1 MW provides a bounding case for the GSTR. While the core would never normally operate at this level, the high power trip would also not activate until the GSTR exceeded the 1.1 MW limit, making it theoretically possible for the GSTR to operate for a significant time period close to 1.1 MW before shutting down. Analyzing the thermal conditions of the core at this power level provides certainty that the GSTR has no credible safety concerns at the expected operating power levels. Thus, the operating full power core was modeled at 915 kW to match the normal operating conditions of the GSTR, while the limiting core was evaluated at a power of 1.1 MW.

Altering the material and cell definitions to represent the temperatures expected when the reactor is operating at full power allows MCNP to predict the neutronic parameters of the full-power limiting core. At full power, the fuel, the cladding, the water within the core, and the structural materials of the core are at an elevated temperature compared to operation at 5 W. A

combination of hand-calculations, measurements from the GSTR, and predictions from the RELAP5 mod 3.3 model of the hot-rod channel of the GSTR (Chapter 4) yielded an initial estimate of the operating conditions of the GSTR based on the reactor power. Iteration between the MCNP and RELAP models of the GSTR refined these initial estimates to provide an accurate estimate of the reactor's temperatures when the reactor is operating at full power.

The full power model divides the reactor's fuel by location and type. This limits the number of different materials in the core model and makes the best use of the limited information available for the GSTR. This simplification creates nine fuel areas within the operating core: one fuel definition for each ring with a single fuel type (8.5 wt.% uranium stainless steel clad fuel in the B- and E-Rings, and 8 wt.% uranium aluminum clad fuel in the F-Ring), two definitions for the C- and D-Rings, (to account for the 12 wt.% and 8.5 wt.% uranium stainless steel clad fuel in these rings), and two definitions for the G ring (for the stainless steel and aluminum clad fuel in this ring).

Averaging fission power tally results across each fuel group gives an average power factor for that fuel group. Multiplying this number by the reactor averaged rod power rod yields that group's average rod power. Comparing this to a RELAP calculation of the average fuel, cladding, and core water temperature as a function of rod power provides a refined estimate of the reactor's operating temperatures. Adjusting the MCNP model to account these new temperatures improves the temperature estimates. Three iterations were sufficient to reduce the changes in the core fuel temperatures to less than 1 K, well within the uncertainty bounds of both the RELAP and MCNP models, and within the accuracy of the measurement capabilities of the GSTR. All MCNP runs used the predicted rod critical positions for that temperature except when stated otherwise. Section 3.4.2. examines the control rod critical positions in detail.

Table 3.3 shows the final average rod powers, fuel average temperature, the predicted and channel coolant and cladding temperatures for each fuel type in the current full power GSTR core. The cladding and water temperatures are consistent to within 9 K over the range of rod powers. As a result, all of the cladding temperatures in the model are set to an average value of 395 K. Similarly, the temperature of the structural materials in the core (i.e. the reflector, grid plates, et. al.) is set to 394 K, while the core water is set to an average temperature of 315 K. The simplifications reduced the preprocessing and memory demands of the model while still providing acceptable results Table 3.4 lists the average water, cladding and structural material temperatures used in the final full power MCNP model of the current GSTR core.

Updating the model temperatures includes changes to the neutron library, TMP card, and S(α,β) data (if applicable). The density of the water in the core is also adjusted based on

Table 3.3. Average calculated rod powers and fuel, cladding, and channel water temperatures by type and ring for the current GSTR core at full power.

Fuel Ring	Wt % uranium	Clad material	Rod Power (kW)	$T_{fuel(avg)}$ (K)	T_{clad} (K)	$T_{coolant}$ (K)
B	8.5	Stainless Steel 304	10.8	530	397	317
C	8.5	Stainless Steel 304	10	521	396	317
C	12.0	Stainless Steel 304	13.2	561	399	319
D	8.5	Stainless Steel 304	8.9	507	395	316
D	12.0	Stainless Steel 304	12.1	547	398	318
E	8.5	Stainless Steel 304	7.5	489	394	315
F	8.0	Aluminum 6061	6.3	474	393	314
G	8.5	Stainless Steel 304	4.1	447	391	313
G	8.0	Aluminum 6061	4.9	456	392	314

temperature; however, the full power model does not alter the temperature of the water outside of the GSTR core, nor does it alter the density of any materials within the model aside from the core water.

Table 3.5 lists the changes made from the low-power to the high-power model. The control rods are modeled independently of the fuel groups, and the fuel follower of each rod is corrected to match the temperature of the 8.5 wt.% stainless steel clad fuel within that ring (excluding the transient rod, which is void- followed). This is conservative as approximately half of the fuel follower is outside of the core when the rod is in the critical position. The same procedure calculated the temperatures in the full power limiting core model, with the peak power

Table 3.4. Average suructual material, core water and cladding temperatures used in the model of the current GSTR core at full power

Component	Mean Temperature (K)
Structural Materials	396
Water	317
Steel Cladding	396
Aluminum Cladding	393

Table 3.5. Changes between the low power and full power MCNP models of the current GSTR configuration.

Value	Low Power Model (5W)	Full Power Model (915 kW)
Fuel Temperature	293.6 K	set according to Table 4
Fuel Cladding Temperature	293.6 K	set according to Table 5
Core Water Temperature	293.6 K	315 K
Bulk Tank Water Temperature	293.6 K	293.6 K
Control Rods	293.6 K	set to match 8.5 wt.% fuel of same ring
All Core Structural Materials	293.6 K	394 K

set to 1.1 MW. Tables 3.6 and 3.7 list the calculated temperatures and those used in the limiting core model. As expected these temperatures are higher than the temperatures predicted at 5W

3.4. Validation

The neutronic characterization of the GSTR requires that the MCNP model is validated against the current core operating conditions, demonstrating the model's ability to represent the current configuration of the GSTR. This validation involved three tests: a control-rod calibration based on experimentally derived control rod worth curves from the GSTR, a critical position and multiplication factor prediction comparison, and a flux characterization across the GSTR core.

3.4.1. Control Rod Calibration

The control rods in the GSTR include two rods installed when the reactor was initially constructed (transient rod and shim rod 2) and two rods installed in December of 1991 (the regulating rod and shim rod 1). Three of the rods (shim rod 1, shim rod 2 and the regulating rod)

Table 3.6. Average calculated rod powers and fuel, cladding, and channel water temperatures by type and ring for the limiting GSTR core at full power.

Fuel Ring	Wt % uranium	Clad material	Rod Power (kW)	$T_{fuel(avg)}$ (K)	T_{clad} (K)	$T_{coolant}$ (K)
B	12.0	Stainless Steel 304	21.8	668	406	325
C	12.0	Stainless Steel 304	20.1	647	405	324
D	8.5	Stainless Steel 304	12.0	546	398	319
E	8.5	Stainless Steel 304	9.8	518	396	317
F	8.5	Stainless Steel 304	6.6	478	394	315
G	8.5	Stainless Steel 304	4.7	454	392	314

Table 3.7. Average structural material, core water and cladding temperatures used in the limiting GSTR core model at full power.

Component	Mean Temperature (K)
Structural Materials	396
Water	317
Stainless Steel Cladding	396

have fuel followers to mitigate the effect they have on the core flux profile while the transient rod is void followed to limit the reactivity added during pulses (Nuclear Installation Safety Division, 2004b). The critical positions of each of the control rods change over time as a result of core configuration changes, fission product buildup, and temperature changes, making an estimation of each rod's effective burnup more complicated than the similar evaluation for the fuel rods.

Time constraints, as well as a lack of complete information on the control rod operating history, resulted in the use of a geometric approximation to determine the control rod worths for the GSTR model based on Oregon State University's TRIGA-relicensing effort (Reese, 2007). Experiments performed at the reactor determined the current control rod worths. Comparing the experimental control rod worths to the model predicted control rod worths for fresh control rods yielded an estimate of the amount of boron depletion in the control rods. Reducing the radius of the control rod region containing the borated graphite simulates this boron depletion. Pure graphite then simulates the depleted material, as seen in Figures 3.8a and 3.8b. However, a single axial segment (Figure 3.8b) did not accurately represent the effects of the axial neutron flux on the control rod depletion, yielding accurate results only when the rod was fully inserted or removed. Breaking the depletion zone into four axial segments better represents the intermediate withdrawal stages. The total volume of depleted graphite within each rod was redistributed between the four axial segments within that rod based on the peak-to-average neutron flux ratio calculated each region with the rod in the critical position (see Figure 3.8c). This provided the spatial resolution needed to accurately represent the boron depletion in the modeled GSTR control rods.

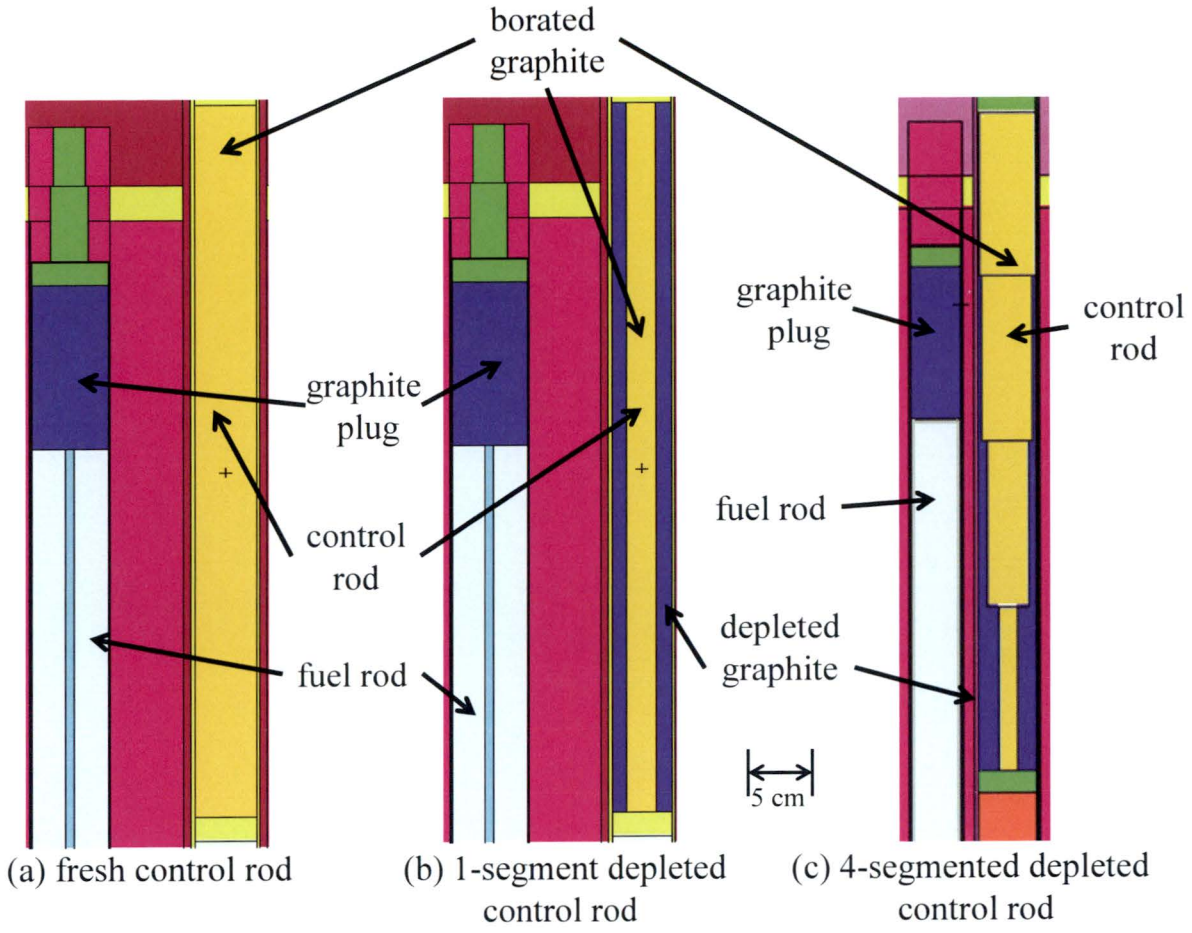

Figure 3.8. Example cross-sections of fresh and depleted GSTR control rods.

Figures 3.9-3.12 show the experimental integral rod worths a function of rod position for axial depletion zones. Dividing the control rods into four axial depletion zones, with the depletion weighted by the neutron flux in each of the axial segments, improved the rod worth calculations for rods with high boron depletion (the transient and shim 1 rods, Figures 3.10 and 3.11, respectively). This method did not significantly alter the rod worth predictions for the rods with little or no boron depletion (the regulating and shim 2 rods, Figures 3.9 and 3.12, respectively). Table 3.8 details the calculated and measured total worths of each control rod, as well as the

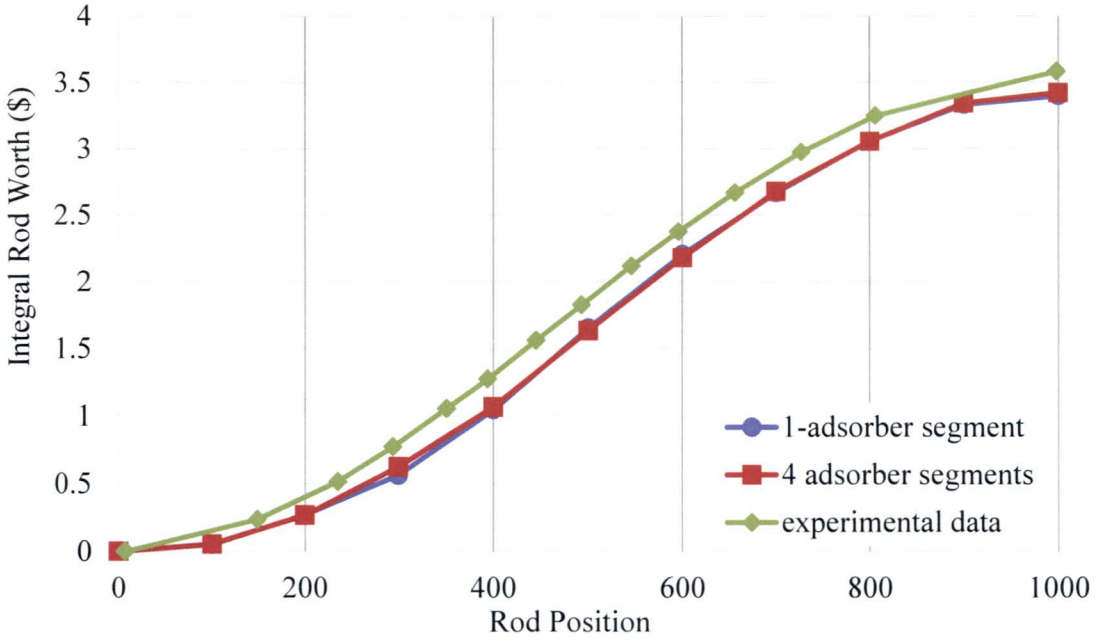

Figure 3.9. Measured and calculated reactivity worth curves for the regulating rod.

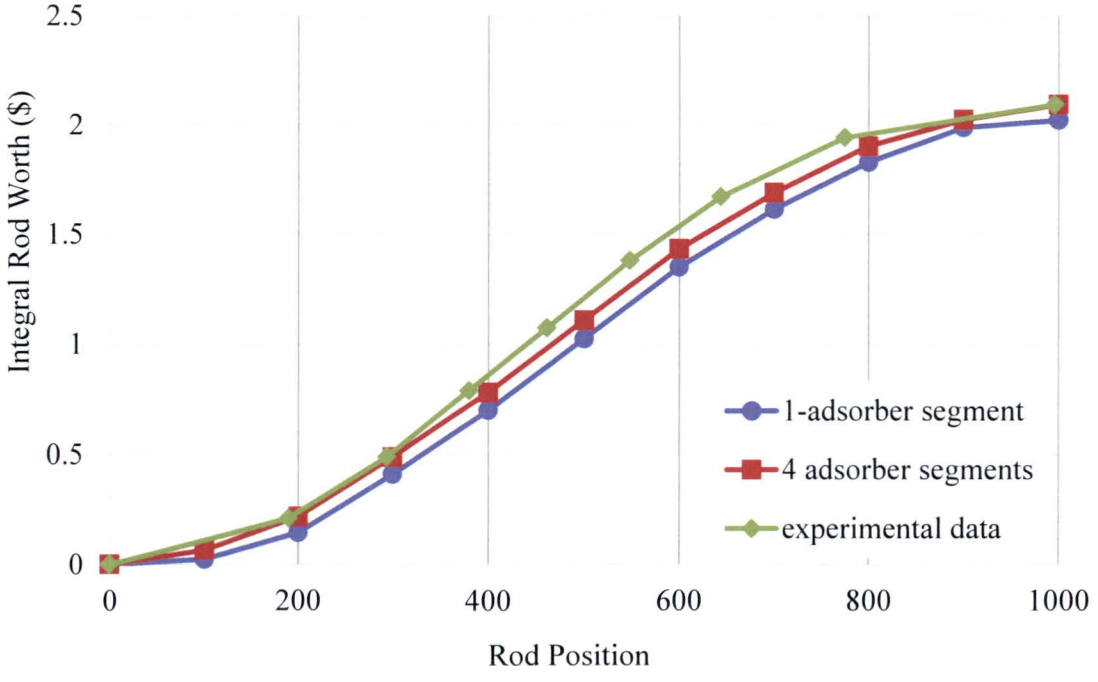

Figure 3.10. Measured and calculated reactivity worth curves for the transient rod.

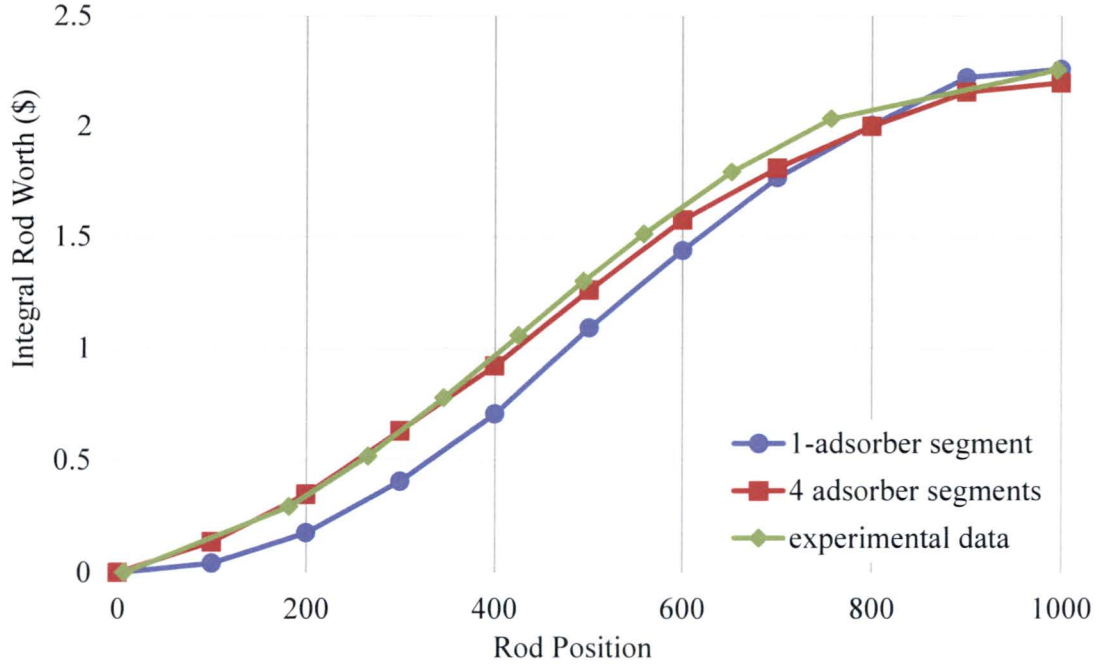

Figure 3.11. Measured and calculated reactivity worth curves for shim rod 1.

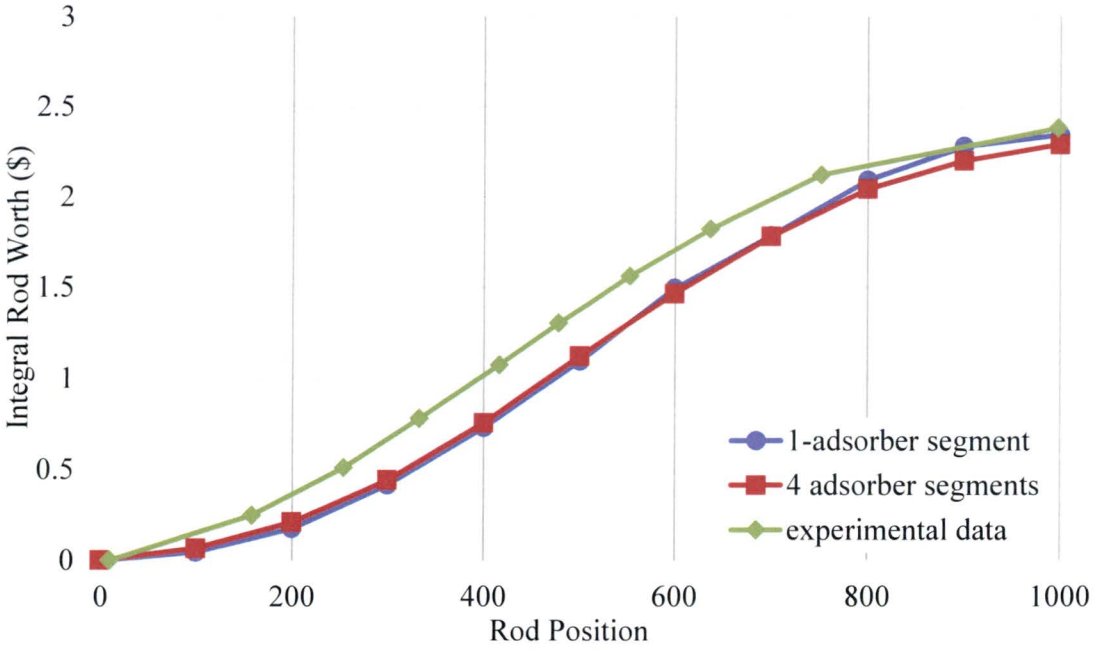

Figure 3.12. Measured and calculated reactivity worth curves for shim rod 2.

Table 3.8. Control rod calibration results.

Value	Regulating Rod	Transient Rod	Shim 1 Rod	Shim 2 Rod
Final Volume[1] (cm^3)	344.064	244.333	208.695	304.674
Calculated Control Rod Worth ($)	3.422	2.091	2.195	2.290
Measured Control Rod Worth ($)	3.582	2.091	2.253	2.382
Difference ($)	0.160	0.000	0.058	0.092

[1] Initial volume is 344.064 cm^3

current absorber volumes in each rod. The combined predicted rod worth for the core is \$0.30 less than the experimentally measured values.

In the case of the regulating rod, the rod worth predicted by MCNP is less than the experimentally determined worth data. In this case, reducing the fuel follower's estimated depletion added reactivity worth to the control rod. It is possible that the material used for the absorber is not consistent between the older and newer control rods. Unfortunately, the documentation available at the GSTR only lists the material as borated graphite, with no detail on the specific composition of each rod, providing no basis for further adjustment of the control rods. The 3σ model uncertainty is around \$0.03 for each rod with a similar level of uncertainty in the experimental data from the GSTR. This indicates that the modeled control rods adequately represent the physical control rods.

3.4.2 Critical Control Rod Position

The current model must be able to accurately predict the critical control rod positions for the current core. This validation examined multiplication factor predictions with the control rods at the measured critical rod heights for both the low power (5 W), and full power (915 kW) cores. Subsequent corrections to the initial model brought the multiplication factor estimates to unity.

Recent research indicates that the ENDF/B-VII.0 neutron cross-section libraries can result in significant biases in MCNP TRIGA reactor models (Snoj, Trkov, and Ravnik, 2007; Snoj, Zerovnik, and Trkov, 2011; Chadwick et al., 2011). Figure 3.13 presents multiplication factor predictions for the four cases presented in Table 3.9 that test the effect of different combinations of neutron cross-sections and S(α,β) data from the ENDF/B-VII.0 and ENDF/B-VI.6 data libraries. The results indicate that the S(α,β) and neutron cross section library choice has an equal effect on the calculated multiplication factor for the GSTR model, with the B-VI.6 libraries lowering the calculated multiplication factor by ~0.0035 for each set of data. While the

Table 3.9. Test cases considered in Figure 3.13.

Test Case	Cross Section Library	S(α,β) data	Multiplication Factor	σ
Case 1	B-VII.0	B/VII.0	1.00071	0.00023
Case 2	B-VI.6	B/VII.0	0.99752	0.00023
Case 3	B-VII.0	B/VI.6	0.99719	0.00023
Case 4	B-VI.6	B/VI.6	0.99446	0.00024

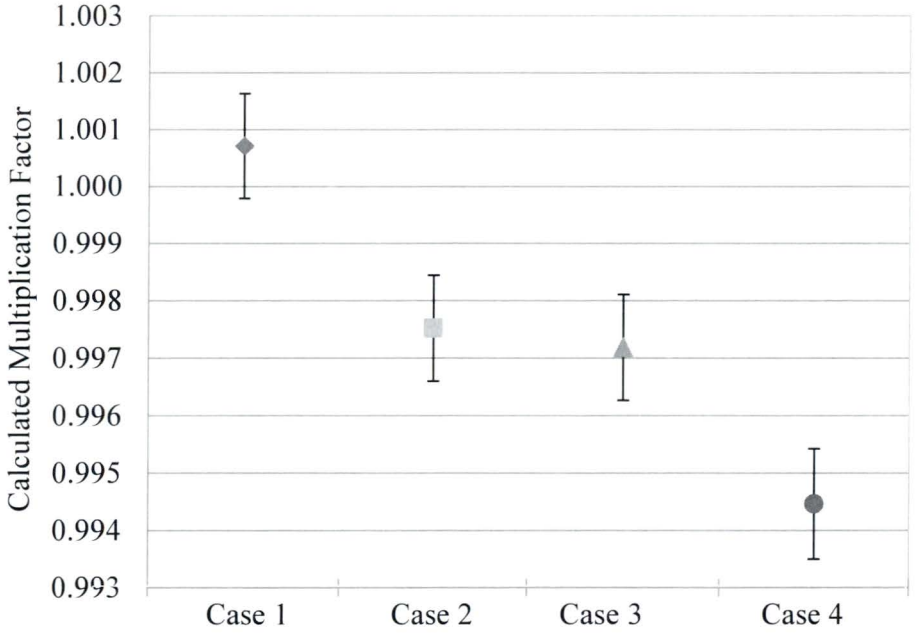

Figure 3.13. Multiplication factors calculated by the GSTR model using the combinations of neutron libraries listed in Table 3.9.

model appears more sensitive to the choice of the S(α,β) library version, the difference between Case 2 and Case 3 is well within the uncertainty of the MCNP calculations. In the GSTR model, the ENDF/B-VII.0 libraries (.70c and .10t) yield a higher predicted multiplication factor than the ENDF/B-VI.6 libraries (.66c and .66t). These findings agree with existing studies (Snoj, Trkov, and Ravnik, 2007; Snoj, Zerovnik, and Trkov, 2011; Chadwick et al., 2011).

While the ENDF/B-VII.0 libraries result in a positive bias to the multiplication factor predicted by the GSTR model, three reasons dictate that the final model includes the ENDF/B-VII.0 libraries. First, many of the fission products needed for the depletion analysis do not exist in the ENDF/B-VI.6 library, requiring the ENDF/B-VII.0 libraries for the burned fuel material definitions. A hybrid model introduces new complications that outweigh the possible benefits of using the ENDF/B-VI.6 libraries exclusively. Second, the ENDF/B-VII.0 libraries contain data at multiple temperatures that make the calculation of the temperature reactivity feedback coefficients easier and more accurate. Finally, since the ENDF/B-VII.0 libraries contain more recent data, and the bias they cause in TRIGA reactor models is documented, it is acceptable to use the most recent libraries while acknowledging the resulting biases.

Table 3.10 lists the measured control rod critical positions and the resulting multiplication factor predicted by the model with all of the control rods at the measured critical position. For the current core, the modeled control rods are withdrawn of 19.05 cm for the 5 W case, and 26.86 cm for the 915 kW (full power) case. The model accurately predicts the criticality of the 915 kW case to within the statistical uncertainty of MCNP and is within \$0.06 of the expected value for the 5 W case.

Table 3.10. Critical control rod position verification data.

Core Configuration (Operating Core)	Measured Critical Rod Height (cm, from bottom of core)	Multiplication Factor	Difference from Critical ($)	3 σ Uncertainty ($)
5 W	19.05	1.00040	0.055	0.041
915 kW	26.86	1.00012	0.016	0.041

For each case, the model slightly over-predicts the multiplication factor, giving a more conservative result. In the GSTR, the critical position actually changes from day to day, as the reactor's operating schedule varies. This allows fission products that act as absorbers (such as samarium and xenon) to build up in variable amounts within the reactor. These fission products alter the actual critical position from day to day, and the modeled fuel composition represents an average value for these fission products. This leads to the actual critical rod positions being slightly elevated from the modeled results; however, the total difference in rod position is less than 1 cm, which is acceptable for this analysis.

3.4.3. Flux Profile

Validation of the MCNP model requires that the model accurately predict the neutron flux profile within the GSTR. The GSTR does not have the facilities to take radial flux measurements, as the GSTR staff currently only measure flux in the central thimble and at the external irradiation facilities. The validation attempts to reproduce the central thimble flux data by comparing the point-to-average normalizations of GSTR experimental data with calculations from the MCNP model.

To predict the flux, the MCNP model employs a series of FMESH tallies using reaction rate multipliers (X-5 Monte Carlo Team, 2003b) to simulate the gold foil reactions measured by the GSTR staff. The actual gold foils used in the experiments are approximately point detectors within the reactor; however, as MCNP tallies represent an average flux over an area, and the

GSTR's measured flux is not highly variable, the FMESH tallies provide an acceptable approximation.

Aside from simple flux tallies, MCNP can also calculate reaction-rates (in units of reactions/barn-cm) for each tally, by using cross-section multipliers for selected materials. To change this to an approximation of activation rate, the number of atoms in a given foil is multiplied by the calculated reaction rate flux to predict the total activation rate for the geometry. MCNP tally data must be denormalized to be meaningfully compared to experimental data. For the present analysis, this denormalization constant corresponds to the source particle rate (*SPR*), which is based on the reactor power:

$$SPR = \frac{P \times \nu}{\delta \times 1.602 \times 10^{-13} J/MeV}. \tag{3.5}$$

This provides the neutron production rate corresponding to the specified reactor power. This constant allows MCNP tallies to be converted to fluxes or reaction rates which can be translated to a predicted activity. The calculations for activity are as follows:

$$\dot{R} = F \times \left(1 \times 10^{-24} \ {cm^2}/{b}\right) \times SPR \times \left(\frac{1}{A_{Au}} \times N_a\right), \tag{3.6}$$

$$A = \dot{R} \times \left(1 - e^{-\frac{ln\,2}{T_{1/2}} \times T}\right). \tag{3.7}$$

Figure 3.14 compares the foil activities calculated by the MCNP model to measurements taken at the GSTR using irradiation foils in January 2012. The values are in rough agreement near the axial center, but diverge below the axial center starting at -5 cm This is consistent with

the model having a more peaked flux profile compared to the actual core and may result from considering fuel depletion to be axially uniform.

Figure 3.15 presents the point to average flux profile from an MCNP FMESH analysis of the central thimble compared to flux measurements taken at the GSTR using irradiation foils in January 2012. The calculated flux in the central thimble from a track length (F4) flux tally over the examined area is 4.51×10^{13} n/cm^{2}s based on a source particle rate of 7.49×10^{16} n/s, while measurements of the thermal flux taken using gold foils at the same location in the core give a flux of 2.01×10^{13} n/cm^{2}s. The higher MCNP result is expected, as MCNP predicts the total neutron flux, while the gold foil activation primarily measures the thermal flux. Since the central-thimble of the reactor produces no neutrons, and is a water-filled cylinder, it is expected that the majority of the flux in this region is thermal. As shown in Figure 3.15, the flux profile

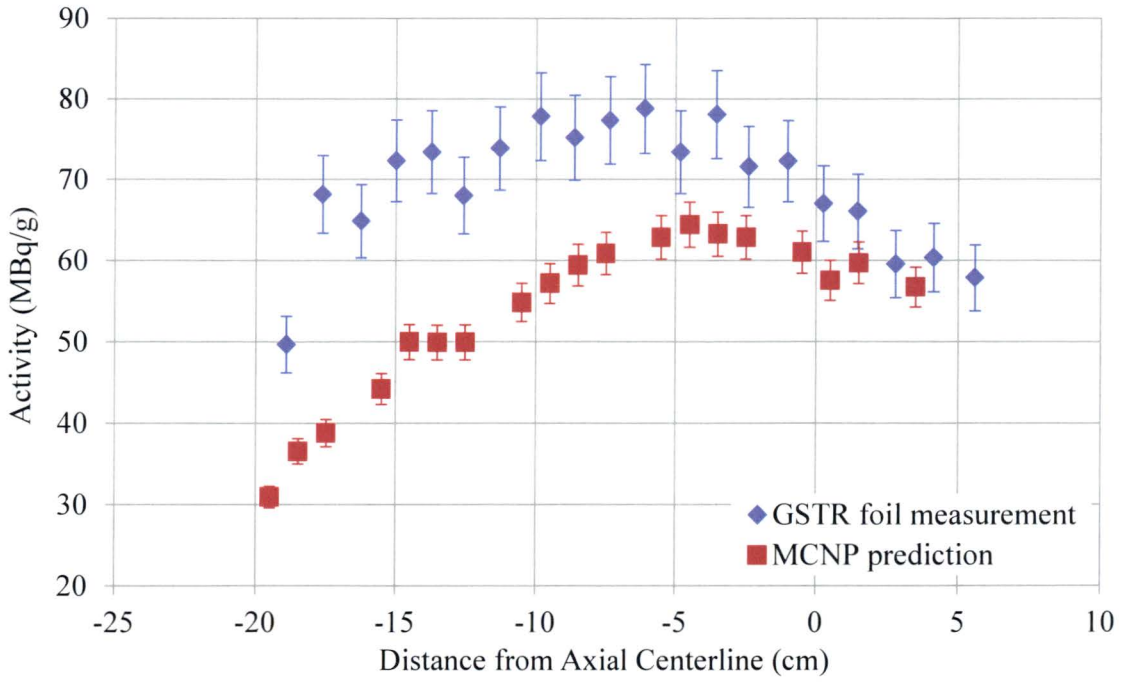

Figure 3.14. Gold foil activity following a one-hour activation as predicted by MCNP and measured by the GSTR staff.

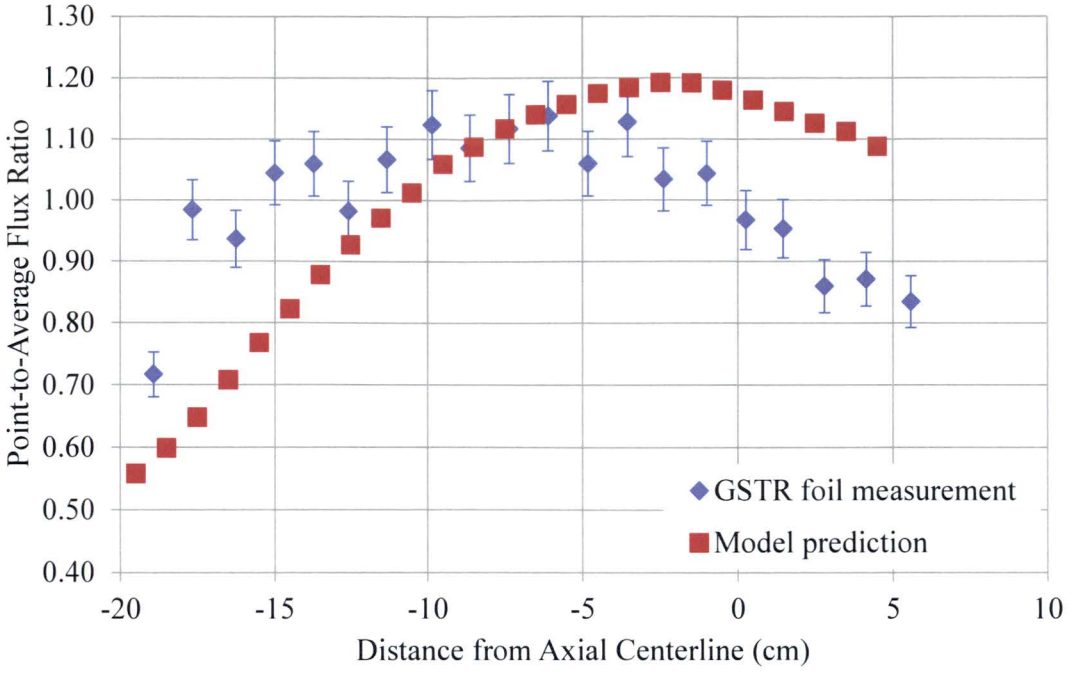

Figure 3.15. Point-to-average flux ratios in the GSTR central thimble.

evaluated by the model peaks ~5 cm higher in the central thimble than the profile measured in the actual core. The predicted flux profile is also less flat than the experimentally determined flux profile. Some of the differences in shape may be due to the lack of axial fidelity in the modeled fuel and the averaging of fuel depletion over the entire element.

3.5. Relicensing Analysis

The validated model analyzed the limiting core to produce the values needed for the updated GSTR Safety Analysis Report (SAR). This analysis included determining the excess and shutdown reactivity margins, determining the critical control rod positions, and determining the fuel temperature, core water temperature, core void and power reactivity coefficients.

3.5.1. Limiting Core Excess and Shutdown Reactivity Margins

The core excess and shutdown margins (the reactivity when the control rods are fully withdrawn or inserted, respectively) are important for the limiting core calculations. The

Table 3.11. Excess and shutdown margins of the limiting core.

Limiting Core Configuration	Multiplication Factor	Difference from Critical ($)	3 σ Uncertainty ($)
1.1 MW Excess	1.01942	2.67	0.041
1.1 MW Shutdown	0.9289	-9.77	0.041
5W Excess	1.04714	6.48	0.041
5W Shutdown	0.95943	-5.57	0.041

limiting core model calculates both of these values during low power (5 W) and full power (1.1 MW) operation (see Table 3.11). These values indicate how much impact the power reactivity coefficient has on the core, and provide bounding limits for the updated GSTR safety analysis. The power reactivity coefficient is determined in Section 3.5.3.4.

As shown in Table 3.11, the full power limiting core has less excess reactivity and a greater shutdown margin than the low power limiting core as a consequence of the negative temperature reactivity feedback from the fuel. This makes the low power (5 W) case the limiting configuration from a criticality safety standpoint, as at low power the control rods provide less negative reactivity margin for the reactor.

3.5.2. Reactor Power Distribution

Calculating the power distribution within the model involves a series of fission power (F7) tallies that track the fission energy produced in each fuel element. The average of these values provides the average power value in the reactor. Dividing the individual tally value for a fuel element by the average power value provides the power factor for that element. In the GSTR limiting core, the power factors range from 0.46 to 2.29, with a power factor of approximately unity existing in the E-Ring fuel of the reactor (with values ranging from 0.93 to 1.06). Multiplying a rod's power factor by the arithmetic average rod power (reactor power

divided by the number of fuel elements, 9.73 kW per rod in the limiting GSTR core) gives an approximate value for the power produced in that rod.

Figure 3.16 shows the calculated power profile for the full power limiting core, operating at the maximum allowed power of 1.1 MW. The GSTR limiting core, as designed, is highly peaked with the G-Ring fuel elements each producing between 4.6 and 4.9 kW, while the peak element in the B-Ring (located slightly to the right and below the central thimble in Figure 3.16) produces over four times that power (22.2 kW) at a peak to average power factor of 2.29. The core is largely symmetrical, with a bias around the peak rod located in the B-Ring. This bias likely results from the control rods, as the transient rod without a fuel follower has a greater impact on the core power profile than the fuel-followed control rods. Since the fuel elements within each ring are identical, the control elements are largely responsible for the polar changes in the power profile.

3.5.3. Reactivity Calculations

The current analysis examines the limiting core at both low (5 W) and full (1.1 MW) power to calculate the fuel temperature, moderator temperature, and void coefficients of reactivity for the GSTR limiting core. For the low power case, any materials not altered to account for the coefficient being calculated are set to 293.6 K. For the full power case, the component temperatures within the reactor have been increased to represent the higher power output, as described in Section 3.3.3. The reactivity calculations are complicated by the

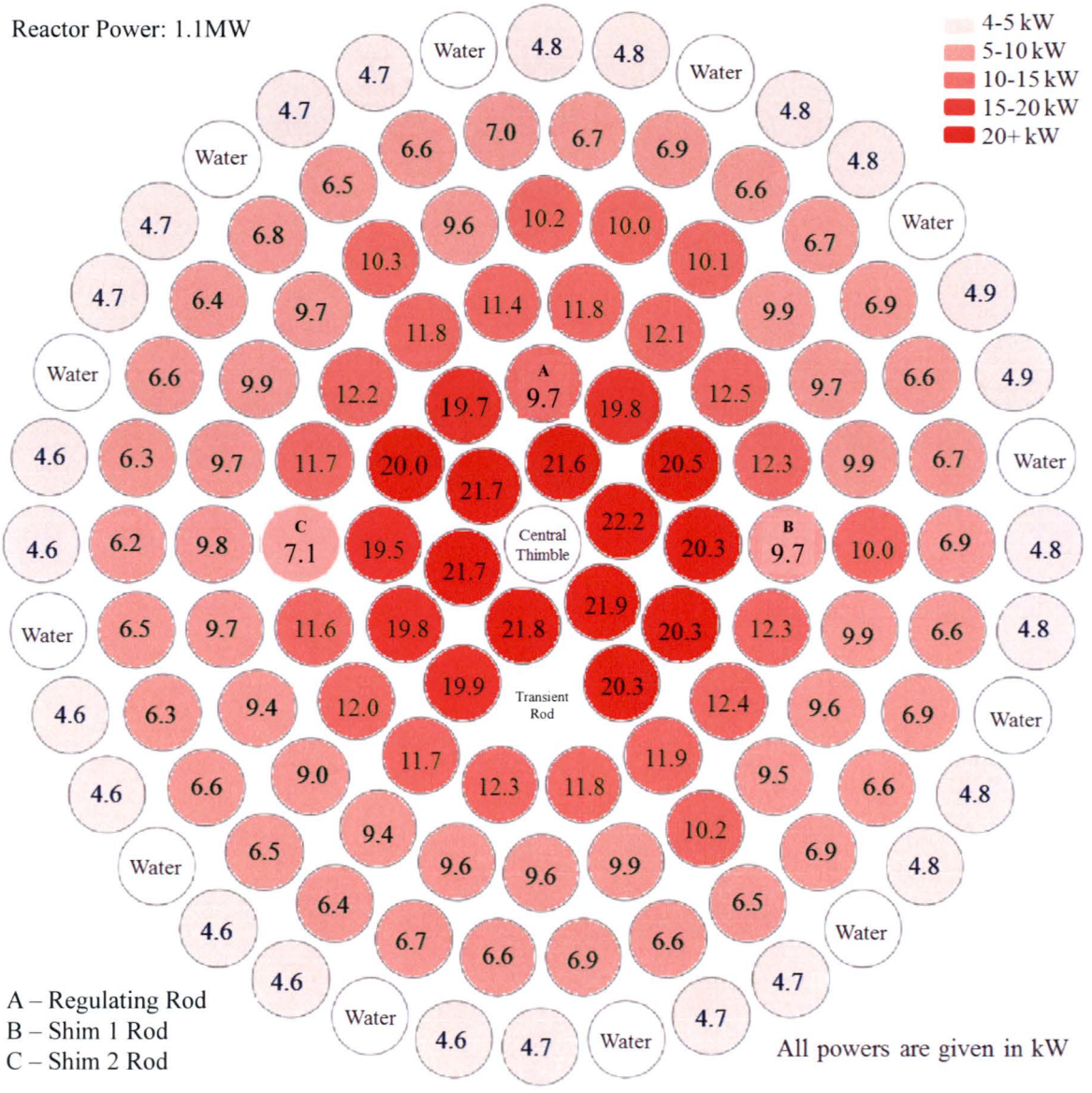

Figure 3.16. Power profile for the GSTR limiting core operating at 1.1 MW.

positions of the control rods. In order to provide consistent results, the control rods are fully withdrawn in all of the reactivity coefficient calculations.

In each case, MCNP predicted an effective multiplication factor as a function of the changing parameter, providing the basis for each reactivity coefficient. Table 3.12 details the changes made to the model to account for each reactivity effect. The slope of each line in a plot of the multiplication factor as a function of a dependent variable in the simulation (temperature or void fraction) give an average reactivity coefficient for that variable in terms of $/K or $/% void.

To provide more detail, the linear derivative between each pair of data points were calculated and plotted individually. This provides a piecewise expression for the reactivity coefficient between each of the calculated data points. Since previous work indicates these coefficients are not constant over the ranges examined, this method provides a more accurate picture of the reactor's behavior (General Atomics, 1967).

3.5.3.1. Fuel Temperature Reactivity Coefficient

Temperature dependent reactivity coefficients can be calculated by varying the necessary parameters in the model across a range of operating temperatures. For the fuel, this comes in

Table 3.12. Input parameters for the reactivity coefficient analysis.

Reactivity Coefficient	Temperature Range (K)	Fuel Temperature	Core Water Temperature	Fuel Density	Core Water Density	Other Component Temperature
fuel temperature	293.6-1200	corrected to temperature	unchanged	unchanged	unchanged	unchanged
core water temperature	293.6-380	unchanged	corrected to temperature	unchanged	corrected to temperature	unchanged
void	unchanged	unchanged	unchanged	unchanged	altered to represent voids	unchanged

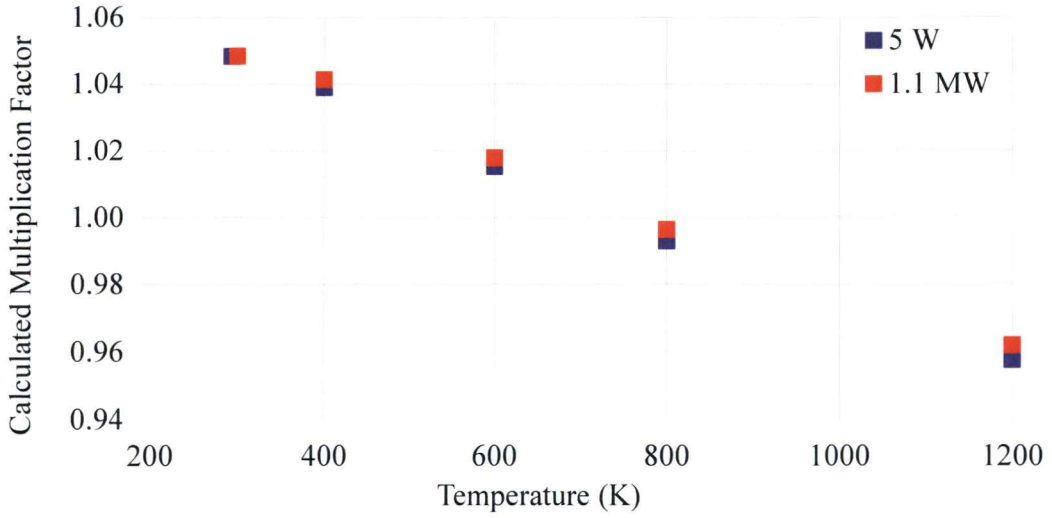

Figure 3.17. Calculated multiplication factor for the GSTR limiting core as a function of fuel temperature.

three parts related to each fuel rod: the specified cross-section data, the specified S(α,β) data, and the specified TMP card value. The makxsf utility included in MCNP5 is capable of Doppler broadening the neutron cross-section libraries to a requested temperature, as well as linearly interpolating the S(α,β) data between available temperatures (Brown, 2006).

Adjusting the cross-section, S(α,β), and TMP card data alters the model to represent the new temperatures. A series of five MCNP runs examined the effect fuel temperatures of 293.6, 400, 600, 800 and 1200 K had on the multiplication factor. This data then determined the fuel temperature reactivity coefficients. Figure 3.17 shows multiplication factors calculated by MCNP, which display the strong negative feedback expected from TRIGA fuel.

Figure 3.18 displays the fuel temperature reactivity coefficient calculated at 347 K, 500 K, 700 K, and 1000 K. These values agree with results published by General Atomics (General Atomics, 1967), with the most negative reactivity coefficient at around 500 K and a general decrease in the magnitude of the reactivity coefficient as the temperature increases above 500 K.

Table 3.13. Integral fuel reactivity as a function of temperature

Temperature (K)	Reactivity at 5W ($)	Reactivity at 1.1 MW($)
293.6	0	0
400	-1.30	-0.98
600	-4.56	-4.21
800	-7.61	-7.16
1200	-12.47	-11.88

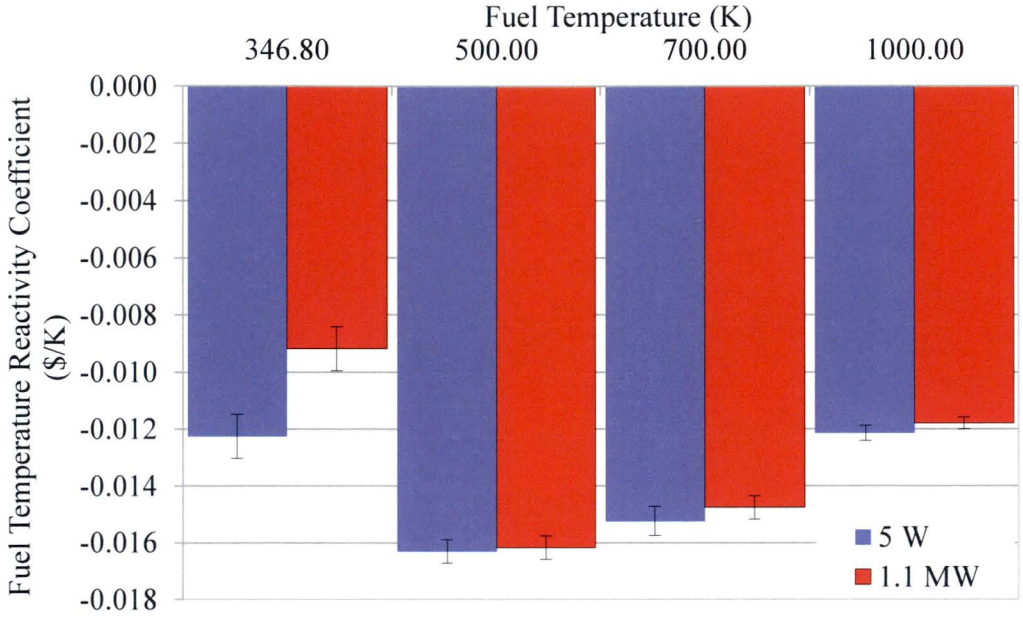

Figure 3.18. Calculated fuel temperature reactivity coefficient for the GSTR limiting core as a function of fuel temperature.

Averaging the fuel temperature reactivity coefficient over the entire temperature range for the limiting core yields a value of -0.0137 $/K for the 5 W case and -0.0135 $/K for the 1.1 MW case.

Table 3.13 lists the integral fuel temperature reactivity (from 293.6 K) as calculated by the MCNP model. While the coefficients are nearly identical, the higher initial coefficient for the 5 W case introduces a difference between the two increasing to $0.59 at 1200 K

3.5.3.2. Core Water Reactivity Coefficient

Calculating the core water temperature reactivity coefficient involves altering the density and temperature of the water within the core of the reactor (where it serves as a neutron moderator and the primary reactor coolant). As density is coupled with temperature, both variables require adjustment over the range of operating temperatures. The makxsf program (Brown, 2006) can alter the cross-section data to represent temperature changes in the water within the core, while density is an input value in the MCNP model, determined through easily available steam tables (American Society of Mechanical Engineers, 2009). The remaining parameters in Table 3.12 remain constant. The MCNP model predicts reactivity at each moderator temperature. Plotting this data and then calculating the derivative yields the moderator temperature reactivity coefficient. Figure 3.19 displays the MCNP calculated

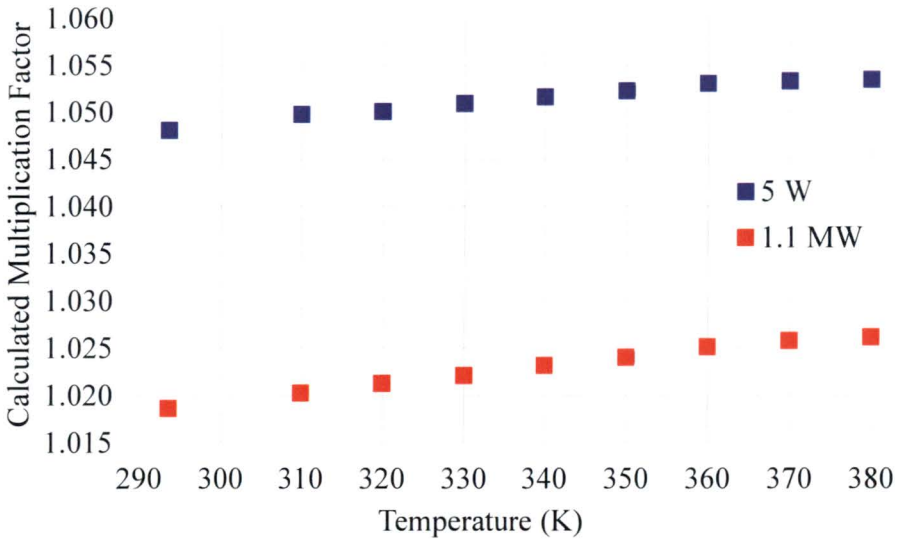

Figure 3.19. Calculated multiplication factor for the GSTR limiting core as a function of core water temperature.

multiplication factor as a function of core water temperature, showing a slight increase with core water temperature.

Figure 3.20 presents the calculated core water temperature reactivity coefficient for the limiting core as a function of temperature. Since the zirconium hydride within the fuel provides the majority of the feedback in a TRIGA reactor, the water is significantly less important. The core water temperature reactivity analysis indicates that the GSTR has a slightly positive core water temperature reactivity coefficient. Previous research has documented this effect, but it has not been extensively studied (Zagar, Ravnik, and Trkov, 2002; Safety Analysis Working Group, 2009). Considering the uncertainty inherent in the MCNP model, there is no significant change in the core water coefficient over the observed temperature range. The average coefficient for the 5 W case is +0.008 $/K while the coefficient for the 1.1 MW case is +0.012 $/K.

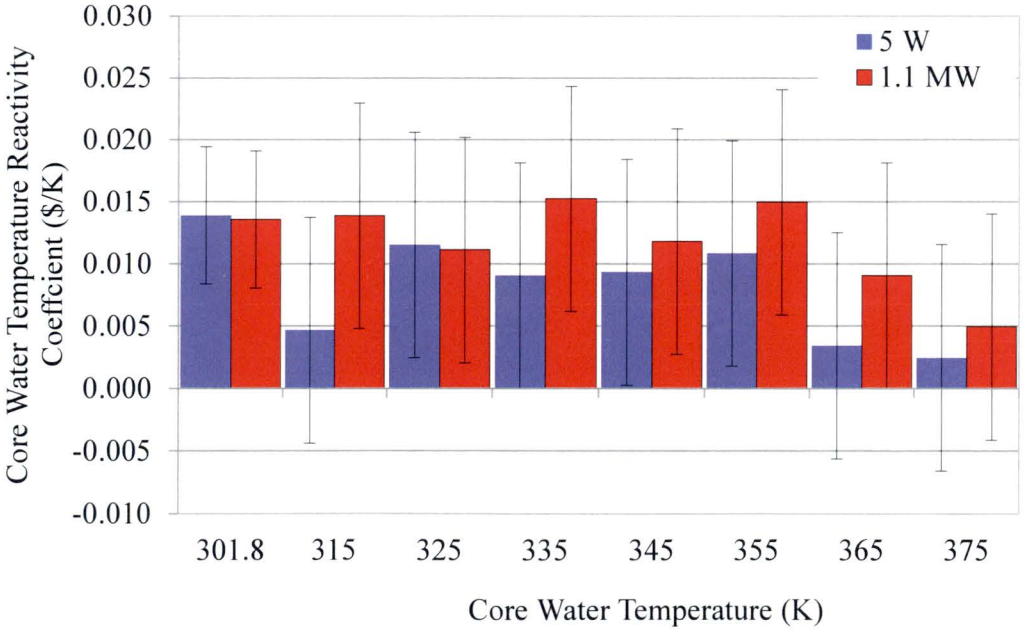

Figure 3.20. Calculated core water temperature reactivity coefficient for the GSTR limiting core as a function of core water temperature.

To further examine this effect, Figure 3.21 displays the multiplication factor versus the core water temperature for the 5 W case in Figure 3.19 as a function the of variables altered in the MCNP model. The cross sections, TMP cards and density changes all result in a slightly negative temperature feedback, which is overridden by the positive S(α,β) feedback (see Figure 3.21). This makes the S(α,β) data is the primary contributor to the increase in core reactivity as a function of core water temperature

3.5.3.3. Void Reactivity Coefficient

The reactor void reactivity coefficient represents the effect that voids within the reactor core will have on the total reactivity of the reactor. The analysis simulates voids by artificially decreasing the density of the water at a constant temperature to represent steam bubbles forming

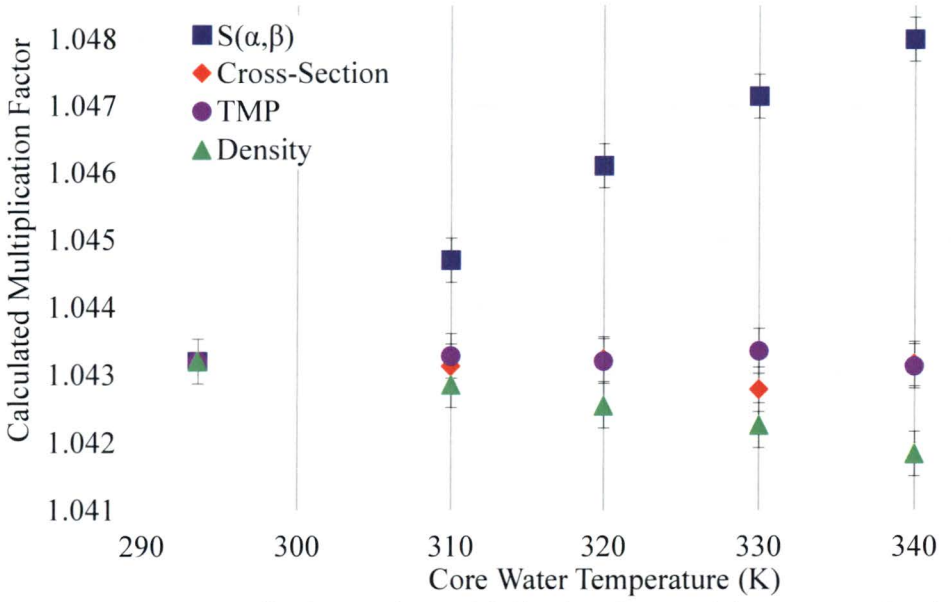

Figure 3.21. Factors contributing to the multiplication factor of the 5W case in Figure 18 as a function of core water temperature.

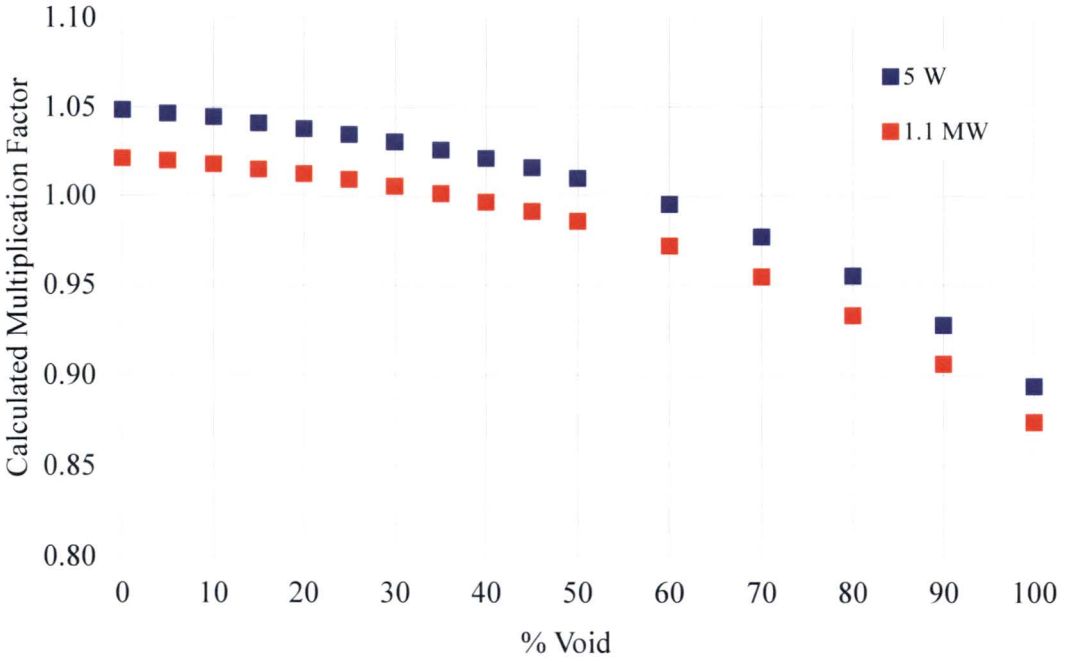

Figure 3.22. Calculated multiplication factor for the GSTR limiting core as a function of core void fraction.

within the coolant. Figure 3.22 displays the calculated multiplication factor as a function of core void fraction, showing the expected decrease in reactivity with a decrease in moderator density.

Figure 3.23 shows the calculated core void reactivity coefficient as a function of the coolant void fraction in the core. As expected, the void reactivity coefficient is highly negative. While a linear fit appears valid over the range of 0-20% void fraction (Figure 3.23), there is a clearly exponential trend above 20%. Assuming a linear trend between 0 and 20% void fraction, the average void reactivity coefficient is -0.075 $/% void for the 5 W case and -0.069 $/% void for the 1.1 MW case within this range.

Table 3.14 shows the integral void reactivity as a function of core void fraction for both the 5 W and 1.1 MW cases. Similar to the fuel temperature reactivity, the 5W case yields a

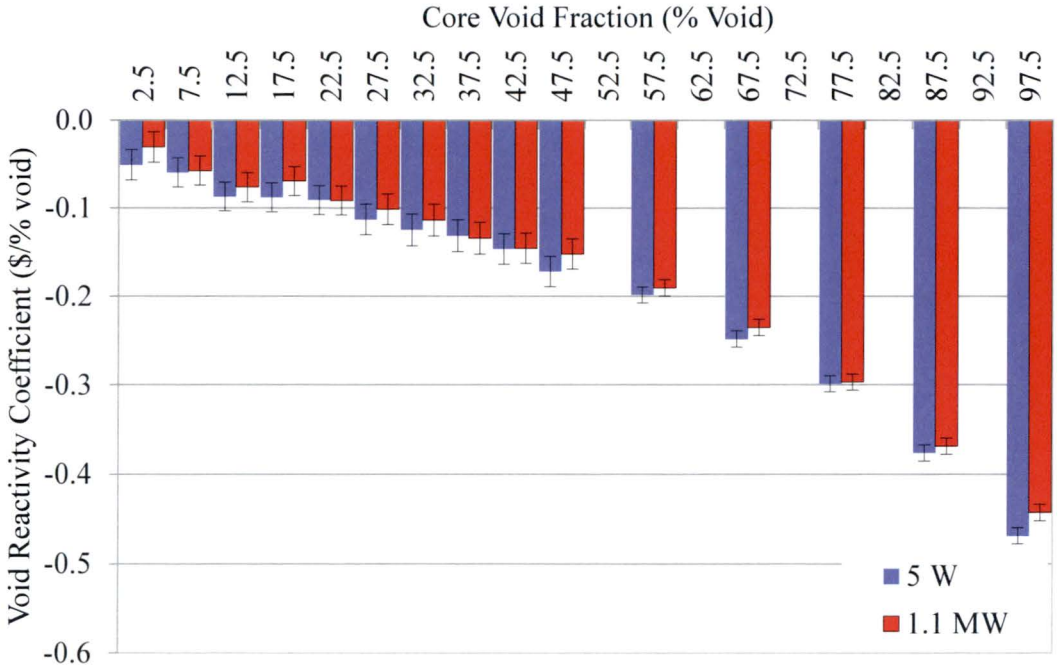

Figure 3.23. Calculated core void reactivity coefficient for the GSTR limiting core as a function of core void fraction.

Table 3.14. Integral void reactivity as a function of core void fraction.

Void Fraction (% Void)	Reactivity at 5 W ($)	Reactivity at 1.1 MW ($)
0	0.00	0.00
5	-0.26	-0.15
10	-0.55	-0.44
15	-1.00	-0.82
20	-1.43	-1.17
25	-1.88	-1.63
30	-2.44	-2.13
35	-3.07	-2.70
40	-3.73	-3.37
45	-4.46	-4.10
50	-5.32	-4.86
60	-7.31	-6.77
70	-9.79	-9.12
80	-12.78	-12.09
90	-16.54	-15.78
100	-21.23	-20.21

greater void reactivity over the examined range (increasing to a difference of $1.02 for a fully voided core); however, the core would be completely shut down well before this point.

3.5.3.4. Power Reactivity Coefficient

The reactor power coefficient considers the effect that power has on the total reactivity of the reactor. Since power effects reactivity through the temperature, and core void effects, the power reactivity coefficient looks at the combination of all of the factors affected by the reactor power. The limiting core model considered the reactor at 5 W and 1.1 MW, so these two points provide the power reactivity coefficient based on the difference in the multiplication factor at these two temperatures. The calculated power coefficient for the GSTR limiting core, taking into account the effects of fuel temperature, core water temperature and density, and core voiding (which is 0% in normal operation) is -0.0037± 0.0007 $/kW.

3.6. Summary and Conclusions

The neutronic analysis of the GSTR core validated the current MCNP model of the GSTR, and then examined the GSTR limiting core to determine the excess, shutdown, and core reactivity coefficients of fuel temperature, core water temperature, void and power. The MCNP model was validated through comparisons of the control rods to experimental rod worth curves, matching the critical rod position to the GSTR measured position, and comparing the MCNP generated flux profile to an experimental flux profile from the central thimble. The total control rod worth is within $0.31 of the experimental results, while the core reactivity calculation with the rods in the critical position is within $0.06 of the expected value of $0.00. The axial flux profile calculated by the MCNP model in the central thimble is less flat than the experimentally measured profile. This may be a consequence of approximating the burnup and fuel depletion as axially uniform.

The limiting core configuration has a maximum excess reactivity of $6.48 and a minimum shutdown margin of $5.57. The limiting core has a highly peaked power distribution with a peak-to-average power ratio of 2.29. The temperature reactivity coefficients calculated for the GSTR limiting core agree with previous analyses from other TRIGA re-licensing efforts, and with General Atomics's original analyses. The model predicts a strongly negative fuel temperature reactivity coefficient (-0.0135 $/K) for the full power limiting core, as well as a slightly positive core water temperature reactivity coefficient (+0.012 $/K) for the full power limiting core. The calculated core void reactivity coefficient is strongly negative (-0.069 $/%void for 0-20% void) for the full power limiting core. These factors combine to provide a core power coefficient of -0.0037 $/kW.

CHAPTER 4
THERMAL-HYDRAULIC ANALYSIS

The thermal-hydraulic analysis involves three models; two designed using the RELAP5 mod 3.3 code, and one using the PARET-ANL v. 7.5 code. The introduction explains the construction of these models, and the analysis performed by them. The following section describes the GSTR as related to these models. Section 4.3 lists the important calculations from the neutronics analysis (Chapter 3), used in the thermal-hydraulic analysis. Section 4.4 describes each of the three models in detail, while section 4.5 explains the results of the model analysis, and the limiting core analysis performed on the GSTR using these models. The chapter ends with a brief summary.

4.1. Introduction

The United States Geological Survey TRIGA Reactor (GSTR) is a 1 MW reactor, located in Lakewood, Colorado. In support of the GSTR's relicensing efforts, this paper describes the development of thermal-hydraulic models for the reactor and the analysis of the GSTR's thermal-hydraulic operating conditions under both steady-state and transient (pulse) operating conditions.

The thermal-hydraulic analysis of the GSTR is based on the RELAP5 Mod 3.3 (Information Systems Laboratories Inc., 2010a) and PARET-ANL version 7.5 (Olson, 2012a) codes. The RELAP models build on previous work performed by Oregon State University (Marcum, 2008; Oregon State University Radiation Center, 2010), while the PARET model was developed independently to provide a comparison to the RELAP data. Both codes use a finite-

difference method to solve for the transient and steady state thermal-hydraulic conditions of the reactor. The implementations of the two models are as similar as possible.

The thermal-hydraulic analysis of the GSTR includes validating the models against the current GSTR operating core. Following this the model calculates the minimum departure from nucleate boiling ratio (DNBR) for a limiting core during normal operations, as well as the peak fuel and cladding temperature of the highest power rod in the limiting core during a number of different pulse insertion events ranging from $2.00 to $3.00 in reactivity insertion

4.2. Description of the Geological Survey TRIGA Reactor

The GSTR is a 1 MW TRIGA Mark I reactor constructed in 1969. As a relatively low power reactor, the GSTR utilizes natural convection to dissipate heat generated during operation into the larger pool. For operations above 1 kW, the GSTR uses a two-loop cooling system to remove heat from the pool. This system has little impact on the actual cooling of the reactor, beyond maintaining the temperature of the pool the reactor is housed in.

The reactor core is contained in a water-filled pool 2.13 meters wide and 7.62 meters deep. Figure 4.1 shows the reactor core of the GSTR. The reactor core is 26.51 cm in radius from the inside of the lazy susan and 66.81 cm tall with 126 fuel locations located around a central thimble (see Figure 4.1). These fuel locations are split into six concentric fuel rings labeled B through G. Four control rods are located in the C- and D-Rings of the core (see Figure 4.1). A radial graphite reflector serves to limit radial neutron leakage (the fuel rods contain inserts to limit axial leakage). The reflector also houses a lazy susan irradiation facility in a groove fixed within the graphite reflector, as shown in Figure 4.1. The circular grid is irregular, with rods located in the center of the reactor having a much smaller pitch than those in the outer

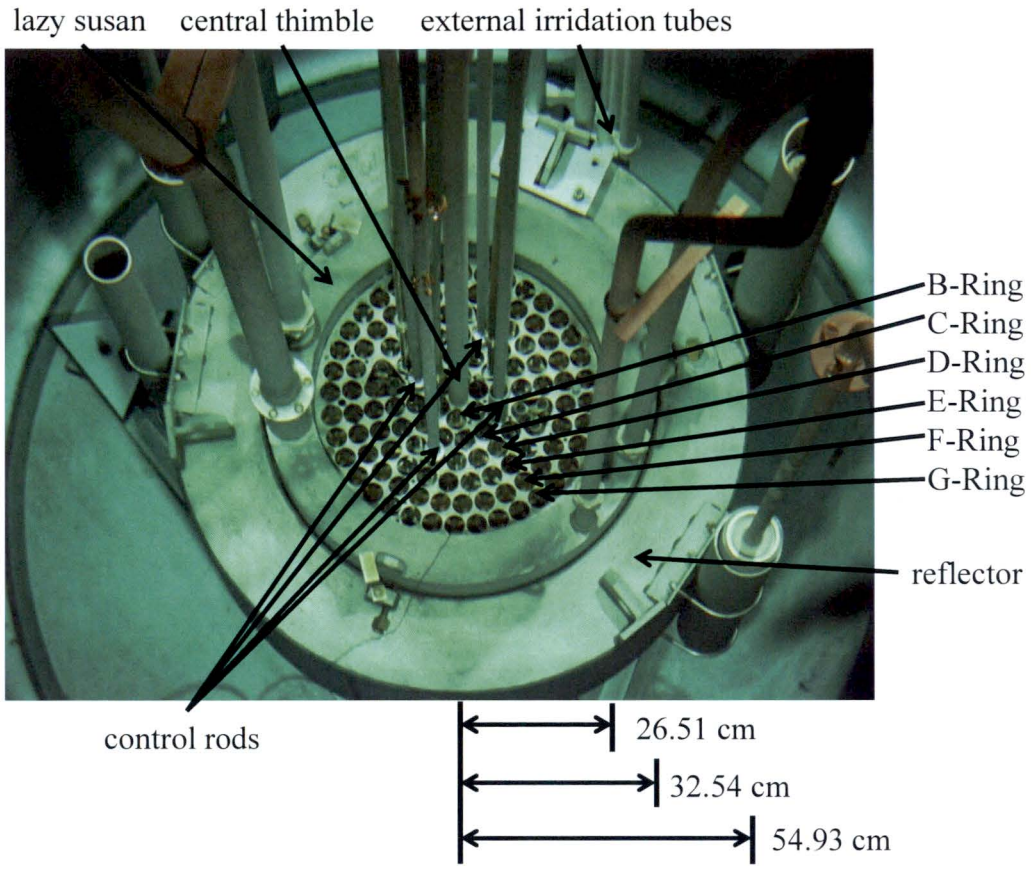

Figure 4.1. The GSTR core, highlighting the reflector, control rods, and fuel.

Table 4.1. GSTR fuel types used in the limiting core thermal-hydraulic analysis.

Fuel Type	Enrichment (%)	Cladding Material	Weight Percent Uranium in Fuel Meat (%)
8.5% stainless steel- clad	< 20	stainless steel	8.5
12 % stainless steel - clad	< 20	stainless steel	12

rings. This complicates heat removal, as the hottest rods in the center have less water flow than those located on the edges. Water enters the core from several holes located in the bottom and sides of the grid plates, and exits through locations in the top.

General Atomics developed several different TRIGA fuel rod configurations (Tomsio, 1986). Table 4.1 describes the two fuel rod types considered in the GSTR limiting core

relicensing analysis: both of which are clad in stainless steel (Figure 4.2). Both types contain a uranium-zirconium hydride fuel enriched to less than 20 wt.% uranium-235 (General Atomics, 2011). Both fuel rod types are 3.73 cm in outer cladding diameter, with a length of 72.06 cm (Tomsio, 1986). The GSTR operating core (Figure 4.3) also includes aluminum clad fuel elements in the outer rings, however, these are not present in the limiting core (Figure 4.4), and are not included in the Chapter 4 analysis.

The stainless-steel clad fuel rods within the GSTR are a mixture of 8.5 and 12 wt.% uranium fuel. The fuel in all of the stainless steel clad fuel elements is 38.1 cm long and 3.63 cm in outer diameter (Figure 4.2). A zirconium plug is located in the middle of the fuel meat (Figure 4.2) as a consequence of the techniques used in manufacturing the U/ZrH fuel (Tomsio, 1986). The dimensions of TRIGA fuel pins are not consistent and vary from reactor to reactor and batch to batch. The dimensions in Figure 4.2 represent a best estimate and form the basis for all of the modeling efforts in this analysis.

There are four control rods within the GSTR (Figure 4.1). Three are fuel-followed borated graphite control rods, while the forth is a void-followed pulse rod. The rod drives above the reactor raise the rods during normal operation. All four rods incorporate an electro-magnetic SCRAM feature. During a SCRAM, the electro-magnet that binds the control rods to their drives deactivates, allowing gravity to pull the rod back into the core. As part of the GSTR technical specifications, the core must shut-down (become subcritical) with three of the four rods inserted to allow for the possibility of a rod becoming stuck. The GSTR's fuel followed control rods are referred to as the shim 1, shim 2, and regulating rods. These rods contain a fuel element following the borated graphite, which reduces the impact of removing the control rod on the core flux profile. The final control rod, the transient rod, is void followed, and uses an electro-

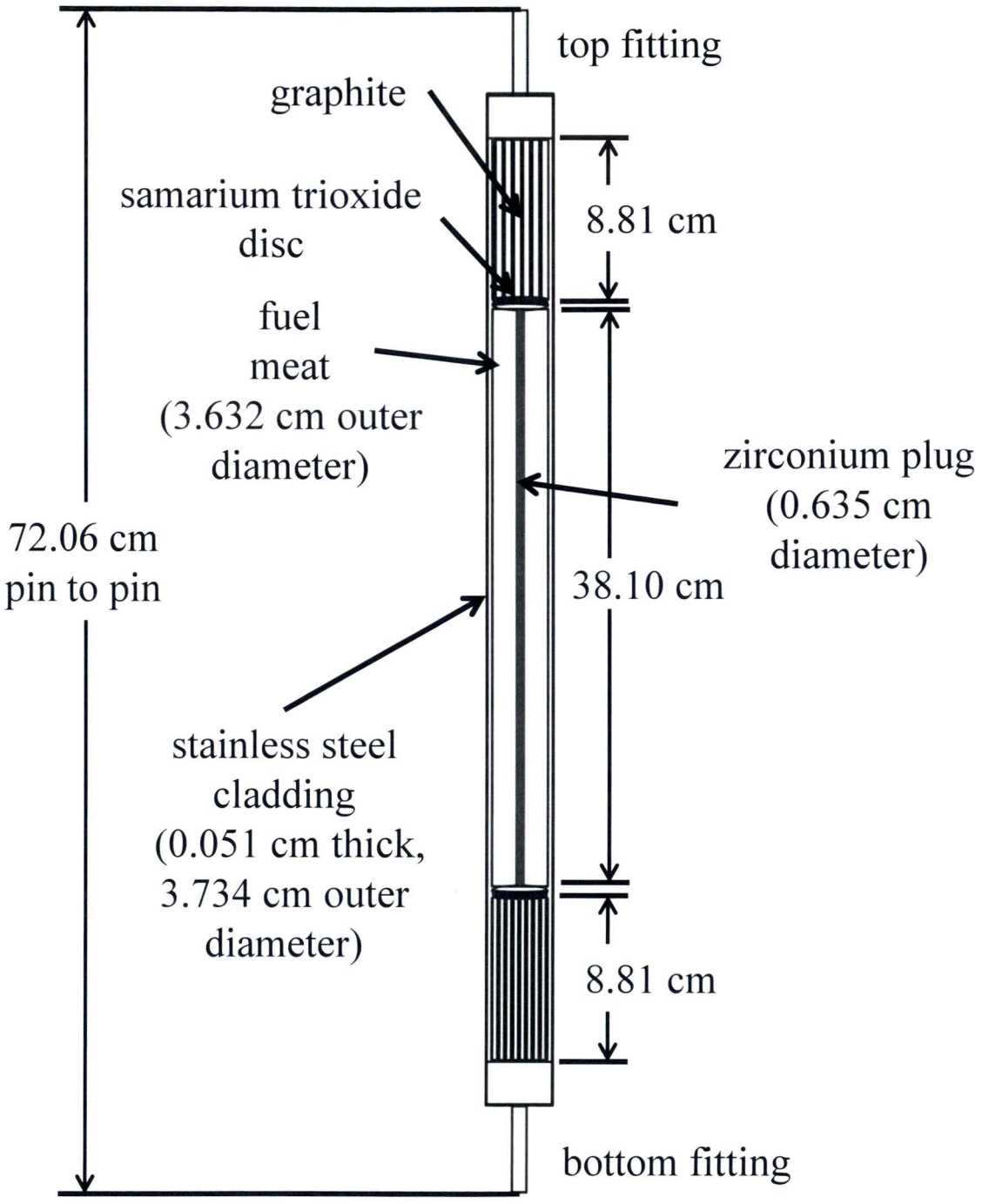

Figure 4.2. TRIGA stainless steel clad fuel rod.

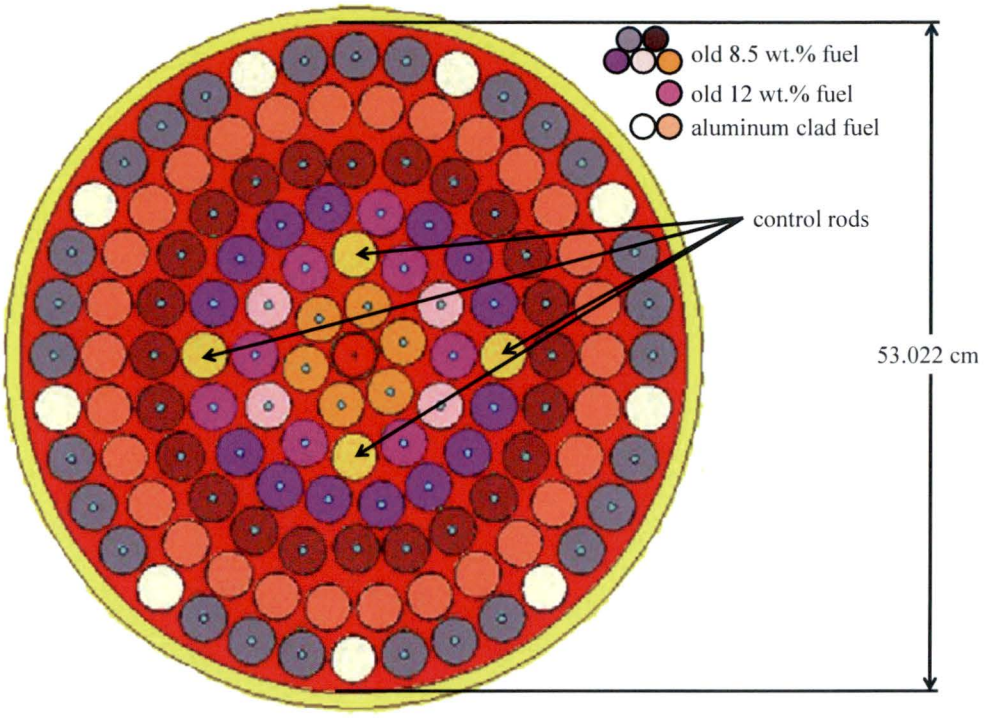

Figure 4.3. Radial view of the GSTR operating core.

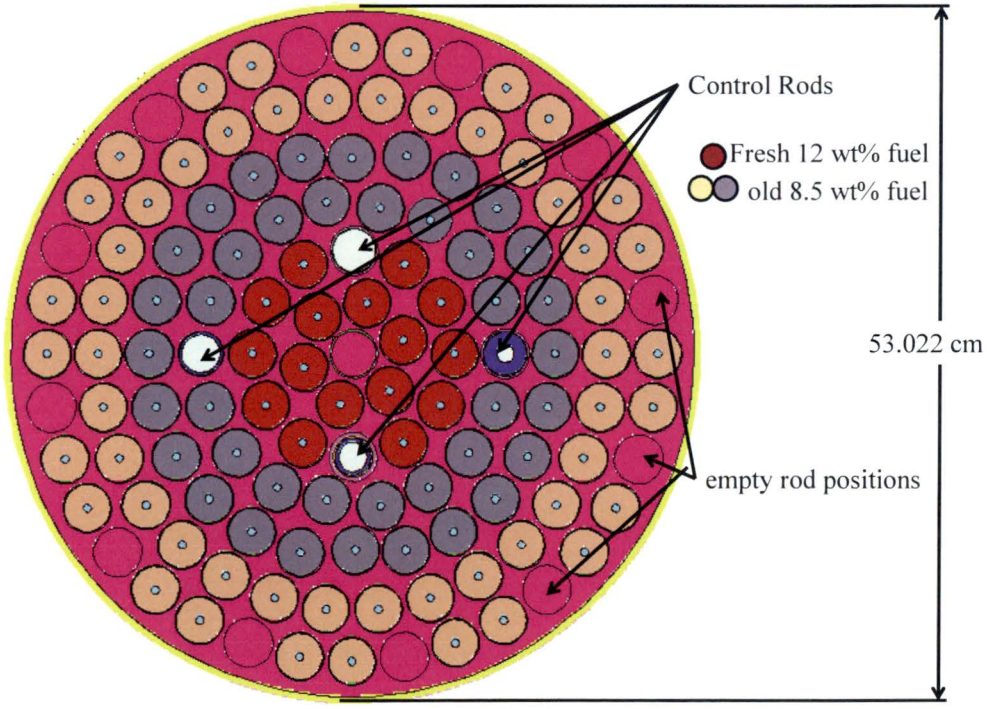

Figure 4.4. Radial view of the GSTR limiting core.

pneumatic rod drive instead of the mechanical system used by the other three control rods. This system can quickly eject the transient rod from the core to initiate a power pulse. Otherwise, the transient rod serves the same function as the other three rods; however, the pneumatic drive is not as sensitive as the mechanical rod drives. The void follower reduces the total reactivity worth of the transient rod.

4.3. Summary of Neutronics Analysis of the GSTR

The neutronic analysis of the GSTR is described in detail in Chapter 3. The neutronics analysis validated the MCNP model of the TRIGA reactor against the operating core (Figure 4.3). The analysis then reconfigured the model to represent the limiting core (Figure 4.4). The neutronics analysis provides the limiting core power profile and the reactivity feedback coefficients for the transient thermal hydraulic models up to a fuel temperature of 1200 K, as well as the other required parameters, such as the neutron generation time and effective delayed neutron fraction. All of the data taken from the MCNP analysis in Chapter 3 used in this chapter refers to the GSTR limiting core; however, as RELAP expect the reactivity in units of $\Delta k/k$ the reactivity coefficients were re-normalized to these units from the ones presented in Chapter 3 with the assumption that the initial value was based on a multiplication factor of 1. Tables 4.2 and 4.3 show the corrected prompt fuel temperature reactivity data and void reactivity data, respectively used in the RELAP and PARET models. A constant value of +\$0.01/K approximates the core water reactivity coefficient, and provides a conservative result in the units required by RELAP. The model uses the standard 6-group decay constants listed in Table 4.4 for uranium-235 (Lewis, 2008). As described in Chapter 3 the limiting core has a prompt neutron generation time of 4.28×10^{-5} s with a delayed neutron fraction of 0.00728.

Table 4.2. Prompt fuel temperature reactivity data for the GSTR limiting core.

Temperature (K)	Prompt Fuel Reactivity ($)
293.6	0.00
400	-0.99
600	-4.34
800	-7.55
1200	-13.00

Table 4.3. Void reactivity data for the GSTR limiting core.

Void Fraction (% Void)	Void Reactivity ($)
5	-0.15
10	-0.44
15	-0.82
20	-1.18
25	-1.65
30	-2.16
35	-2.75
40	-3.45
45	-4.23
50	-5.04
60	-7.12
70	-9.77
80	-13.26
90	-17.83
100	-23.70

Figures 4.5 and 4.6 display the axial and radial power factors, respectively, determined by the MCNP model of the reactor. These factors were calculated from a fission power conservative tally within the highest power fuel element within the limiting core, and provide the largest radial and axial power factors as the thermal-hydraulic models only allow one radial and one axial power factor. These power factors provide the power distribution within the hot rod

Table 4.4. Six-group delayed neutron fractions used in the transient thermal-hydraulic models (Lewis, 2008).

Group	Decay Constant (1/s)	Fraction of Delayed Neutrons
1	0.0124	0.0323
2	0.0301	0.2185
3	0.1118	0.1969
4	0.3013	0.3954
5	1.1361	0.1154
6	3.0130	0.0415

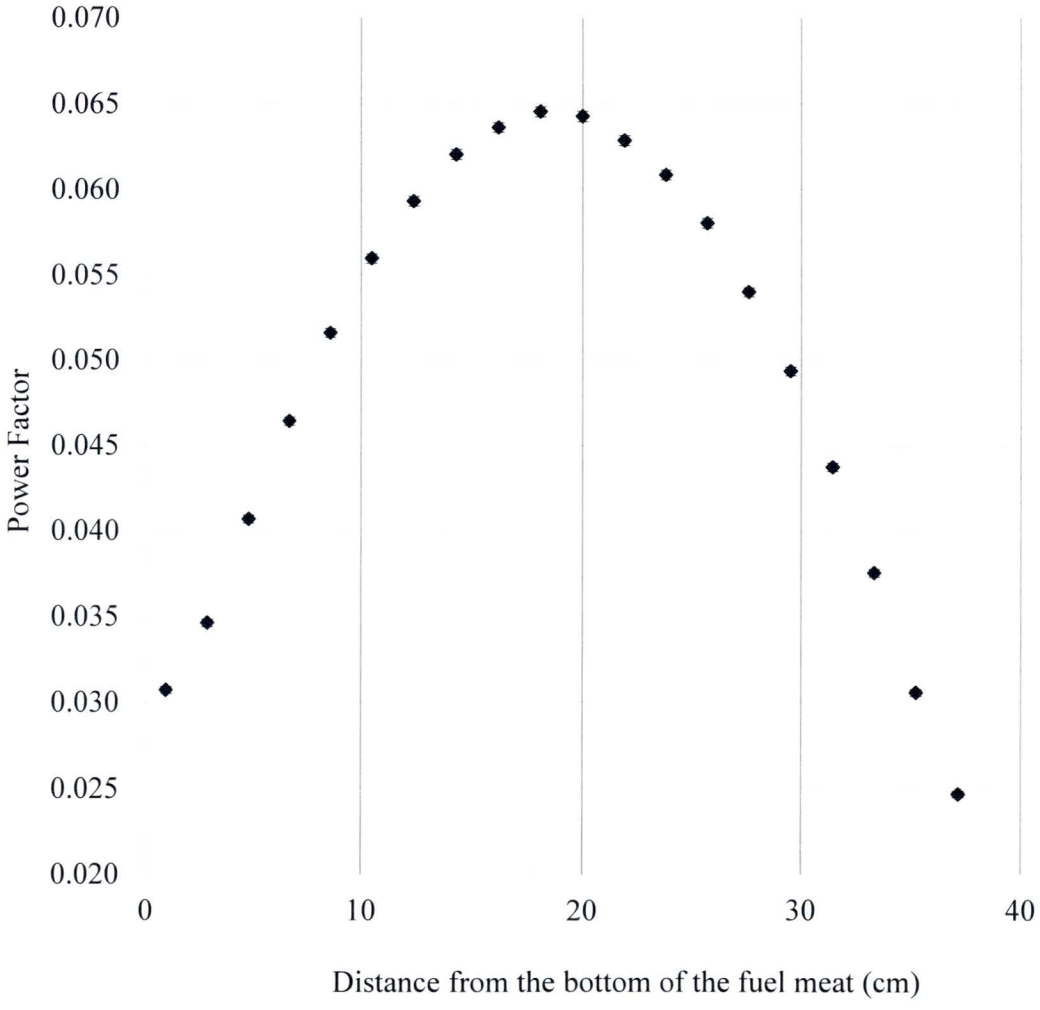

Figure 4.5. Axial power factor calculated by the MCNP model of the GSTR limiting core.

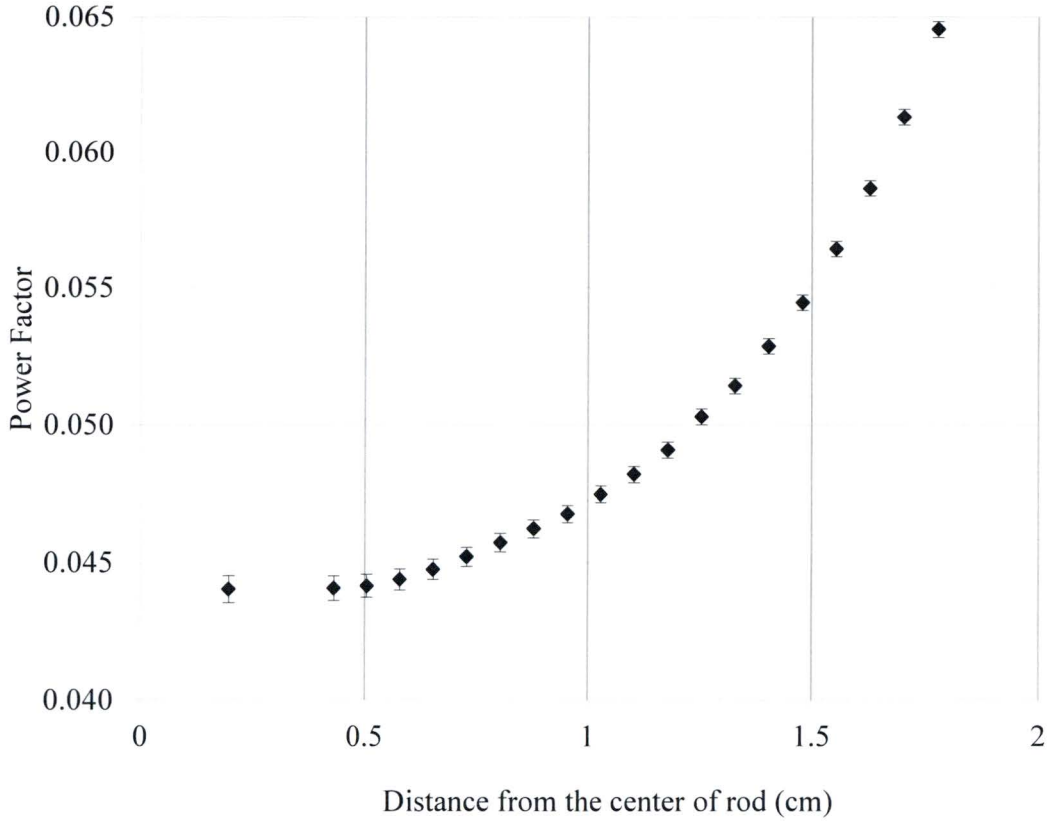

Figure 4.6. Radial power factor calculated by the MCNP model of the GSTR limiting core.

fuel element used in the transient thermal-hydraulic analysis, and represent the normalized power distribution in the rod.

4.4. Description of the Thermal-Hydraulic Models

The thermal-hydraulic analysis of the GSTR involves three models, two developed using the Reactor Excursion and Leak Analysis Program (RELAP) code (Information Systems Laboratories, Inc., 2010a and 2010b), and a third model developed using the Program for the Analysis of Reactor Transients (PARET) (Woodruff, 1982). The RELAP5 mod 3.3 models produce the majority of the modeling results, while the PARET-ANL v. 7.5 models provides a second set of verification data. The steady state RELAP model uses a single channel to represent

the hot rod for the DNBR analysis. The transient RELAP model utilizes two channels, and an average channel to represent the bulk core behavior and a hot channel representing the core hot rod. The PARET model contains a single average channel. The geometries in all three models are as similar as possible.

4.4.1. Steady-State RELAP Model

The steady-state RELAP model represents a single fuel channel with a source and sink that provide boundary conditions for a natural convection flow upwards through the fuel channel (Figure 4.7). The calculated hydrostatic pressure at the top of the core is 160443 Pa, while the hydrostatic pressure at the bottom is 167188 Pa. The initial conditions of the model set the water temperature to 60 °C to match the GSTR's Technical Specifications limit during steady state operation.

RELAP models the fuel rod as a heat structure with twenty axial nodes. Each axial node contains twenty radial nodes representing the radial geometry of the fuel rod. Data from the MCNP model of the core (Chapter 3) provides the axial and radial power factors within the heat structure (Figures 4.5 and 4.6 respectively). RELAP does not track the power factor for each cell in the heat structure, but instead uses one set of axial and radial factors. While the results from the neutronic model provided a detailed power profile for the entire rod, RELAP uses 40 unique factors (20 radial and 20 axial) to represent the full geometry of 400 heated cells that make upthe fuel within the fuel element. To be conservative, the RELAP model uses the most limiting axial and radial profiles available from the neutronics analysis (Figure 4.5 and 4.6 respectively) Each

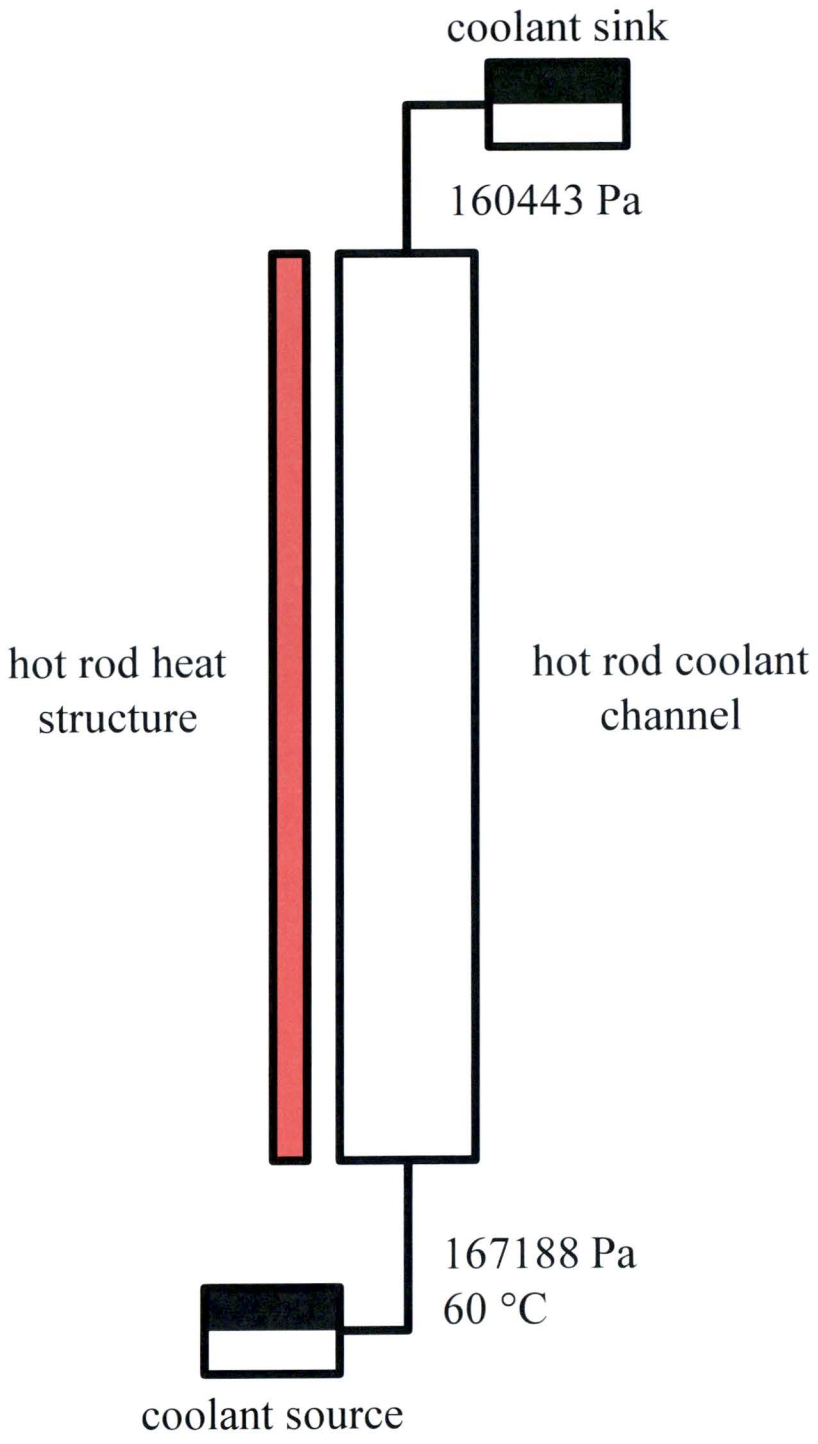

Figure 4.7. Steady state RELAP model of the GSTR.

axial segment of the heat structure has one boundary on a corresponding segment of the hot rod channel to allow heat to flow from the rod into the channel (see Figure 4.8).

Tables 4.5 and 4.6 list the axial node lengths of the hot channel and the radial node lengths of the heat-structure, respectively. The hot rod channel is broken into a series of 24 axial nodes, representing the fuel and the non-fueled sections of the fuel rod (Figure 36 and Table 4.5). Twenty of these nodes link to the fuel heat structure which is also represented by 20 axial segments consisting of 20 radial nodes (see Figure 4.8). The first and last pair of nodes in the hot rod channel represents the fixtures and graphite reflectors above and below the fuel meat makeup of the fueled portion of the element (Figure 4.8 and Table 4.6). The innermost section represents the zirconium plug in the center of the element, while the outer two elements represent

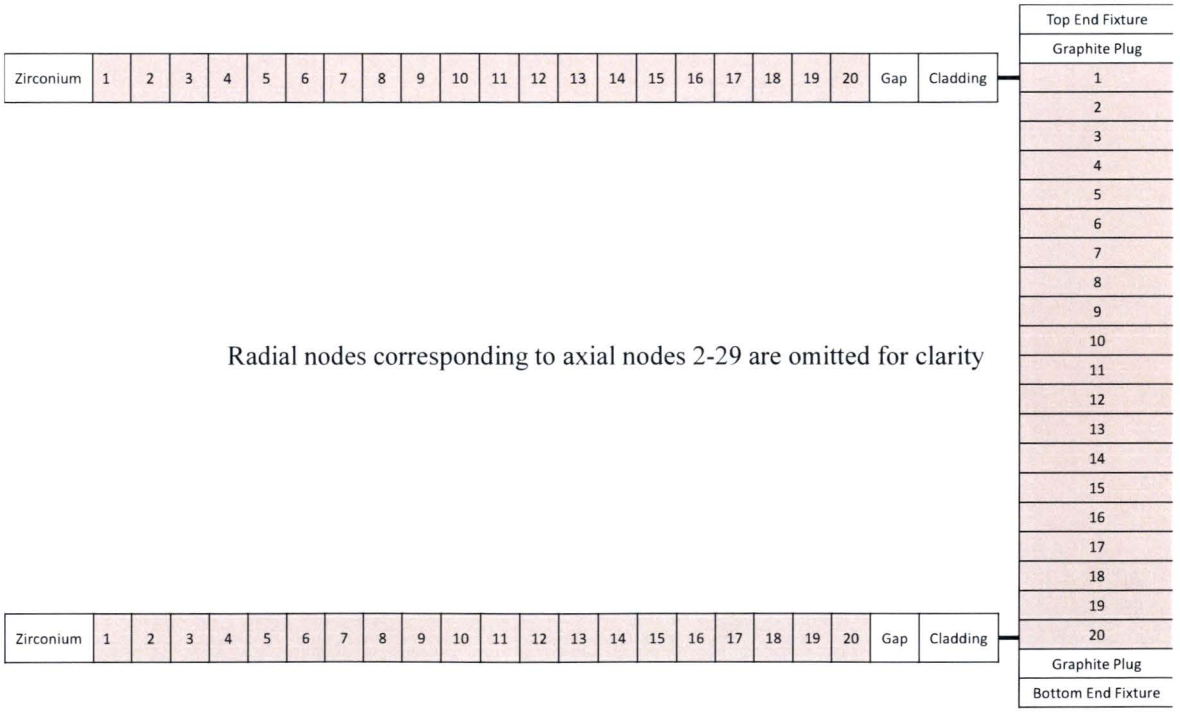

Figure 4.8. Layout of the axial and radial nodes of the fuel rod in the RELAP and PARET models of the GSTR limiting core.

Table 4.5. Axial node lengths in the hot channel segments of the GSTR.

Node	Node Length
1	2.13×10^{-2}
2	1.33×10^{-1}
3	1.91×10^{-2}
4	1.91×10^{-2}
5	1.91×10^{-2}
6	1.91×10^{-2}
7	1.91×10^{-2}
8	1.91×10^{-2}
9	1.91×10^{-2}
10	1.91×10^{-2}
11	1.91×10^{-2}
12	1.91×10^{-2}
13	1.91×10^{-2}
14	1.91×10^{-2}
15	1.91×10^{-2}
16	1.91×10^{-2}
17	1.91×10^{-2}
18	1.91×10^{-2}
19	1.91×10^{-2}
20	1.91×10^{-2}
21	1.91×10^{-2}
22	1.91×10^{-2}
23	1.33×10^{-1}
24	2.13×10^{-2}

Table 4.6. Radial node lengths in the heat structure segment of thickness in the RELAP model of the GSTR.

Node	Node Length
1	3.175×10^{-3}
2	7.443×10^{-4}
3	7.443×10^{-4}
4	7.443×10^{-4}
5	7.443×10^{-4}
6	7.443×10^{-4}
7	7.443×10^{-4}
8	7.443×10^{-4}
9	7.443×10^{-4}
10	7.443×10^{-4}
11	7.443×10^{-4}
12	7.443×10^{-4}
13	7.443×10^{-4}
14	7.443×10^{-4}
15	7.443×10^{-4}
16	7.443×10^{-4}
17	7.443×10^{-4}
18	7.443×10^{-4}
19	7.443×10^{-4}
20	7.443×10^{-4}
21	7.443×10^{-4}
22	1.000×10^{-4}
23	5.080×10^{-4}

the gap between the fuel meat and the cladding, and the cladding of the fuel (see Figure 4.8).

(Figure 4.8). Radially, the fuel rod axial elements consist of 23 sections representing the internal

An external file sets the power within the rod, and the axial and radial peaking factors present in the geometry description distribute this heat throughout the heat structure. Following

the process used by Oregon State University, the model has an inlet pressure loss coefficient of 2.26 and an exit pressure loss coefficient of 0.63 (Marcum, 2008).

The channel dimensions for the steady state model are based on the average B-Ring flow area between the point halfway between the central thimble and the middle of the B-Ring, and the mid-point of the B-and C-Rings. The area of the six fuel elements in the B-Ring is then subtracted, and the remaining area is divided by 6 to give the flow area per fuel element in the B-Ring, as presented in Table 4.7. The resulting flow area of 5.855 cm^2 with an effective hydraulic diameter of 1.997 cm provides a realistic flow area for the steady-state analysis.

4.4.2. Transient RELAP Model

The RELAP transient model provides a comparison to the PARET model, as well as an examination of the reactor during the two-phase flow conditions PARET is unable to resolve, such as high-reactivity pulses (Olson, 2012b). Figure 4.9 shows the RELAP transient model used for this project. The transient model includes a single channel that represents the average behavior of the GSTR during pulse or transient operations to drive the point-kinetics model in RELAP. A second channel that does not provide any data for the point-kinetics calculations

Table 4.7. Calculation of the flow area used in the steady state thermal-hydraulic analyses.

Parameter	Value
B-Ring Distance from Center (cm)	4.053
C-Ring Distance from Center (cm)	7.981
Inner Radius of Flow Channel (cm)	2.026
Outer Radius of Flow Channel (cm)	6.017
Fuel Element Cross Section (cm^2)	10.949
Wetted Perimeter of a Single Fuel Element (cm)	11.730
B-Ring Total Flow Area (cm^2)	35.132
Flow Area/Rod (cm^2)	5.855
Effective Hydraulic Diameter (cm)	1.997

represents the hot rod for the GSTR core. The fuel geometry for both channels matches the steady-state model (Figure 4.8); however, the flow areas are based on an average flow area per pin, calculated as shown in Table 4.8. The limiting core case includes the added flow area from the twelve empty fuel spaces in the grid. The resulting flow area is higher than the single

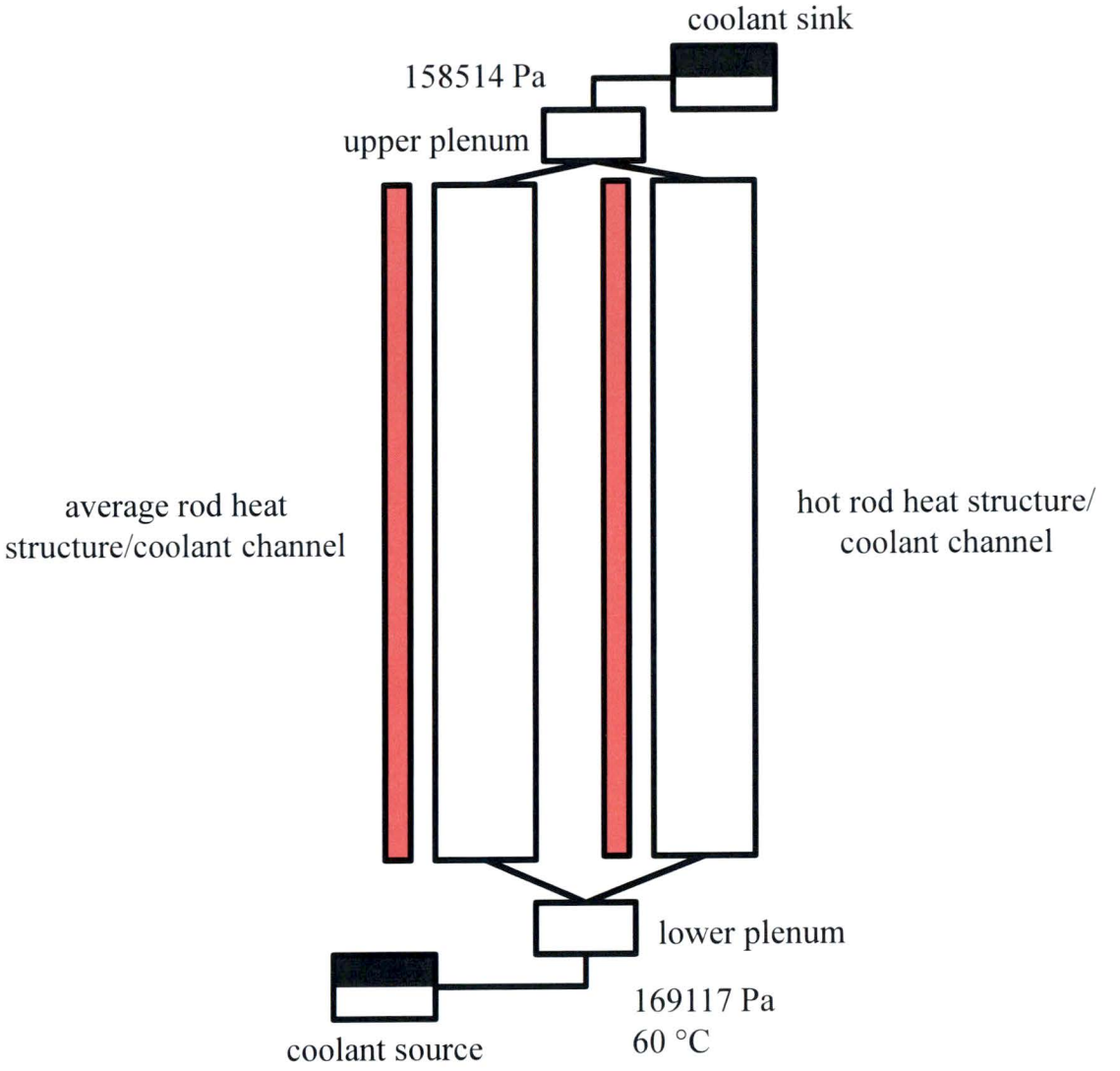

Figure 4.9. Transient RELAP model of the GSTR.

Table 4.8. Flow area calculations for the GSTR limiting core used in the transient analysis.

Parameter	Value
# Elements	110
# Control Rods	4
Element Cross Section (cm^2)	10.949
Control Rod Cross Section[1] (cm^2)	9.580
Transient Rod Cross Section (cm^2)	7.917
Central Thimble Cross Section (cm^2)	11.401
Core Cross Section (cm^2)	2208.099
Total Flow Area (cm^2)	824.209
Area/Rod[2] (cm^2)	8.382
Hydraulic Diameter (cm)	2.858

[1] Shim 1, Shim 2 and Regulating Rods
[2] Includes the four control rods

channel flow area in the B-Ring used in the steady-state analysis, and yields more realistic transient analysis results. With the expanded flow area, the hydraulic diameter becomes 2.858 cm.

The peaking factor for the average rod is assumed to be 1.0, while the hot rod has a peaking factor of 2.29 based on the MCNP analysis of the limiting core (Chapter 3). In addition, upper and lower plenums added to the channel to provide additional geometry for heat exchange before the boundaries of the tank, and for mixing the inlets and outlets of the two channels. These are loosely based on the geometry of the GSTR, and effectively extend the fuel channel. For the purpose of simplicity, the plenum dimensional area is equal to that of the channel dimensions (8.382 cm^2), and the height is 10.0 cm for both the upper and lower plenums.

The transient model uses the point-kinetics model included in the RELAP5 Mod 3.3 code to calculate the reactor power. From this calculation, the model places a fraction of the total power into each fuel element based on the element's peaking factor (PF), based on Equation 4.1:

$$\text{Rod Power} = \frac{\text{Reactor Power}}{\text{\# Rods in Core}} \times \text{PF} \tag{4.1}$$

RELAP's point-kinetics model includes terms for the fuel temperature, core water temperature, and void reactivities (see Section 4.3) as components of the total reactivity change at a given temperature.

4.4.3. PARET Model

Unlike RELAP, PARET uses a pre-defined geometry representing one or more fuel channels and includes data for upper and lower plenums and pressure differentials (Olson, 2012a). To maintain consistency, the PARET model uses the same geometric information, including the node lengths from Tables 4.5 and 4.6, as the RELAP model.

Like the RELAP model, PARET uses the dimensions shown in Table 4.8 to describe the channel dimensions, and includes a 0.1 m plenum above and below the hot-rod channel in both steady state and transient models. The PARET model does not include a hot-rod channel, as a single average rod channel provides an adequate comparison to the RELAP model.

The differences in the models came from differences in the code. While RELAP reads many of the feedback coefficients directly from calculated tables, PARET uses a continuous function to model the feedback coefficients. The PARET model uses a constant value of 0.0135 \$/K for the fuel temperature feedback coefficient, which approximates the neutronics results assuming a linear trend. The PARET model otherwise uses the point-kinetics parameters listed in Tables 4.2 through 4.4.

4.4.5. Testing Methodology

For the steady-state analysis, the models use a rod-power of 22.17 kW. The initial temperature of the entire system is set to 333.15 K, based on Technical Specifications for the reactor. The initial coolant velocity is set to 0.2 m/s. The transient analysis examined the prompt behavior of the GSTR limiting core during a series of pulses at different reactivity insertions. The GSTR initiates a pulse by expelling the transient control rod to a pre-set height through its pneumatic drive. The rod is then held at this height for 1.5 seconds before dropping fully into the core, returning the reactor to the same external reactivity conditions as before the pulse. Finally, the remaining rods drop 15 seconds after the pulse is initiated. Table 4.9 lists the pulse procedure for the GSTR, based on a $3.00 reactivity insertion. Both the RELAP and PARET models linearly interpolate the external reactivity between the points in Table 4.9. The models assume that it takes 0.2 s to remove a rod from the GSTR during a pulse. The reactor Technical Specifications provide SCRAM rates of 2.0 seconds for the transient (pulse) rod and 1.0 seconds for the other rods. The current GSTR Technical Specifications limit the pre-pulse steady-state power to below 1 kW. This upper bound is the starting point for all pulse tests. The initial physical conditions of the transient models match those of the steady-state analysis.

Table 4.9. Reactivity insertion sequence for a $3 pulse.

Time (s)	Inserted Reactivity($)
0	0
1	0
1.2	3.0
2.5	3.0
4.5	0
16	0
17	-5
3600	-5

4.5. Thermal-Hydraulic Results

The thermal hydraulic results are broken into three sections: the calibration of the thermal-hydraulic RELAP model, the steady-state results from the RELAP model, and the transient pulse results generated by both PARET and RELAP. As the PARET model was developed based on the RELAP model to provide verification results to compare to RELAP, the PARET model was only compared to the RELAP model to provide an idea of the uncertainties in the thermal hydraulic analysis.

4.5.1 Model Calibration

The gap included in TRIGA fuel is initially filled with air (Tomsio, 1986), but over time fission products from the fuel join the composition. Furthermore, the thickness of the gap varies over time as the fuel swells. Both of these functions are tunable in the model, and are useful for calibrating the general ability of the RELAP model to predict the behavior of the GSTR outside of the specific relicensing situations examined in this paper.

4.5.1.1 Fuel Gap Size Analysis

The manufacture of TRIGA fuel contains enough non-uniformity to make the gap between the fuel meat and cladding an approximate value for each rod (Marcum, 2008). Further, as the rod produces power in a reactor, the fuel swells from the buildup of fission products, leading to the gap size decreasing over time. The peak fuel temperature is highly dependent on the gap size, as seen in Figure 4.10. While the relationship between the temperature and gap thickness is strong, the actual gap size is nearly impossible to determine, and the model uses this parameter to calibrate the results with the actual temperature measurements from the GSTR.

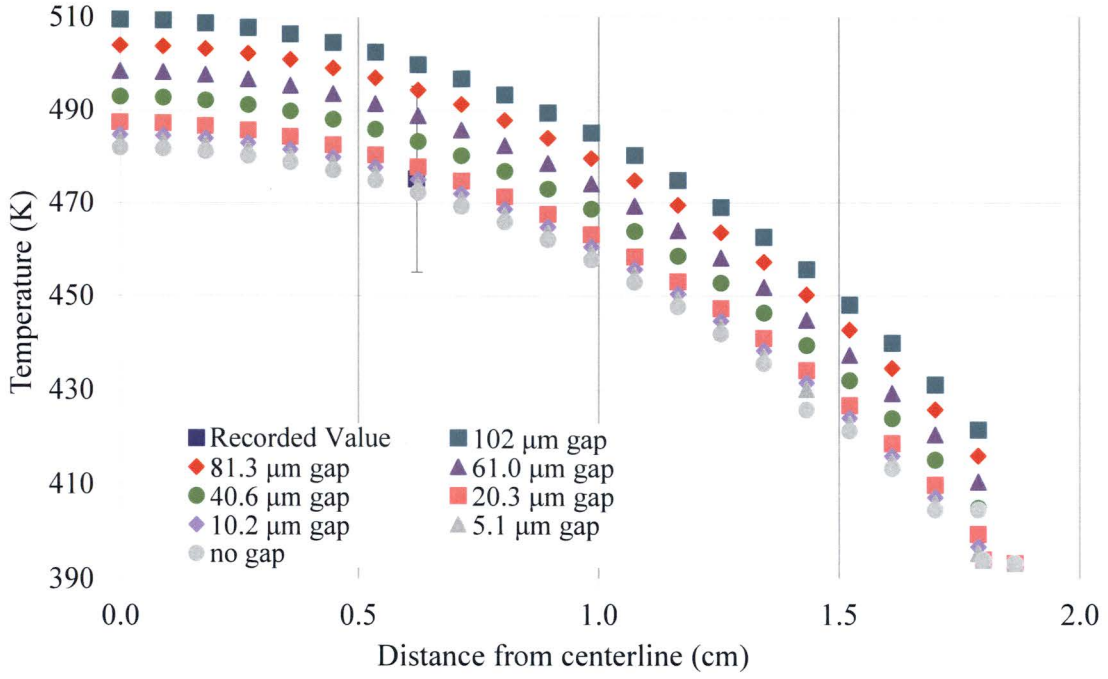

Figure 4.10. Fuel temperature profiles as a function of gap thickness.

The GSTR's instrumented fuel elements determine fuel temperature with an uncertainty of ± 20 °C, which covers a large portion of the plausible gap size. This makes any gap calibration based on temperature measurements from the GSTR invalid. To compensate, the model's gap thickness has been selected to match the gap size (0.1 mm) used in the Oregon State and other subsequent TRIGA reactor analyses (Oregon State University Radiation Center, 2010; Marcum, 2008; Hartman, 2011).

4.5.1.2 Generalized Power-Temperature Curves for the GSTR

Generalized power curves that determine the relationship between the powers generated in a rod, and the temperatures at various locations within the rod are a useful tool for the GSTR staff. Figures 4.11 and 4.12 present this relationship for the aluminum and stainless steel clad GSTR fuel rods, respectively. A comparison of Figures 4.11 and 4.12 demonstrate that the

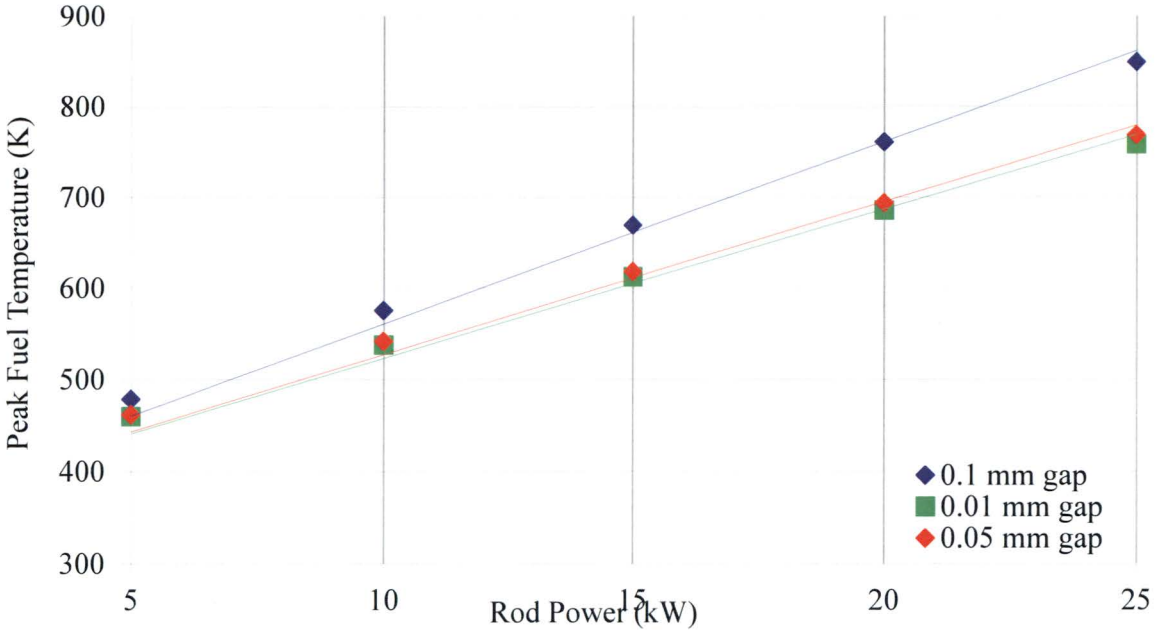

Figure 4.11. Peak fuel temperatures as a function of rod power at different gap sizes in an aluminum clad rod.

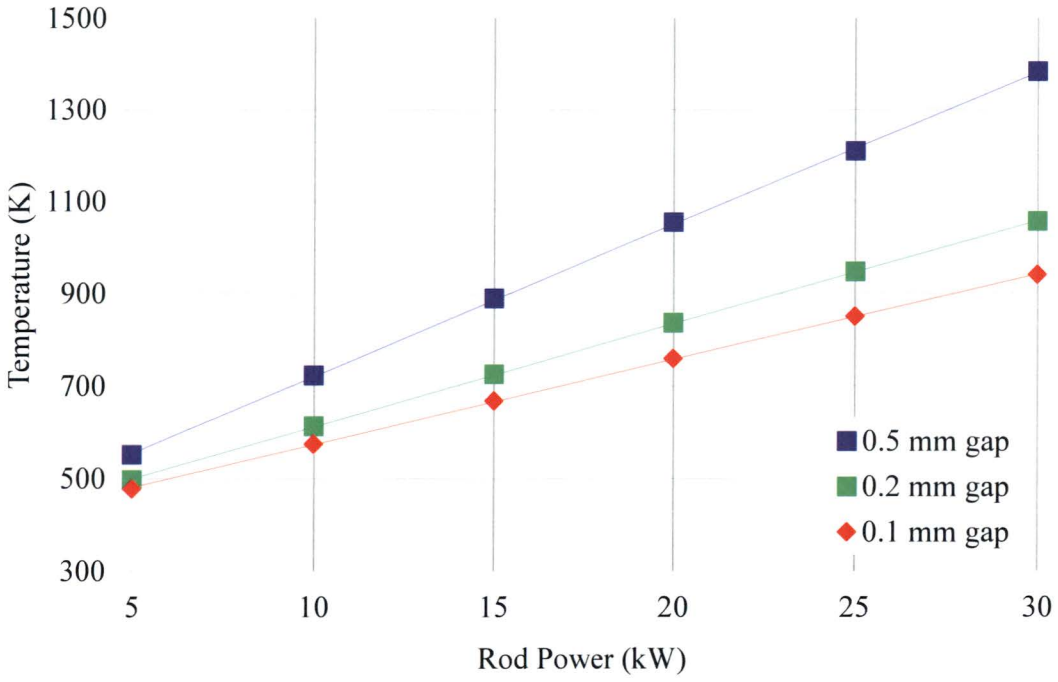

Figure 4.12. Peak fuel temperature as a function of rod power at different gap sizes in a stainless steel clad rod.

model is insensitive to the thermal properties of the cladding. At the same power and gap thickness there is no appreciable difference in the peak fuel temperature between the two cladding types. The lines for the 0.1 mm gap (the largest gap size in the aluminum clad fuel case (Figure 4.11), and the smallest case examined in the stainless-steel clad fuel (Figure 4.12)) are identical to within modeling uncertainty. Thus, a single model, using stainless steel cladding, can represent the entire reactor. Based on this assumption, Figure 4.13 presents a generalized temperature profile for the rods and channels in the GSTR, assuming a gap thickness of 0.1 mm.

4.5.2. Steady-State Results

The RELAP steady-state model predicts the normal operating conditions of the hot-rod channel for the GSTR limiting core. Figure 4.14 shows the steady state temperature profile at the axial center of the fuel element for the hot rod with the reactor operating at 1.1 MW. Since the limiting core is highly peaked compared to the current GSTR configuration, this data cannot

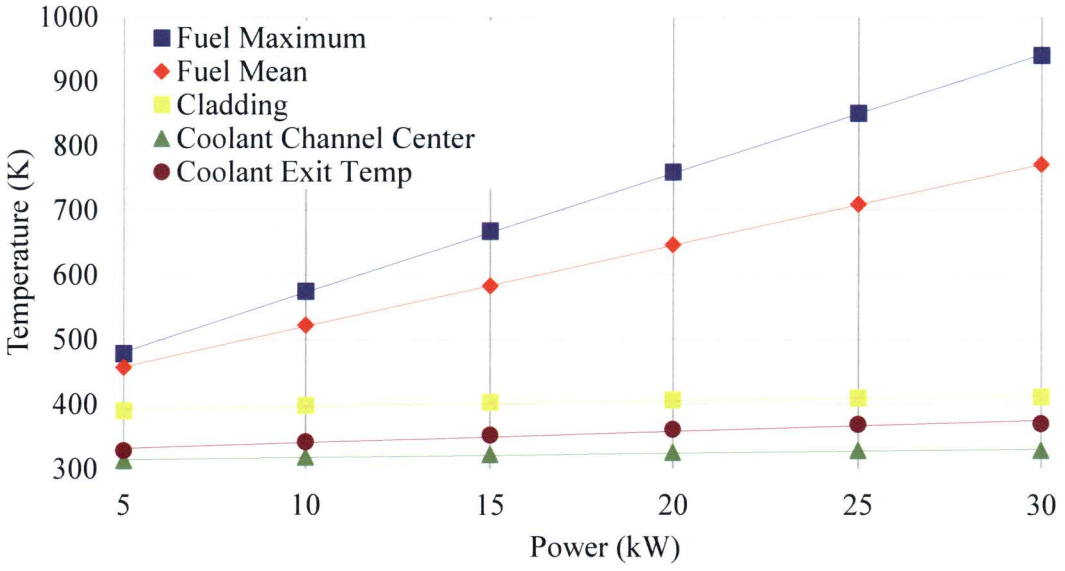

Figure 4.13. Generalized temperature curves for the GSTR fuel rods and channels as a function of power.

be compared to current data from the reactor facility, as no instrumented rods in the current core produce as much power as the limiting core hot-rod. When compared to work done for the TRIGA re-licensing effort sat Oregon State University and Reed College, the GSTR data is within 50 K of the trends predicted by both analyses (Marcum, 2008; Oregon State University Radiation Center, 2010). Given the differences in the reactors, core configurations, and model uncertainty, this is acceptable for the purpose of the safety analysis, as this difference is still within the safety limits of the GSTR. The steady state model indicates that the peak fuel temperature under steady-state conditions is 830 K. Under these conditions, the minimum Departure for Nucleate Boiling Ratio (DNBR) is 2.16 at 23.81 cm from the bottom of the fuel meat. This is higher than the location of the peak fuel temperature, as the interplay between heat flux (proportional to peak fuel temperature at steady state) and water temperature push the location of the minimum DNBR slightly further up the element to a point where the water

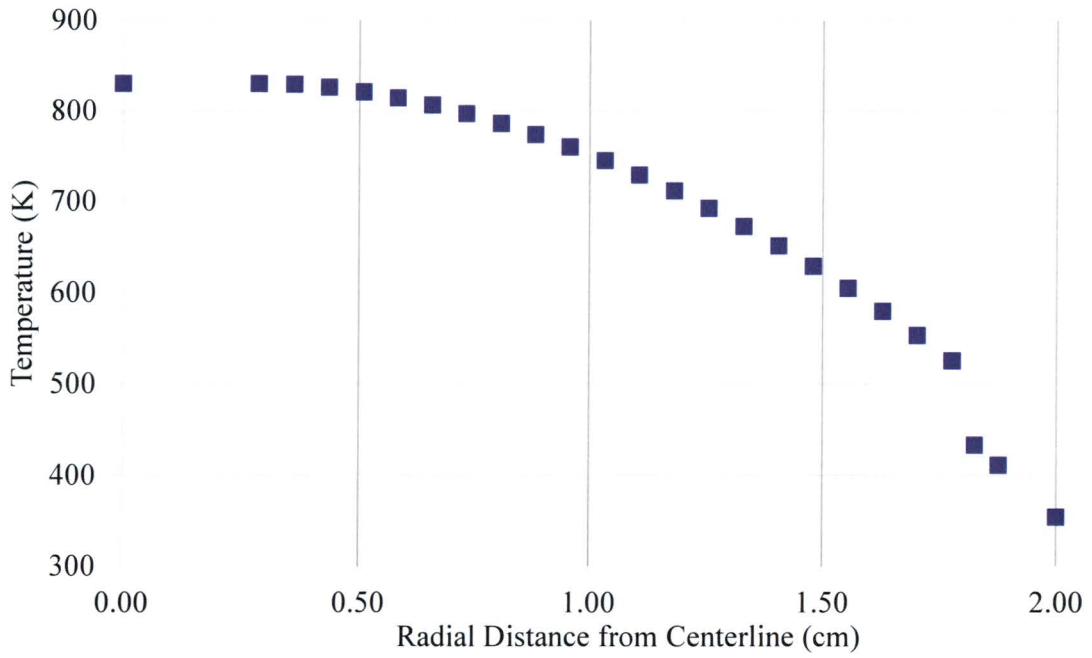

Figure 4.14. Steady state hot-rod temperature profile for the middle of the hot-rod for the GSTR at full power (1.1 MW).

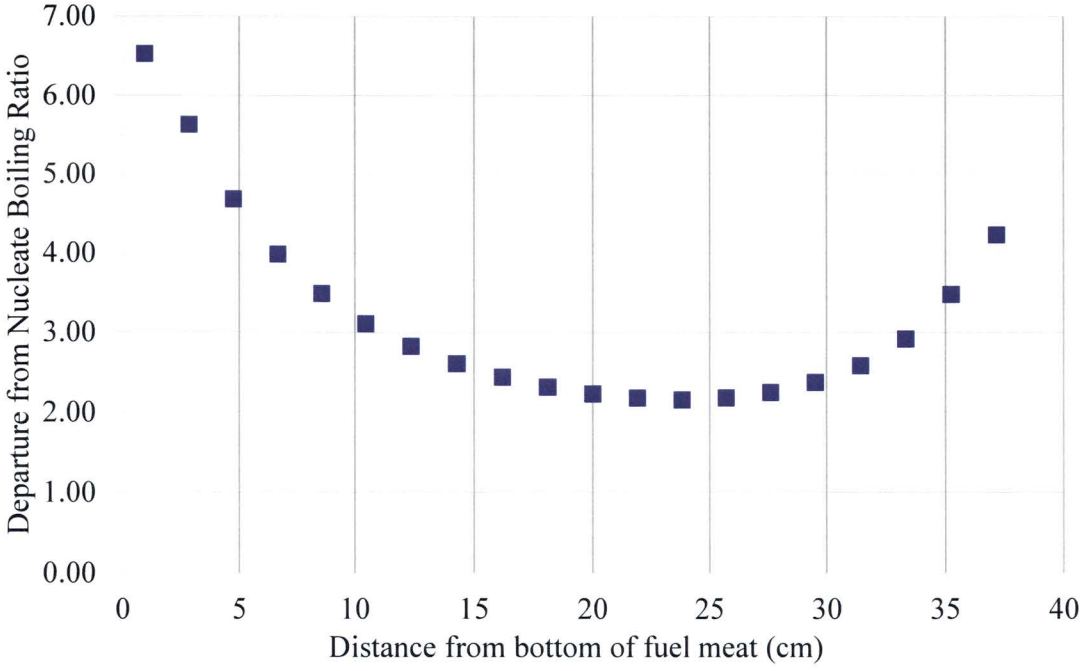

Figure 4.15. Departure from nucleate boiling ratio as a function of position along the hot-rod fuel element

temperature is higher. Figure 4.15 shows the DNBR in the hot channel as a function of distance along the fuel meat.

4.5.3. Transient Results

The analysis examines the inherent sensitivities of the model based on a $1.50 pulse modeled with two different codes (RELAP5 mod 3.3 and PARET-ANL v. 7.5) before looking at a range of pulses modeled in RELAP. The transient analysis then characterizes the behavior of the limiting core during a pulse at the $3.00 limit currently set by the Technical Specifications of the GSTR.

4.5.3.1. Comparison of the RELAP and PARET models

The transient analysis includes results from both the RELAP and PARET models of the GSTR. PARET has difficulties analyzing conditions when the peak void jumps above 0.2

(Olson, 2012b), and so a $1.50 pulse serves to show the simularities between the two models, and to provide some insight into the uncertanities and possible weakness of the current modeling strategy for the GSTR. To ensure that the PARET model did not exceed PARET's void limits, both models focused on an average rod with a peaking factor of 1.0, and did not consider the hot rod. While unsuitable for relicensing, these results do provide a comparison between the two models.

Figures 4.16 through 4.18 show the predicted power, maximum fuel temperature, and reactivities, respectively, for a $1.50 pulse simulated by both RELAP and PARET. The power behaviors shown in Figure 4.16 for a $1.50 pulse show similar behavior, although the models deviate as time goes on, with the power decreasing much faster in the RELAP model than in the PARET model. The remaining uncertainty in both models comes from the approximations made in modeling a pool-type reactor as one or two channels. PARET does not model cross-

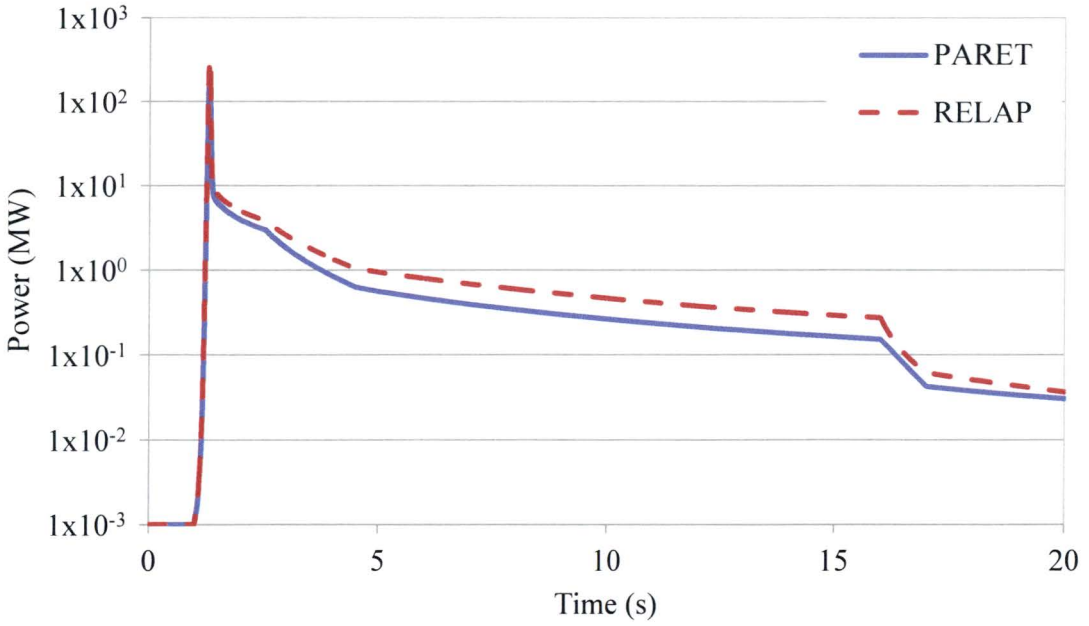

Figure 4.16. Power during a $1.50 pulse modeled in both PARET and RELAP.

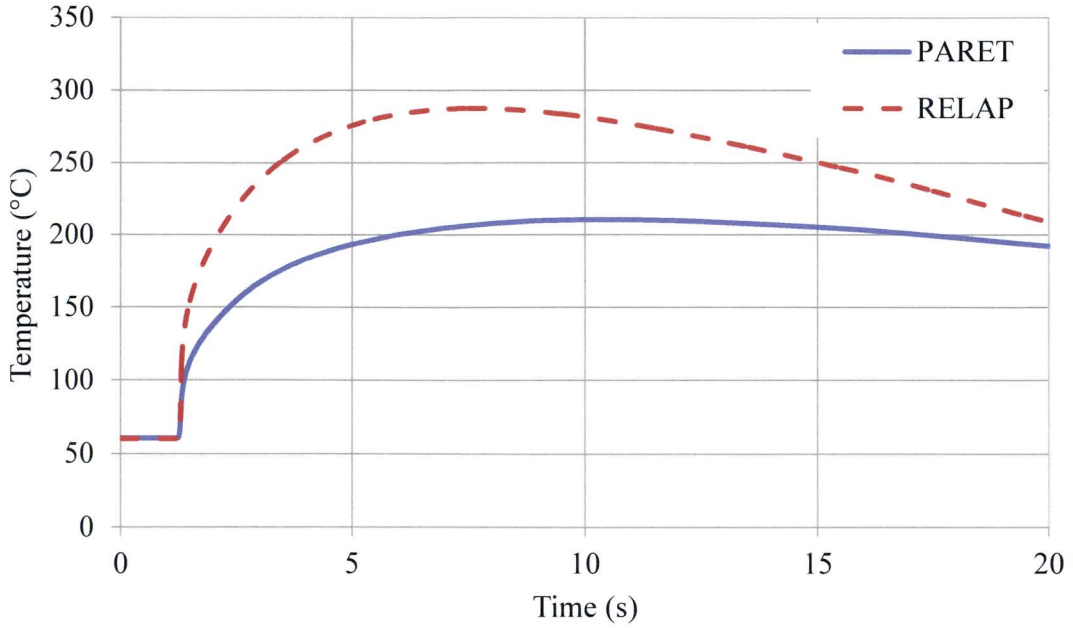

Figure 4.17. Peak fuel temperature during a $1.50 pulse modeled in both PARET and RELAP.

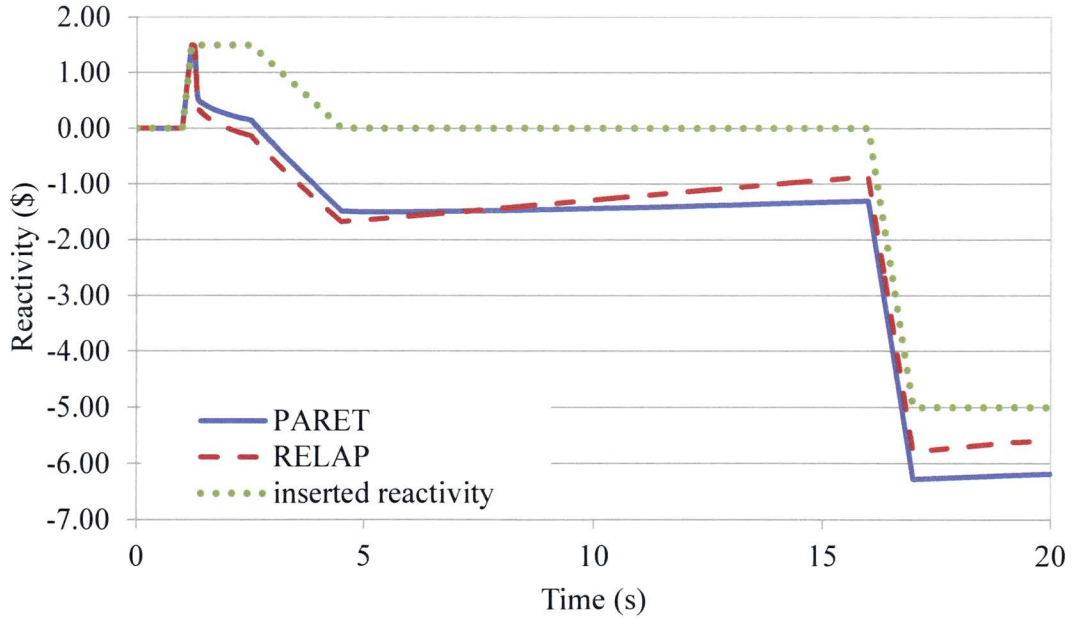

Figure 4.18. Inserted and total reactivity during a $1.50 pulse modeled in both PARET and RELAP.

flow, and the two-channel RELAP model does not include this effect. Figure 4.17 shows the innermost fuel temperature for both models during the pulse. While very similar during the prompt effects, both models eventually diverge by ~80 °C, well outside any feasible uncertainty bounds for either simulation RELAP's inherent calculation uncertainty is ~1%, ignoring errors in geometry and simplifying assumptions (Pawel and Mesina, 2011). For this to be a result of uncertainty, both models would need about a 50% uncertainty in their calculations, which is greater than the findings of RELAP uncertainty studies on other models (Fletcher and Beaton, 2006; Gertman and Mesina, 2012). Figure 4.18 shows the calculated total reactivity for the first 20 seconds of the pulse, with the program-inserted reactivity shown as a dotted line. PARET shows a higher total reactivity for the first 5 seconds, likely resulting from to the approximation of the fuel reactivity feedback coefficient as a linear function.

The difference in the predicted peak temperatures is the only significant difference between the two models. While RELAP uses a detailed table produced from the MCNP results to represent reactivity as a function of temperature, the PARET model uses a simple linear model based on the same data. The PARET model predicts a lower peak power, 204 MW, while RELAP predicts a peak power of nearly 319 MW for the same pulse and core (Figure 4.16). This appears to be caused by differences in how the two codes assign power to the average rod, leading to differences in the magnitude of the temperature feedback. The PARET model distributes the power throughout the rod more uniformly, which leads to an early peak in the fuel temperature (as seen in Figure 4.17). This earlier peak retards the rising power, resulting in the lower power peak in the PARET model. According to the PARET model, the peak fuel temperature for a $1.50 pulse is 483 K while the RELAP model predicts a peak fuel temperature

of 561 K. This implies that the RELAP model is more conservative than the PARET model, as RELAP predicts a higher peak temperature for the same reactivity insertion.

Another cause of uncertainty may be from the simplicity of the models. Since the entire reactor is represented by a single channel (the hot-rod channel does not contribute to the point-kinetics in the RELAP model), it is possible that this approximation is adding further uncertainty to the analysis. In general, it appears that modeling the non-prompt effects of a pulse in a TRIGA type reactor requires a more robust model than the one- and two channel models produced in either PARET or RELAP. Cross-flow appears to play a significant part in the post-pulse heat transfer into the coolant; however, neither model is capable of adequately modeling or simulating this effect. Work by Oregon State University confirms this hypothesis (Marcum, 2008). Based on these results, the two channel model provides an extremely conservative estimate of the temperatures beyond the fist second following a pulse and should be considered as an extreme upper bound.

4.5.3.2. RELAP Pulse Analysis

The primary scenario for the GSTR pulse analysis was a $3.00 reactivity insertion, which is the reactivity insertion limit for the reactor established by the reactor Technical Specifications. As a consequence of void formation after the pulse, the PARET model had difficulties resolving this high-reactivity insertion. The PARET developers recommend that PARET should not be used for high-reactivity insertions into a natural-convection model (Olson, 2012b).

The RELAP model examined a $3.00 pulse using the reactivity insertion sequence given in Table 4.9. Figure 4.19 shows the RELAP calculated results for the hot-rod during a $3.00 pulse, showing the innermost fuel temperature, the fuel surface temperature (the majority of

fissions in a TRIGA reactor take place at the fuel surface), the temperature at the point of the inserted thermocouple (~2/3 of the way into the fuel meat) and the reactor power. The limit line represents a temperature limit of 830 °C (1103 K) for TRIGA pulses established by the Nuclear Regulatory Commission. The surface temperature drives the temperature feedback and the prompt effects. Heat transfer after the prompt power pulse follows the classically predicted pattern for a heated cylinder as seen in the innermost fuel and thermocouple location readings following the pulse. The temperature at the thermocouple following the prompt power pulse slightly leads the temperature at the innermost edge of the fuel. The behavior of the fuel temperature in Figure 4.19 is indicative of the limits of the RELAP model following the prompt-behavior of the reactor. The thermocouple and innermost fuel temperatures reach 1070 K for a

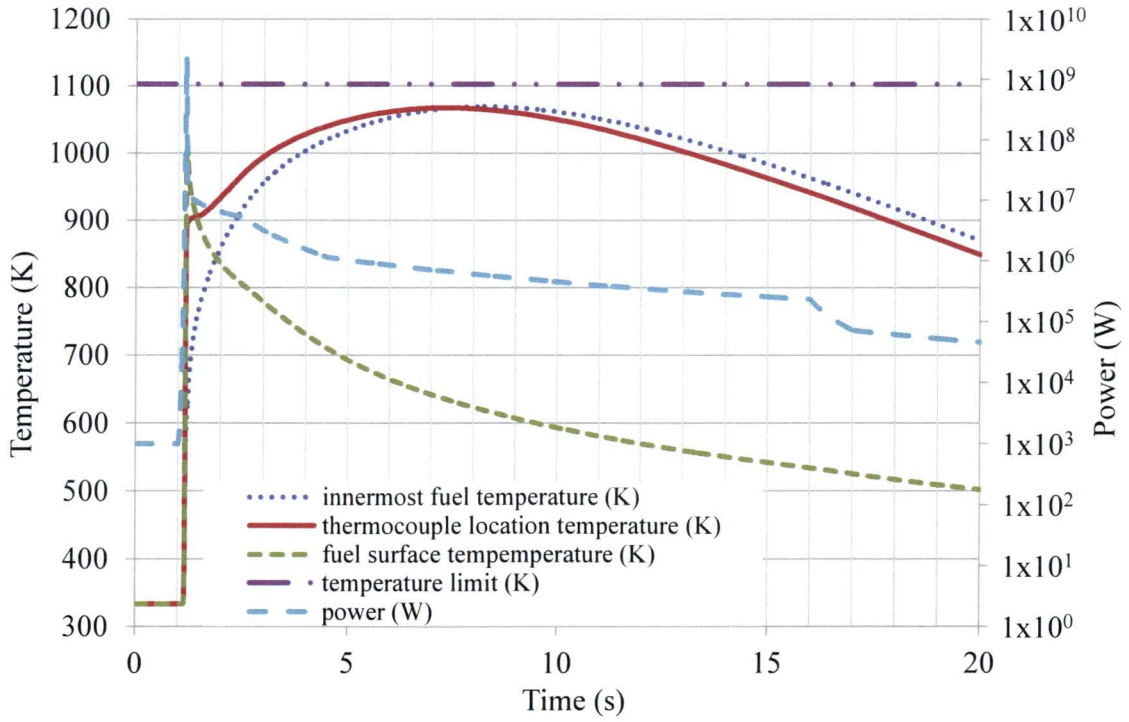

Figure 4.19. Temperatures and powers calculated as a function of time for the GSTR hot rod during a $3.00 pulse.

few seconds after the $3.00 pulse before decreasing rapidly as heat is removed to the GSTR pool.

Following the $3.00 pulse, the void fraction of the hot channel reaches a peak value of 0.16 before dropping back to single-phase flow at about 10 seconds (see Figure 4.20). In theory TRIGA type reactors should operate in single phase flow during a pulse, however, given the high power reached during the $3.00 pulse, some voiding may be an effect of the pulse. Figure 4.21 shows the reactivities calculated during the pulse. The predictions in Figure 4.21 are comparable with the findings from other TRIGA reactors (Agasie, 2009; Hartman, 2011; Marcum, 2008).

The void generation may be the result of the extremely conservative nature of the model's flow channel, and while voids may form during a pulse, the powers and temperatures predicted by the RELAP model are consistent with similar studies performed on TRIGA reactors, although these studies do not mention core voiding (Marcum, 2008; Hartman, 2011).

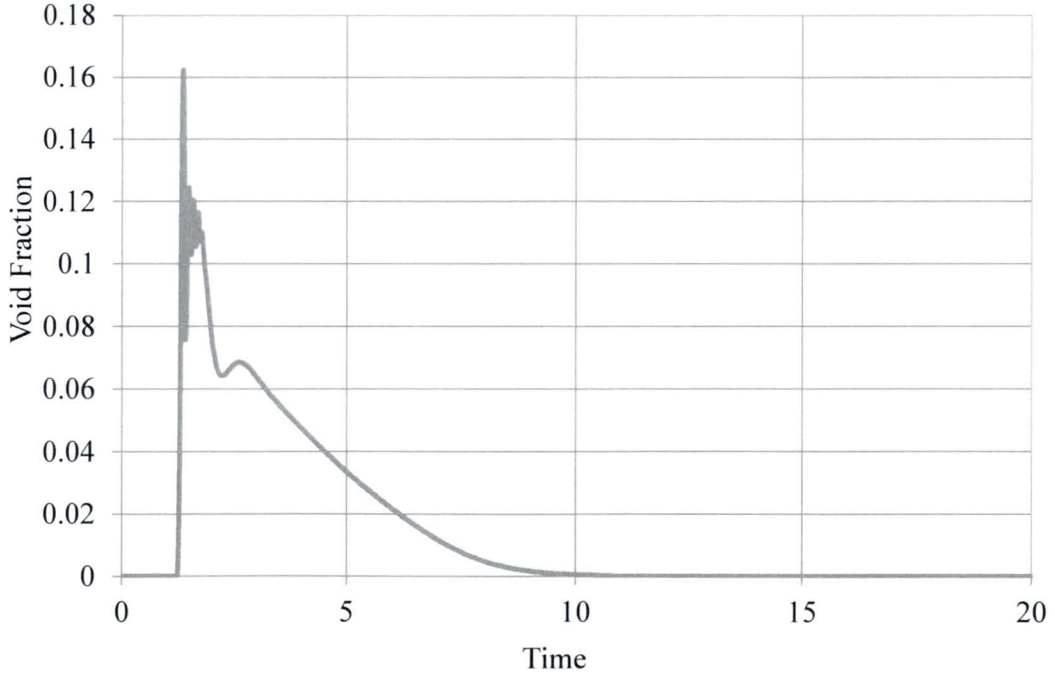

Figure 4.20. Calculated void fraction in the hot-channel as a function of time during a $3.00

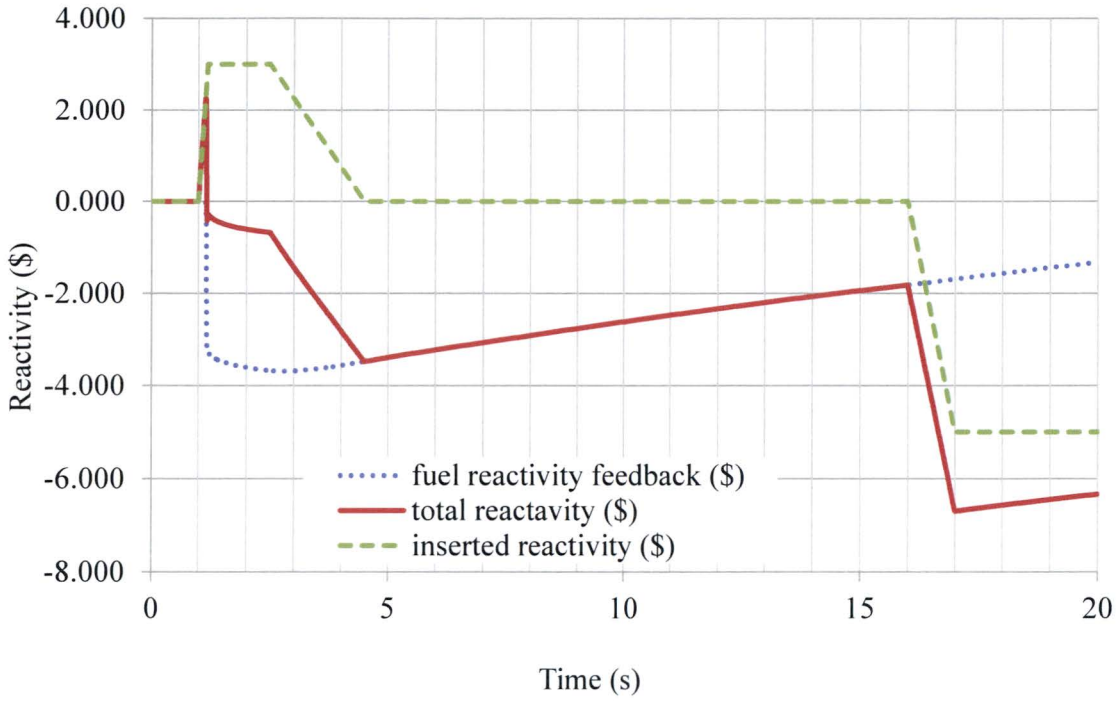

Figure 4.21. Inserted and calculated reactivities as a function of time during $3.00 pulse.

Because the RELAP model does not simulate the cross flows present in the GSTR, it is likely that the actual cooling capacity of the GSTR is much greater than predicted by the RELAP model. Unfortunately, there is no way to test this with the current model. These effects also take place well after the pulse event has concluded, and do not appear to effect the limiting core peak temperatures predicted by the model. A more detailed fluid flow analysis using a more complete model of the core is needed to resolve this issue, which appears to be an inherent weakness of this modeling strategy (Agasie, 2009). The present two-channel model serves as a very conservative upper bound on temperatures expected during a pulse.

Pulses of $2.75, $2.50, and $2.00 were also analyzed to test the behavior of the reactor, and to provide further data in case the $3.00 pulse was insufficiently limiting. Figures 4.22-4.24 display the temperature and power predictions for a $2.75, $2.50 and $2.00 pulse, respectively.

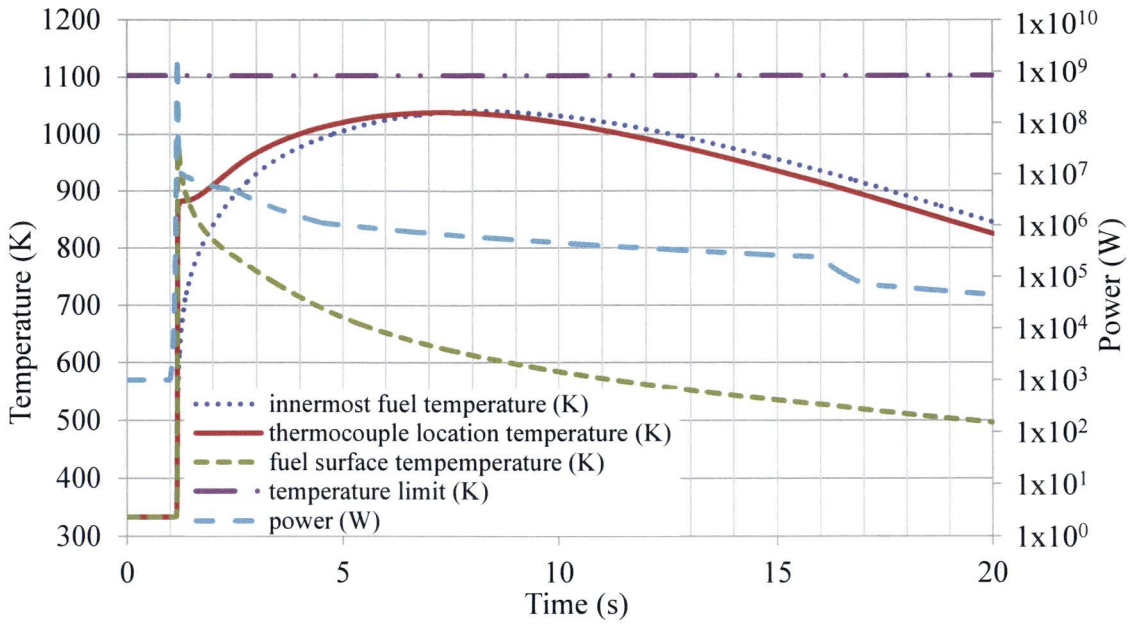

Figure 4.22. Temperatures and powers calculated as a function of time for the GSTR hot rod during a $2.75 pulse.

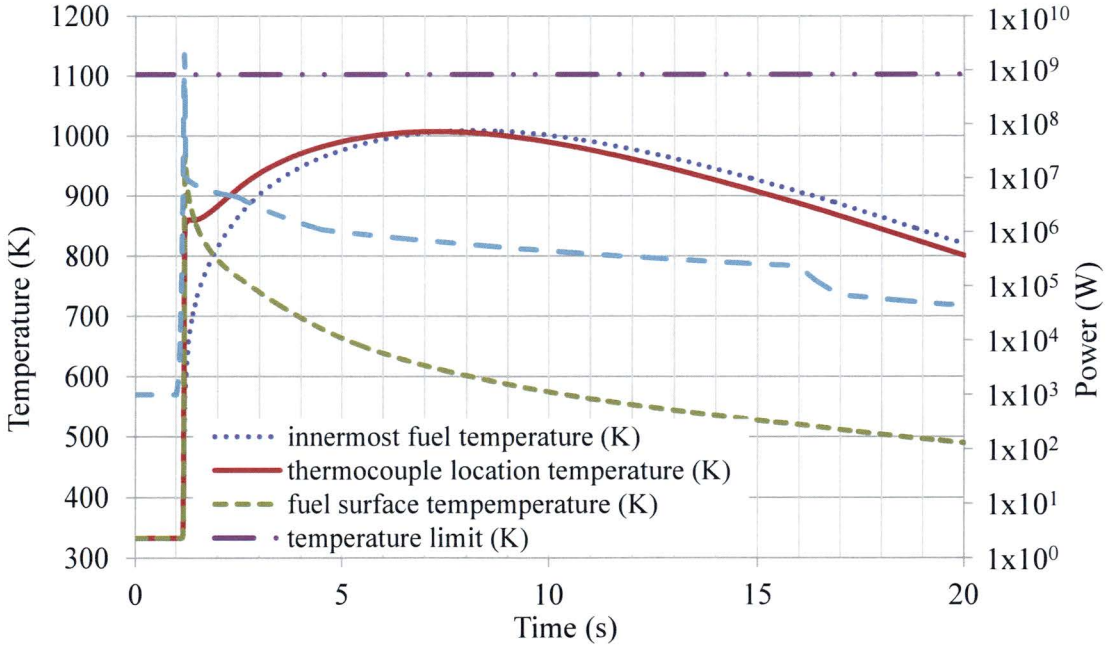

Figure 4.23. Temperatures and powers calculated as a function of time for the GSTR hot rod during a $2.50 pulse.

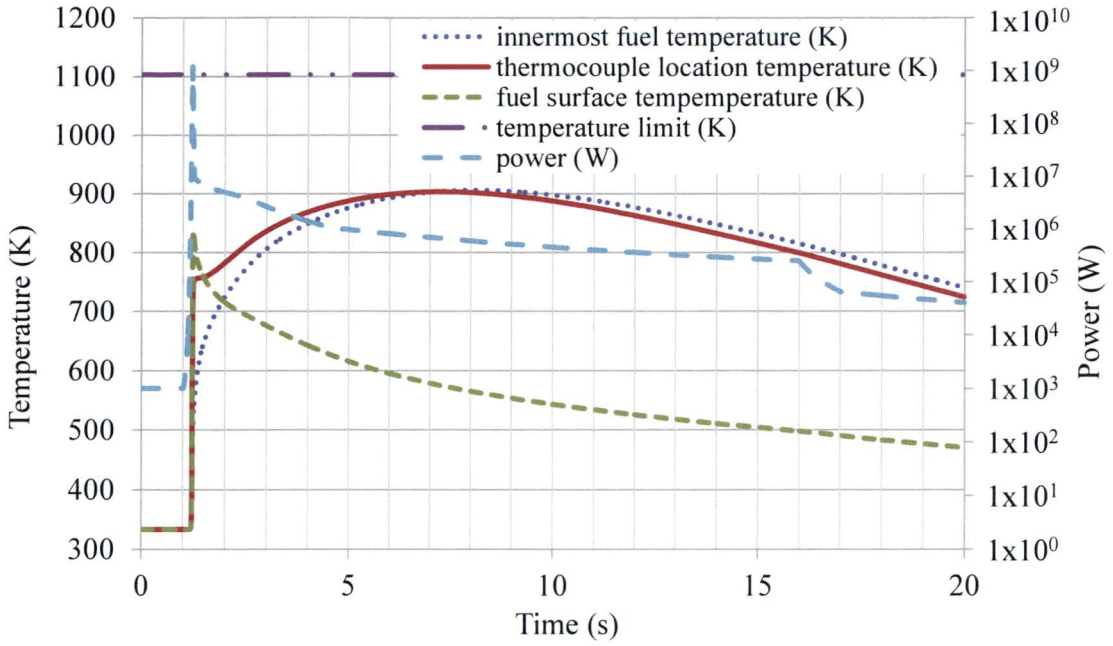

Figure 4.24. Temperatures and powers calculated as a function of time for the GSTR hot rod during a $2.00 pulse.

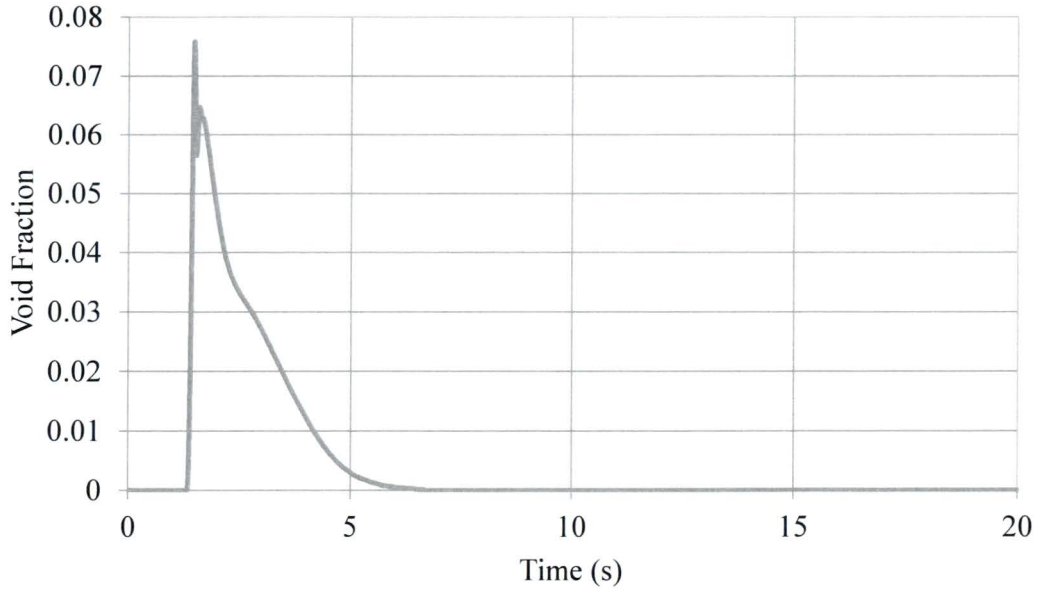

Figure 4.25. Calculated void fraction in the hot-channel as a function of time during a $2.00 pulse.

Table 4.10. Peak powers and temperatures predicated by the hot channel analysis for a $3.00 pulse of the GSTR limiting core.

	$3.00	$2.75	$2.50	$2.00
Peak Power (MW)	2397	2193	1992	1193
Peak Fuel Surface Temperature (K)	1018	995	969	838
Peak Thermocouple Location Temperature (K)	1068	1038	1007	903
Peak Fuel Temperature	1070	1040	1010	906
Pulse full width half maximum (s)	0.013	0.014	0.014	0.018

As expected, the peak temperature and oscillations decrease as the reactive insertion decreases; however, the model still predicts some voiding in the hot-rod channel during the $2.00 pulse, as seen in Figure 4.25. The peak void fraction is lower in the $2.00 pulse than during the $3.00 pulse (0.075 vs. 0.16 respectively), but in theory should not be occurring for such a low reactivity insertion. The cause for this is unknown, and is another sign that the two-channel RELAP model does not accurately model the non-prompt behavior in the GSTR fuel channels following a pulse. Table 4.10 displays the temperature results and full width half maximum for all of the analyzed pulses. The peak temperatures during a $3.00 pulse is below the limit placed on peak pulse by the Nuclear Regulatory Commission. For lower reactivities, the peak temperatures decrease, while the full width half maximum increases slightly as the pulse insertion amount decreases.

4.6. Summary and Conclusions

The thermal-hydraulic analysis of the GSTR limiting core examined the steady-state operating conditions in the hot-rod channel as well as the behavior of the reactor during transient pulses of up to $3.00. The analysis used the RELAP5 mod 3.3 code for the steady state and transient The analysis used the RELAP5 mod 3.3 code for the steady state and transient analysis, and PARET-ANL v. 7.5 to provide a comparison analysis to RELAP during low reactivity insertions.

Comparisons between the RELAP and PARET models indicate a general agreement between the core powers, temperatures, and reactivities predicted by the models. Differences in the results coming from differences in the way each code models the point-kinetics and hydraulic effects are likely responsible for the differences between the two models.

The steady-state analysis examined the core hot-rod during normal operations at 1.1 MW. In this analysis, the peak fuel temperature is 830 K, while the minimum departure from nucleate boiling ratio is 2.16. The pulse analysis examined reactivity pulses from \$3.00 to \$2.00 using the RELAP model. The thermocouple and innermost fuel temperatures in the GSTR after a \$3.00 reactivity pulse reach 1070 K for a few seconds before decreasing rapidly as heat is removed to the GSTR pool. Lower reactivity insertions result in lower coolant and fuel temperatures. In all of the pulse insertions, some amount of void appears in the hot-channel following the pulse.

The RELAP model appears to be overly conservative as a result of the lack of cross-flow within the model, and the use of a single channel to represent the core average conditions. This leads to non-realistic behavior several seconds after a high-reactivity pulse, resulting in significant voiding in the hot channel. These predictions may be an artifact of the simplicity of the model, and a more detailed analysis is necessary to understand the non-prompt behavior of the coolant in the GSTR following a pulse event. The present RELAP models represent a bounding case for the temperatures expected in the hot channel and fuel during steady state and transient operations.

CHAPTER 5
SUMMARY AND CONCLUSIONS

The neutronic analysis of the GSTR core validated the current MCNP model of the GSTR and then examined the GSTR limiting core to determine the excess and shutdown reactivities, reactivity coefficients of fuel temperature, core water temperature, void and power reactivity coefficient. The MCNP model was validated through comparisons of the control rods to experimental rod worth curves, matching the critical rod position to the GSTR measured position, and comparing the MCNP generated flux profile to an experimental flux profile from the central thimble. The total control rod worth is within \$0.30 of the experimental results, while the reactivity calculated with the control rods in the measured critical positions is within \$0.06 of the expected value of \$0.00. The flux profiles generated by the MCNP model are more peaked than those measured at the GSTR. This is likely due to the model using an axially uniform definition for fuel composition, as opposed to the real burnup distribution likely found within the GSTR fuel elements.

The limiting core configuration has a maximum excess reactivity of \$6.48 and a minimum shutdown margin of \$5.57. The limiting core has a highly peaked power distribution with a peak-to-average power ratio of 2.29. The temperature reactivity coefficients calculated for the GSTR limiting core agree with previous analyses from other TRIGA re-licensing efforts, and with General Atomics's original analyses. The model predicts a strongly negative fuel temperature reactivity coefficient (-0.0135 \$/K), as well as a slightly positive core water temperature reactivity coefficient (0.012 \$/K) for the full power limiting core. The calculated void reactivity coefficient is strongly negative (-0.069 \$/%void for 0-20% void). These factors combine to provide a core power reactivity coefficient of -0.0037 \$/kW.

The thermal-hydraulic analysis of the GSTR limiting core examined the steady-state operating conditions of the hot-rod channel as well as the behavior of the reactor during transient pulses of up to $3.00. The analysis used the RELAP5 mod 3.3 code for the steady state and transient analysis, and PARET-ANL v. 7.5 to provide a comparison analysis to RELAP during low reactivity insertions. Comparisons between the RELAP and PARET models indicate a general agreement between the models. Differences in the way each code models the point-kinetics and hydraulic effects are likely responsible for the discrepancy between the two models.

The steady-state analysis examined the core hot-rod during normal operations at 1.1 MW. In this analysis, the peak fuel temperature is 830 K, while the minimum departure from nuclide boiling ratio is 2.16. The pulse analysis examined reactivity pulses from $3.00 to $2.00 using the RELAP model. The thermocouple and innermost fuel temperature in the GSTR reach 1070 K for a few seconds after a $3.00 reactivity pulse before decreasing rapidly as heat is removed to the GSTR pool. Lower reactivity insertions result in lower coolant and fuel temperatures. In all of the pulse insertions, some amount of void appears in the channel following the pulse.

The RELAP model appears to be overly conservative as a result of the lack of cross-flow within the model, and the use of a single channel to represent the core average conditions. This leads to non-realistic behavior several seconds after a high-reactivity pulse, with significant voiding in the hot channel. These predictions may be an artifact of the simplicity of the model, and a more detailed analysis is necessary to understand the non-prompt behavior of the coolant in the GSTR following a pulse event. The RELAP models serves as a bounding case for the temperatures expected in the hot channel and fuel during steady state and transient operations.

CHAPTER 6
SUGGESTIONS FOR FUTURE RESEARCH

The RELAP model does not appear sufficient for analyzing the non-prompt effects of a high-reactivity insertion during a TRIGA pulse. A more detailed model that includes cross flow, and is preferably capable of modeling the reactor core in three dimensions is likely needed to accurately simulate the reactor behavior following a pulse. Such a model would need to be constructed using a more rigorous analysis code than RELAP5. This is compounded by the relative lack of information on this topic, as the GSTR is one of the final TRIGA reactors to be analyzed for relicensing, and the majority of the previous efforts have used models similar to the ones presented in Chapter 4.

The GSTR MCNP model could also be improved. While the current model is acceptable for the core, further analysis can always be done; however, any serious changes would likely be limited by the data available at the reactor facility. The GSTR's age, as well as the multiple fuel types, and fuel ages made modeling the GSTR model a unique challenge. One perhaps obvious path for improvement may be attempting to refine the burnup of the fuel using multiple axial segments like in the control rod depletion analysis. This may improve the model's ability to match the recorded axial flux data from the GSTR. A detailed uncertainty analysis of the core with an attempt to characterize some of the unknowns currently approximated in the model may provide greater insight into the full capabilities of the model.

A more realistic goal would be expanding the model to include some of the facilities used by the GSTR staff and researchers not currently present in the core. The facilities outside of the core have little to no impact on the operation of the reactor, which is why they were ignored in

the model; however, they may serve as locations for future experiments and expansions to the capabilities of the GSTR. Therefore, adding these geometries to the core model will improve the model's usefulness to the GSTR following the relicensing analysis.

REFERENCES CITED

Adoo, N. A., Nyarko, B.J. B., Akaho, E.H. K., Alhassan, E., Agbodemegbe, V. Y., Bansah, C. Y., Della, R. (2011), "Determination of the thermal hydraulic data of GHARR-1 under reactivity insertion transients using the PARET/ANL code," *Nuclear Engineering and Design,* 241(12), 5203-5210.

Agasie, R. J. (2009), "Response to Request for Additional Information Regarding HEU/LEU Conversion," U.S. Nuclear Regulatory Commission, License # R-74, Docket # 50-156: University of Wisconsin-Madison.

American Society of Mechanical Engineers (2009), "ASME International Steam Tables for Industral Use, Second Edition," New York, American Society of Mechanical Engineers, 802809.

Anderson, N. A. (2010), "Modeling a Printed Circuit Heat Exchanger with RELAP5-3D for the Next Generation Nuclear Plant," Idaho National Laboratory, INL/EXT-10-20619.

Antariksawan, A. R., Zmitkova, J., Huda, Q., Allison, C. M., Tiancai, L., and Hohorst, J. K. (2005), "Validation of RELAP/SCDAPSIM/Mod3.4 for research reactor applications," *13th International Conference on Nuclear Engineering (ICONE-13),* Beijing, China, May 16-20.

Artstein, Z., and Vitale, R. A. (1975), "A Strong Law of Large Numbers for Random Compact Sets," *The Annals of Probability,* 3(5), 179-882.

Binh, Q. D., Lan, P. N. (2007), "Application of a genetic algorithm to the fuel reload optimization for a research reactor," *Applied Mathematics and Computation,* 187(2) 977-988.

Beddingfield, D. H., and Swinhoe, M. T. (2004), "Curium Concentration in Spent Nuclear Fuel." *Institute of Nuclear Materials Management 45th Annual Meeting,*. Orlando, Flordia, July 18-22.

Bess, J. D., Marshall, M. A., and Maddock, T. L. (2011), "Benchmark Evaluation of the NRAD Reactor LEU Core Startup Measurements," *International Conference on Nuclear Criticality (ICNC2011),* Endinburgh, United Kingdom, September 19-22

Brewer, R. (2009), "Criticality Calculations with MCNP5: A Primer," Los Alamos National Laboratory, LA-UR-09-00380.

Brown, F. B. (2006), "The makxsf Code with Doppler Broadening," Los Alamos National Laboratory. LA-UR-06-7002.

Carter, L. L., and Cashwell, E. D. (1975), "Particle-Transport Simulation with the Monte Carlo Method," Los Alamos National Laboratory, TID-26607.

Chadwick, M.B., Herman, M., Oblozinsky, P., Dunn, M. E., Danon, Y., Kahler, A. C., Smith, D. L., Pritychenko, B., Arbanas, G., Arcilla, R., Brewer, R., Brown, D. A., Capote, R., Carlson, A. D., Cho, Y. S., Derrien, H., Guber, K., Hale, G. M., Hoblit, S., Holloway, S., Johnson, T. D., Kawano, T., Kiedrowski, B. C., Kim, H., Kunieda, S., Larson, N. M., Leal, L., Lestone, J. P., Little, R. C., McCutchan, E. A., MacFarlane, R. E., MacInnes, M., Mattoon, C. M., McKnight, R. D., Mughabghab, S. F., Nobre, G.P.A., Palmiotti, G., Palumbo, A., Pigni, M. T., Pronyaev, V. G., Sayer, R. O., Sonzogni, A. A., Summers, N. C., Talou, P., Thompson, I. J., Trkov, A., Vogt, R. L., van der Marck, S. C., Wallner, A., White, M. C., Wiarda, D., Young, P. G. (2011), "ENDF/V-VII.1 Nuclear Data for Science and Technology: Cross Sections, Covariances, Fission Product Yields and Decay Data," *Nuclear Data Sheets,* 112(12), 2887-2996.

Cheng, Y.-H., Wang, J.-R., Lin, H.-T., and Shih, C. (2009), "Benchmark calculations of pressurizer model for Maanshan nuclear power plant using TRACE code," *Nuclear Engineering and Design,* 239(11), 2343-2348.

Clifford, C. E., Hopkins, G. R., and West, G. B. (1966), "Nuclear Power Reactor Having a High Negative Temperature Coefficient of Reactivity", United States of America Patent No. 3,257,285.

D'Auria, F., and Galassi, G. M. (1998), "Code Validation and Uncertainties in System Thermalhydraulics," *Progress in Nuclear Energy,* 33(1-2), 175-216.

Day, W. (2004), "License amendment request to use aluminum-clad fuel in the GSTR," U. S. Nuclear Regulatory Commission, License # R-113, Docket # 50-274, United Stated Department of the Interior.

England, T. R., and Rider, B. F. (1994), "Evaluation and Compilation of Product Yields," Los Alamos National Laboratory, LA-UR-94-3106.

Ferreri, J. C., Ambrosini, W., D'Auria, F. (1995), "On the convergence of RELAP5 calculations in a single-phase, natural circulation test problem." National Nuclear Regulator, PI-1/96, 303-307.

Fletcher, C. D., and Beaton, R. M. (2006), "Evaluation of Uncertanties in SCDAP/RELAP 5 Station Blackout Simulations," Information Systems Laboratores, Inc., RES-CO5-340.

Fouquet, D. M., Razvi, J., and Whittemore, L. W. (2003), "TRIGA research reactors: A pathway to the peaceful applications of nuclear energy," *Nuclear News*, November, 2003, 46-56.

General Atomics, (1967), "Kinetic Behavior of TRIGA Reactors," General Atomics Technologies Inc., GA-7882.

General Atomics, (2011a), "TRIGA Projects," http://www.ga-esi.com/triga/projects/index.php, retrieved March 19 2013.

General Atomics, (2011b), "About TRIGA," http://www.ga-esi.com/triga/about/index.php, retrieved March 19 2013.

Gertman, A. E., and Mesina, G. L., (2012), "Uncertanity Analysis of RELAP5-3D©," *Mathematics Graduate Projects and Theses*, Boise State University, Paper 1, http://scholarworks.boisestate.edu/math_gradproj/1

Haake, E. V., and Krase, J. M. (1967), "Forced Curculation Boiling Nuclear Power Reactor," United States of America Patent No. 3,296,083.

Hamidouche, T., Bousbia-Salah, A., Adorni, M., and D'Auria, F. (2004), "Dynamic calculations of the IAEA safety MTR research reactor Benchmark program using RELAP5/3.2 code," *Annals of Nuclear Energy,* 31(12), 1385-1402.

Hartman, M. R. (2011), "Analysis of the Thermal Hydraulic and Reactivity Insertion Behavior of the DOW TRIGA Research Reactor," U.S. Nuclear Regulatory Comission, License # R-108, Docket # 50-264, Dow Chemical.

Hendricks, J. S., Adams, K. J., Booth., T. E., Briesmeister, J. F., Carter, L. L., Cox, L. J., Favorite, J. A., Forster, R. A., McKinney, G. W., Prael, R. E. (2000), "Present and future capabilities of MCNP," *Applied Radiation and Isotopes*, 53(4-5) 857-861.

Housiadas, C. (2002), "Lumped parameters analysis of coupled kinetics and thermal-hydraulics for small reactors," *Annals of Nuclear Energy,* 29(11), 1315-1325.

Huda, M. Q., and Rahman, M. (2004), "Thermo-hydrodynamic design and Safety parameter studies of the TRIGA MARK II research reactor," *Annals of Nuclear Energy,* 31(10), 1101-1118.

Information Systems Laboratories, Inc. (2010a), "RELAP5/Mod3.3 Code Manual Volume I: Code Structure, System Models, and Solution Methods," U.S. Nuclear Regulatory Commission, NUREG/CR-5535/Rev P4-Vol I: U.S.

Informations Systems Laboratories, Inc. (2010b), "RELAP5/Mod3.3 Code Manual Volume II: User Guide-Input Requirements," U.S. Nuclear Regulatory Commission, NUREG/CR-5535/Rev 1-Vol II.

Jensen, R. T., and Newell, D. L. (1998), "Thermal hydraulic calculations to support increase in operating power in McClellan Nuclear Radiation Center (MNRC) TRIGA reactor," *RELAP 5 International User's Seminar*, College Station, Texas, May 17-22.

Jonah, S. A. (2011), "Measured and Simulated Reactivity Insertion Transients Characheristics of NIRR-1," *Annals of Nuclear Energy,* 38(2-3), 295-297.

Kazeminejad, H., (2008), "Thermal-hydraulic modeling of flow inversion in a research reactor," *Annals of Nuclear Energy,* 35(10), 1813-1819.

Kiedrowski, B. C., Booth, T. E., Brown, F. B., Bull, J. S., Favorite, J. A., Forster, R. A., Martz, R. I. (2012), "MCNP5-1.60 Feature Enhancements and Manual Clarifications," Los Alamos National Laboratory, LA-UR-10-06217.

Lewis, E. E. (2008), Fundamentals of Nuclear Reactor Physics, San Diego, California, Elsevier Inc.

Marcum, W. (2008), "Thermal Hydraulic Analysis of the Oregon State TRIGA Reactor Using RELAP-3D," Oregon State University, Master's Thesis.

Marcum, W. R., Woods, B. G., and Reese, S. R. (2009), "Experimental and theoretical comparison of fuel temperature and bulk coolant characteristics in the Orgeon State TRIGA reactor during steady state operation," *Nuclear Engineering and Design,* 240(1), 151-159.

Maria, C. P., (2010), "Thermal hydraulic analysis of the IPR-R1TRIGA research reactor using a RELAP5 model," *Nuclear Engineering and Design,* 240(6), 1487-1494.

Merroun, O., Al Mers, A., Veloso, M. A., El Bardouni, T., El Bakkari, B., and Chakir, E. (2009), "Experimental validation of the thermal-hydraulic code SACATRI," *Nuclear Engineering and Design,* 239(12), 2875-2884.

Mesquita, A. Z. (2006), "Experimental Heat Transfer Analysis of the IPR-R1 TRIGA Reactor," *3rd World TRIGA User's Conference,* Belo Horizonte, Brazil, August 22-25.

Miller, W. S., and Feltus, M. A. (2000), "Three-dimesnional coupled kinetics/thermal hydraulic benchmark TRIGA experiments," *Annals of Nuclear Energy,* 27(9), 771-790.

Muir, D. W., and MacFarlane, R. E. (1994), "The NJOY Nuclear Data Processing System Version 91," Los Alamos National Laboratory, LA-12740-M.

Nuclear Installation Safety Division (2004a), "TRIGA Reactor Characteristics," International Atomic Energy Agency, Pers/JCH/nbb/ior/NSNI/Rev.1.

Nuclear Installation Safety Division., (2004b), "Triga Reactor Main Systems," International Atomic Energy Agency, Pers/JCH/nbb/ior/NSNI/Rev.1.

Olson, A. P. (2012a), "A Users guide to the PARET-ANL Code," Argonne National Laboratory, ANL/RERTR/TM-11-38.

Olson, A. P., (2012b), Personal Correspondance (E-Mail), August 17.

Oregon State University Radiation Center (2010), "Analysis of the Thermal Hydraulic Behavior of the Reed Research Reactor," U.S. nuclear Regulatory Commission, License # R-112, Docket # 50-288, Corvallis, Oregon.

Pawel, A. J., and Mesina, G. L., (2011), "Uncertanity Analysis for RELAP5-3D," Idaho National Laboratory, INL/EXT-11-22936.

Pelowitz, D. B. (2008), "MCNPX User's Manual," Los Alamos National Laboratory, LA-UR-02-2067.

Ranson, V. H., and Hicks, D. L. (1984), "Hyperbolic Two-Pressure Models for Two-Phase Flow," *Journal of Computational Physics,* 53(1), 124-151.

Reese, S. (2007), "Safety Analysis Report fot the Conversion of the Oregon State TRIGA Reactor from HEU to LEU Fuel," U.S. Nuclear Regulatory Comission, License # R-106, Docket # 50-243, Oregon State University.

Riemke, R. A., Davis, C. B., and Schultz, R. R. (2008), "Heat Transfer Boundary Conditions in the RELAP5-3D Code," Idaho National Laboratory, INL/CON-08-13692.

Safety Analysis Working Group (2009), "Documented Safety Analysis Addendum for the Neutron Radiography Reactor Facility Core Conversion," Idaho National Laboratory, INL/CON-09-15854

Simnad, M. T. (1981), "The U-ZrH Alloy: It's Properties and use in TRIGA Fuel," *Nuclear Engineering and Design,* 10(64), 403-422.

Snoj, L., Trkov, A., and Ravnik, M. (2007), "Testing of Cross Section Libraries for TRIGA Criticality Benchmark," *Nuclear Energy for New Europe*, Portorož, Slovenia, September 10-13.

Snoj, L., Zerovnik, G., and Trkov, A. (2011), "Analysis of Cross Section Libraries on Zirconium Benchmarks." The 12th *International Conference on Nuclear Cardiology.* Edinburgh, Scotland, September 19-22.

Takasuo, E. (2006), "Modeling of Pressurizer Using APROS and TRACE Thermal Hydraulic Codes," VTT Technical Research Center of Finland, Research Notes 2339.

Tomsio, N. (1986), "Characterization of TRIGA Fuel," General Atomics Technologies Inc., GA-C18542.

United States Geological Survey. (2008), "*REVISED SAFETY ANALYSIS REPORT, TECHNICAL SPECIFICATIONS, AND ENVIRONMENTAL REPORT,"* License # R-113, Docket # 50-274, United States Geological Survey.

Woodruff, W. L. (1982), "The PARET code and the Analysis of the SPERT I Transients," Argonne National Laboratory, CONF-821155-9

Woodruff, W. L. (1984), "A Kinetics and Thermalhydraulics Capability for the Analysis of Research Reactors," *Nuclear Technology,* 64(2), 196-206.

Woodruff, W. L., and Smith, R. S., (2001), "A Users Guide for the ANL Version of the PARET Code PARET/ANL (2001 Rev.)," Argonne National Laboratory, ANL/RERTR/TM-16.

Woodruff, W. L., Hanan, N. A., Smith, R. S., and Matos, J. E., (1996), "A Comparison of the PARET/ANL and RELAP5/MOD3 Codes for the Analysis of the IAEA Benchmark Transients," *International Meeting on Reduced Enrichment for Research and Test Reactors (RERTR-1996),* Seoul, Korea, October 7-10.

X-5 Monte Carlo Team. (2003a), "MCNP5 Manual Volume I: Overview and Theory," Los Alamos National Labortory, LA-UR-03-1987.

X-5 Monte Carlo Team. (2003b), "MCNP5 Manual Volume II: User's Guide," Los Almos National Laboratory, LA-CP-03-0245.

Zagar, T., Ravnik, M., and Trkov, A. (2002), "Isothermal Temperature Reactivity Coefficient Measurement in TRIGA Reactor," *Nuclear Energy for New Europe 2002,* Kranjska Gora, Slovenia, September 9-12.

APPENDIX A
GSTR MCNP5 MODEL

This appendix contains the MCNP model used for the neutronics analysis of the GSTR. The specific model presented represents the operating core at 5W with the control rods located in the critical positions. It includes the necessary components to configure the limiting core at 5W, but significant changes to the material definitions in the data section would be needed to match either full power model, as described in Chapter 3. The model is set to run using the parameters described in Chapter 3, and includes an input parameter to automatically rename the output file to GSTR_Feb22_2012.o. Details on the model are found in Chapter 3.

```
MESSAGE: o=GSTR_Feb22_2012.o

GSTR 12/09/2011
c
c  changed fuel burn up to more accurately show what is in the core,  don't know
c  why it wasn't this way in the first place.
c Final core model based on ENDFB/VII.0 libraries and S(a,b) data
c
c Removed legacy code from bottom shortening file
c Also set code to run 50K neutrons per cycle, 1015 cycles w/ 15 inactive cycles
c
c ********************************************************************
c                                Cells
c ********************************************************************
c
c
c %%%%%%%%%%%%%%%%%%%%%%%%%%%%%%
c  Stainless steel fuel rod universe 8.5 w/o Bring
c %%%%%%%%%%%%%%%%%%%%%%%%%%%%%%
c
  1 4 -7.86       2 -12 imp:n=1 u=1  $top pin
  2 4 -7.86      -2 3 -13 imp:n=1 u=1  $spacer
  3 4 -7.86      -3 4 -14 imp:n=1 u=1  $top cladding
  4 4 -7.86      -4 5 -14 imp:n=1 u=1  $inner spacer
  5 2  -1.56      -5 6 -14 imp:n=1 u=1  $upper graphite plug
  6 100 0.0973663 -6 7 -14 15 imp:n=1 u=1  $8.5 w/o fuel
  7 2  -1.56      -7 8 -14 imp:n=1 u=1  $lower graphite plug
  8 4 -7.86      -8 9 -14 imp:n=1 u=1  $inner spacer
  9 4 -7.86     -9 10 -14 imp:n=1 u=1  $bottom cladding
10 4 -7.86       -10 -12 imp:n=1 u=1  $bottom pin
11 4 -7.86      -3 10 14 -31 imp:n=1 u=1  $side cladding
12 1 -1      -2 500 13 imp:n=1 u=1  $upper grid plate
13 3 -2.7        12 -501 imp:n=1 u=1  $lower grid plate
14 1 -1     (-430 2 12):(-12 -430 1)  imp:n=1 u=1 $water above gridplate
15 1 -1        -500 3 13 -31 imp:n=1 u=1  $water below gridplate
16 1 -1       -10 501 12 -31 imp:n=1 u=1  $water above lower gridplate
17 5 -5.8       -15 -6 7 imp:n=1 u=1  $zr plug
285 1 -1     31 -500 501 imp:n=1 u=1  $water around fuel rod
c
c %%%%%%%%%%%%%%%%%%%%%%%%%%%%%%
c  Stainless steel fuel rod universe 12 w/o
c %%%%%%%%%%%%%%%%%%%%%%%%%%%%%%
c
```

```
18 4 -7.86      2 -12 imp:n=1 u=2  $top pin
19 4 -7.86     -2 3 -13 imp:n=1 u=2  $spacer
20 4 -7.86     -3 4 -14 imp:n=1 u=2  $top cladding
21 4 -7.86     -4 5 -14 imp:n=1 u=2  $inner spacer
22 2  -1.56     -5 6 -14 imp:n=1 u=2  $upper graphite plug
23 90 0.0967479 -6 7 -14 15 imp:n=1 u=2  $12 w/o fuel
24 2  -1.56     -7 8 -14 imp:n=1 u=2  $lower graphite plug
25 4 -7.86     -8 9 -14 imp:n=1 u=2  $inner spacer
26 4 -7.86    -9 10 -14 imp:n=1 u=2  $bottom cladding
27 4 -7.86       -10 -12 imp:n=1 u=2  $bottom pin
28 4 -7.86      -3 10 14 -31 imp:n=1 u=2  $side cladding
29 1 -1      -2 500 13 imp:n=1 u=2  $upper grid plate
30 3 -2.7     12 -501 imp:n=1 u=2  $lower grid plate
31 1 -1     (-430 2 12):(-12 -430 1)  imp:n=1 u=2 $water above gridplate
32 1 -1        -500 3 13 -31 imp:n=1 u=2  $water below gridplate
33 1 -1       -10 501 12 -31 imp:n=1 u=2  $water above lower gridplate
34 5 -5.8       -15 -6 7 imp:n=1 u=2  $zr plug
286 1 -1     31 -500 501 imp:n=1 u=2  $water around fuel rod
c
c %%%%%%%%%%%%%%%%%%%%%%%%%%%%%%
c  Aluminum fuel rod universe 8.0 w/o F ring
c %%%%%%%%%%%%%%%%%%%%%%%%%%%%%%
c
35    3 -2.7     -12 2 imp:n=1 u=3  $top pin
36    3 -2.7   -2 -13 16 imp:n=1 u=3  $spacer
37    3 -2.7  -16 3 -22 imp:n=1 u=3  $top claddng
38    3 -2.7  -3 18 -22 imp:n=1 u=3  $inner spacer
39    2 -1.56  -18 23 -22 imp:n=1 u=3  $upper graphite
50   10 .161768 -23 19 -22 imp:n=1 u=3  $sm poison
40 101 0.0766967 -19 20 -22 imp:n=1 u=3  $8 w/o fuel
51   10 .161768 -20 24 -22 imp:n=1 u=3  $sm Poison
41    2 -1.56  -24 8 -22 imp:n=1 u=3  $lower graphite
42    3 -2.7  -8 10 -22 imp:n=1 u=3  $lower cladding
43    3 -2.7     -10 -12 imp:n=1 u=3  $bottom pin
44    3 -2.7   -16 10 22 -32 imp:n=1 u=3  $side cladding
45    1 -1   -2 500 13 imp:n=1 u=3  $upper gridplate
46    3 -2.7  12 -501 imp:n=1 u=3  $lower gridplate
47    1 -1 (-430 2 12):(-12 -430 1)  imp:n=1 u=3 $water above upper gridplate
48    1 -1  -500 16 13 -32 imp:n=1 u=3  $water blow upper gridplate
49    1 -1  -10 501 12 -32 imp:n=1 u=3  $water above lower gridplate
295   1 -1     32 -500 501 imp:n=1 u=3  $water around fuel rod
c
c %%%%%%%%%%%%%%%%%%%%%%%%%%%%%%
c  Stainless steel fuel rod universe 8.5 w/o
c %%%%%%%%%%%%%%%%%%%%%%%%%%%%%%
c
52 4 -7.86      2 -12 imp:n=1 u=4  $top pin
53 4 -7.86     -2 3 -13 imp:n=1 u=4  $spacer
54 4 -7.86     -3 4 -14 imp:n=1 u=4  $top cladding
55 4 -7.86     -4 5 -14 imp:n=1 u=4  $inner spacer
56 2  -1.56     -5 6 -14 imp:n=1 u=4 $upper graphite plug
57 102 0.0973709 -6 7 -14 15 imp:n=1 u=4  $8.5 w/o fuel
58 2  -1.56     -7 8 -14 imp:n=1 u=4  $lower graphite plug
59 4 -7.86     -8 9 -14 imp:n=1 u=4  $inner spacer
60 4 -7.86    -9 10 -14 imp:n=1 u=4  $bottom cladding
61 4 -7.86       -10 -12 imp:n=1 u=4  $bottom pin
62 4 -7.86      -3 10 14 -31 imp:n=1 u=4  $side cladding
63 1 -1      -2 500 13 imp:n=1 u=4  $upper grid plate
64 3 -2.7        12 -501 imp:n=1 u=4   $lower grid plate
65 1 -1     (-430 2 12):(-12 -430 1)  imp:n=1 u=4 $water above gridplate
66 1 -1        -500 3 13 -31 imp:n=1 u=4  $water below gridplate
67 1 -1       -10 501 12 -31 imp:n=1 u=4  $water above lower gridplate
68 5 -5.8       -15 -6 7 imp:n=1 u=4  $zr plug
```

```
288 1 -1     31 -500 501 imp:n=1 u=4  $water around fuel rod
c
c %%%%%%%%%%%%%%%%%%%%%%%%%%%%%
c  Stainless steel fuel rod universe 8.5 w/o D ring
c %%%%%%%%%%%%%%%%%%%%%%%%%%%%%
c
69 4 -7.86      2 -12 imp:n=1 u=5  $top pin
70 4 -7.86     -2 3 -13 imp:n=1 u=5  $spacer
71 4 -7.86     -3 4 -14 imp:n=1 u=5  $top cladding
72 4 -7.86     -4 5 -14 imp:n=1 u=5  $inner spacer
73 2  -1.56     -5 6 -14 imp:n=1 u=5  $upper graphite plug
74 103 0.097383 -6 7 -14 15 imp:n=1 u=5  $8.5 w/o fuel
75 2  -1.56     -7 8 -14 imp:n=1 u=5  $lower graphite plug
76 4 -7.86     -8 9 -14 imp:n=1 u=5  $inner spacer
77 4 -7.86    -9 10 -14 imp:n=1 u=5  $bottom cladding
78 4 -7.86       -10 -12 imp:n=1 u=5  $bottom pin
79 4 -7.86      -3 10 14 -31 imp:n=1 u=5  $side cladding
80 1 -1      -2 500 13 imp:n=1 u=5  $upper grid plate
81 3 -2.7        12 -501 imp:n=1 u=5  $lower grid plate
82 1 -1     (-430 2 12):(-12 -430 1)  imp:n=1 u=5 $water above gridplate
83 1 -1        -500 3 13 -31 imp:n=1 u=5  $water below gridplate
84 1 -1      -10 501 12 -31 imp:n=1 u=5  $water above lower gridplate
85 5 -5.8       -15 -6 7 imp:n=1 u=5  $zr plug
289 1 -1     31 -500 501 imp:n=1 u=5  $water around fuel rod
c
c %%%%%%%%%%%%%%%%%%%%%%%%%%%%%
c  Stainless steel fuel rod universe 8.5 w/o E ring
c %%%%%%%%%%%%%%%%%%%%%%%%%%%%%
c
86 4 -7.86      2 -12 imp:n=1 u=6  $top pin
87 4 -7.86     -2 3 -13 imp:n=1 u=6  $spacer
88 4 -7.86     -3 4 -14 imp:n=1 u=6  $top cladding
89 4 -7.86     -4 5 -14 imp:n=1 u=6  $inner spacer
90 2  -1.56     -5 6 -14 imp:n=1 u=6   $upper graphite plug
91 104 0.0973888 -6 7 -14 15 imp:n=1 u=6  $8.5 w/o fuel
92 2  -1.56     -7 8 -14 imp:n=1 u=6  $lower graphite plug
93 4 -7.86     -8 9 -14 imp:n=1 u=6  $inner spacer
94 4 -7.86    -9 10 -14 imp:n=1 u=6  $bottom cladding
95 4 -7.86       -10 -12 imp:n=1 u=6  $bottom pin
96 4 -7.86      -3 10 14 -31 imp:n=1 u=6  $side cladding
97 1 -1      -2 500 13 imp:n=1 u=6  $upper grid plate
98 3 -2.7        12 -501 imp:n=1 u=6  $lower grid plate
99 1 -1     (-430 2 12):(-12 -430 1) imp:n=1 u=6  $water above gridplate
230 1 -1       -500 3 13 -31 imp:n=1 u=6  $water below gridplate
231 1 -1      -10 501 12 -31 imp:n=1 u=6  $water above lower gridplate
232 5 -5.8       -15 -6 7 imp:n=1 u=6  $zr plug
292 1 -1     31 -500 501 imp:n=1 u=6  $water around fuel rod
c
c %%%%%%%%%%%%%%%%%%%%%%%%%%%%%
c  Stainless steel fuel rod universe 8.5 w/o G ring
c %%%%%%%%%%%%%%%%%%%%%%%%%%%%%
c
233 4 -7.86      2 -12 imp:n=1 u=7  $top pin
234 4 -7.86     -2 3 -13 imp:n=1 u=7  $spacer
235 4 -7.86     -3 4 -14 imp:n=1 u=7  $top cladding
236 4 -7.86     -4 5 -14 imp:n=1 u=7  $inner spacer
237 2  -1.56     -5 6 -14 imp:n=1 u=7   $upper graphite plug
238 105 0.0974108 -6 7 -14 15 imp:n=1 u=7  $8.5 w/o fuel
239 2  -1.56     -7 8 -14 imp:n=1 u=7   $lower graphite plug
240 4 -7.86     -8 9 -14 imp:n=1 u=7  $inner spacer
241 4 -7.86    -9 10 -14 imp:n=1 u=7   $bottom cladding
242 4 -7.86       -10 -12 imp:n=1 u=7  $bottom pin
243 4 -7.86      -3 10 14 -31 imp:n=1 u=7  $side cladding
```

```
244 1 -1      -2 500 13 imp:n=1 u=7  $upper grid plate
245 3 -2.7        12 -501 imp:n=1 u=7  $lower grid plate
246 1 -1     (-430 2 12):(-12 -430 1)   imp:n=1 u=7 $water above gridplate
247 1 -1        -500 3 13 -31 imp:n=1 u=7   $water below gridplate
248 1 -1       -10 501 12 -31 imp:n=1 u=7   $water above lower gridplate
249 5 -5.8       -15 -6 7 imp:n=1 u=7  $zr plug
293 1 -1     31 -500 501 imp:n=1 u=7  $water around fuel rod
c
c %%%%%%%%%%%%%%%%%%%%%%%%%%%%%
c  Aluminum fuel rod universe 8.0 w/o G ring
c %%%%%%%%%%%%%%%%%%%%%%%%%%%%%
c
250    3 -2.7     -12 2 imp:n=1 u=8  $top pin
251    3 -2.7   -2 -13 16 imp:n=1 u=8  $spacer
252    3 -2.7  -16 3 -22 imp:n=1 u=8  $top claddng
253    3 -2.7  -3 18 -22 imp:n=1 u=8  $inner spacer
254    2 -1.56  -18 23 -22 imp:n=1 u=8  $upper graphite
255   10 .161768 -23 19 -22 imp:n=1 u=8  $sm poison
256 106 0.0766921 -19 20 -22 imp:n=1 u=8  $8 w/o fuel
257   10 .161768 -20 24 -22 imp:n=1 u=8  $sm Poison
258    2 -1.56  -24 8 -22 imp:n=1 u=8  $lower graphite
259    3 -2.7  -8 10 -22 imp:n=1 u=8  $lower cladding
260    3 -2.7     -10 -12 imp:n=1 u=8  $bottom pin
261    3 -2.7   -16 10 22 -32 imp:n=1 u=8  $side cladding
262    1 -1   -2 500 13 imp:n=1 u=8  $upper gridplate
263    3 -2.7  12 -501 imp:n=1 u=8  $lower gridplate
264    1 -1 (-430 2 12):(-12 -430 1)  imp:n=1 u=8 $water above upper gridplate
265    1 -1  -500 16 13 -32 imp:n=1 u=8   $water blow upper gridplate
266    1 -1  -10 501 12 -32 imp:n=1 u=8   $water above lower gridplate
296    1 -1     32 -500 501 imp:n=1 u=8  $water around fuel rod
c
c %%%%%%%%%%%%%%%%%%%%%%%%%%%%%
c  Stainless steel fuel rod universe 12 w/o fresh
c %%%%%%%%%%%%%%%%%%%%%%%%%%%%%
c
267 4 -7.86      2 -12 imp:n=1 u=9  $top pin
268 4 -7.86     -2 3 -13 imp:n=1 u=9  $spacer
269 4 -7.86     -3 4 -14 imp:n=1 u=9  $top cladding
270 4 -7.86     -4 5 -14 imp:n=1 u=9  $inner spacer
271 2  -1.56     -5 6 -14 imp:n=1 u=9  $upper graphite plug
272 110 0.0967479 -6 7 -14 15 imp:n=1 u=9 $12 w/o fuel
273 2  -1.56     -7 8 -14 imp:n=1 u=9  $lower graphite plug
274 4 -7.86     -8 9 -14 imp:n=1 u=9  $inner spacer
275 4 -7.86    -9 10 -14 imp:n=1 u=9  $bottom cladding
276 4 -7.86       -10 -12 imp:n=1 u=9  $bottom pin
278 4 -7.86      -3 10 14 -31 imp:n=1 u=9  $side cladding
279 1 -1      -2 500 13 imp:n=1 u=9  $upper grid plate
280 3 -2.7     12 -501 imp:n=1 u=9  $lower grid plate
281 1 -1     (-430 2 12):(-12 -430 1) imp:n=1 u=9  $water above gridplate
282 1 -1        -500 3 13 -31 imp:n=1 u=9  $water below gridplate
283 1 -1       -10 501 12 -31 imp:n=1 u=9  $water above lower gridplate
284 5 -5.8       -15 -6 7 imp:n=1 u=9 $zr plug
294 1 -1     31 -500 501 imp:n=1 u=9  $water around fuel rod
c
c %%%%%%%%%%%%%%%%%%%%%%%%%%%%%
c  Aluminum fuel rod universe 8.0 w/o fresh
c %%%%%%%%%%%%%%%%%%%%%%%%%%%%%
c
520    3 -2.7     -12 2 imp:n=1 u=15  $top pin
521    3 -2.7   -2 -13 16 imp:n=1 u=15  $spacer
522    3 -2.7  -16 3 -22 imp:n=1 u=15  $top claddng
523    3 -2.7  -3 18 -22 imp:n=1 u=15  $inner spacer
524    2 -1.56  -18 23 -22 imp:n=1 u=15  $upper graphite
```

```
525   10 .161768 -23 19 -22 imp:n=1 u=15  $sm poison
526 111 0.076689132 -19 20 -22 imp:n=1 u=15  $8 w/o fuel
527   10 .161768 -20 24 -22 imp:n=1 u=15  $sm Poison
528    2 -1.56  -24 8 -22 imp:n=1 u=15  $lower graphite
529    3 -2.7  -8 10 -22 imp:n=1 u=15  $lower cladding
530    3 -2.7     -10 -12 imp:n=1 u=15  $bottom pin
531    3 -2.7   -16 10 22 -32 imp:n=1 u=15  $side cladding
532    1 -1   -2 500 13 imp:n=1 u=15  $upper gridplate
533    3 -2.7  12 -501 imp:n=1 u=15  $lower gridplate
534    1 -1 (-430 2 12):(-12 -430 1)  imp:n=1 u=15 $water above upper gridplate
535    1 -1  -500 16 13 -32 imp:n=1 u=15   $water blow upper gridplate
536    1 -1  -10 501 12 -32 imp:n=1 u=15   $water above lower gridplate
537    1 -1     32 -500 501 imp:n=1 u=15  $water around fuel rod
c
c %%%%%%%%%%%%%%%%%%%%%%%%%%%%%
c  water cylinder
c %%%%%%%%%%%%%%%%%%%%%%%%%%%%%
c
290 1 -1 -30 501 imp:n=1  u=14
291 3 -2.7 -30 -501 imp:n=1  u=14
c
c %%%%%%%%%%%%%%%%%%%%%%%%%%%%%
c  full at grid positions
c %%%%%%%%%%%%%%%%%%%%%%%%%%%%%
c
c b ring
100 0 -100 -1 11 fill=1(1) imp:n=1 $b-1
101 0 -101 -1 11 fill=1(2) imp:n=1 $b-2
102 0 -102 -1 11 fill=1(3) imp:n=1 $b-3
103 0 -103 -1 11 fill=1(4) imp:n=1 $b-4
104 0 -104 -1 11 fill=1(5) imp:n=1 $b-5
105 0 -105 -1 11 fill=1(6) imp:n=1 $b-6
c
c c-ring
106 0 -106 -1 11 fill=2(7) imp:n=1
107 0 -107 -1 11 fill=4(8) imp:n=1
108 0 -108 -1 11 fill=4(9) imp:n=1
109 0 -109 -1 11 fill=4(10) imp:n=1
110 0 -110 -1 11 fill=4(11) imp:n=1
111 0 -111 -1 11 fill=2(12) imp:n=1
112 0 -112 -1 11 fill=2(13) imp:n=1
113 0 -113 -1 11 fill=2(14) imp:n=1
114 0 -114 -1 11 fill=2(15) imp:n=1
115 0 -115 -1 11 fill=2(16) imp:n=1
116 0 -116 -430 431 fill=13(203) imp:n=1
117 0 -117 -430 431 fill=12(204) imp:n=1
c
c d ring
118 0 -118 -430 431 fill=11(201) imp:n=1
119 0 -119 -430 431 fill=10(202) imp:n=1
120 0 -120 -1 11 fill=5(21) imp:n=1
121 0 -121 -1 11 fill=2(22) imp:n=1
122 0 -122 -1 11 fill=5(23) imp:n=1
123 0 -123 -1 11 fill=5(24) imp:n=1
124 0 -124 -1 11 fill=5(25) imp:n=1
125 0 -125 -1 11 fill=5(26) imp:n=1
126 0 -126 -1 11 fill=5(27) imp:n=1
127 0 -127 -1 11 fill=5(28) imp:n=1
128 0 -128 -1 11 fill=5(29) imp:n=1
129 0 -129 -1 11 fill=5(30) imp:n=1
130 0 -130 -1 11 fill=5(31) imp:n=1
131 0 -131 -1 11 fill=5(32) imp:n=1
132 0 -132 -1 11 fill=5(33) imp:n=1
```

```
133 0 -133 -1 11 fill=2(34) imp:n=1
134 0 -134 -1 11 fill=5(35) imp:n=1
135 0 -135 -1 11 fill=5(36) imp:n=1
c
c e ring
136 0 -136 -1 11 fill=6(37) imp:n=1
137 0 -137 -1 11 fill=6(38) imp:n=1
138 0 -138 -1 11 fill=6(39) imp:n=1
139 0 -139 -1 11 fill=6(40) imp:n=1
140 0 -140 -1 11 fill=6(41) imp:n=1
141 0 -141 -1 11 fill=6(42) imp:n=1
142 0 -142 -1 11 fill=6(43) imp:n=1
143 0 -143 -1 11 fill=6(44) imp:n=1
144 0 -144 -1 11 fill=6(45) imp:n=1
145 0 -145 -1 11 fill=6(46) imp:n=1
146 0 -146 -1 11 fill=6(47) imp:n=1
147 0 -147 -1 11 fill=6(48) imp:n=1
148 0 -148 -1 11 fill=6(49) imp:n=1
149 0 -149 -1 11 fill=6(50) imp:n=1
150 0 -150 -1 11 fill=6(51) imp:n=1
151 0 -151 -1 11 fill=6(52) imp:n=1
152 0 -152 -1 11 fill=6(53) imp:n=1
153 0 -153 -1 11 fill=6(54) imp:n=1
154 0 -154 -1 11 fill=6(55) imp:n=1
155 0 -155 -1 11 fill=6(56) imp:n=1
156 0 -156 -1 11 fill=6(57) imp:n=1
157 0 -157 -1 11 fill=6(58) imp:n=1
158 0 -158 -1 11 fill=6(59) imp:n=1
159 0 -159 -1 11 fill=6(60) imp:n=1
c
c f ring
160 0 -160 -1 11 fill=3(61) imp:n=1
161 0 -161 -1 11 fill=3(62) imp:n=1
162 0 -162 -1 11 fill=3(63) imp:n=1
163 0 -163 -1 11 fill=3(64) imp:n=1
164 0 -164 -1 11 fill=3(65) imp:n=1
165 0 -165 -1 11 fill=3(66) imp:n=1
166 0 -166 -1 11 fill=3(67) imp:n=1
167 0 -167 -1 11 fill=3(68) imp:n=1
168 0 -168 -1 11 fill=3(69) imp:n=1
169 0 -169 -1 11 fill=3(70) imp:n=1
170 0 -170 -1 11 fill=3(71) imp:n=1
171 0 -171 -1 11 fill=3(72) imp:n=1
172 0 -172 -1 11 fill=3(73) imp:n=1
173 0 -173 -1 11 fill=3(74) imp:n=1
174 0 -174 -1 11 fill=3(75) imp:n=1
175 0 -175 -1 11 fill=3(76) imp:n=1
176 0 -176 -1 11 fill=3(77) imp:n=1
177 0 -177 -1 11 fill=3(78) imp:n=1
178 0 -178 -1 11 fill=3(79) imp:n=1
179 0 -179 -1 11 fill=3(80) imp:n=1
180 0 -180 -1 11 fill=3(81) imp:n=1
181 0 -181 -1 11 fill=3(82) imp:n=1
182 0 -182 -1 11 fill=3(83) imp:n=1
183 0 -183 -1 11 fill=3(84) imp:n=1
184 0 -184 -1 11 fill=3(85) imp:n=1
185 0 -185 -1 11 fill=3(86) imp:n=1
186 0 -186 -1 11 fill=3(87) imp:n=1
187 0 -187 -1 11 fill=3(88) imp:n=1
188 0 -188 -1 11 fill=3(89) imp:n=1
189 0 -189 -1 11 fill=3(90) imp:n=1
c
c g ring
```

```
190 0 -190 -1 11 fill=7(91) imp:n=1
191 0 -191 -1 11 fill=7(92) imp:n=1
192 0 -192 -1 11 fill=7(93) imp:n=1
193 0 -193 -1 11 fill=8(94) imp:n=1
194 0 -194 -1 11 fill=7(95) imp:n=1
195 0 -195 -1 11 fill=7(96) imp:n=1
196 0 -196 -1 11 fill=7(97) imp:n=1
197 0 -197 -1 11 fill=8(98) imp:n=1
198 0 -198 -1 11 fill=7(99) imp:n=1
199 0 -199 -1 11 fill=7(100) imp:n=1
200 0 -200 -1 11 fill=7(101) imp:n=1
201 0 -201 -1 11 fill=7(102) imp:n=1
202 0 -202 -1 11 fill=7(103) imp:n=1
203 0 -203 -1 11 fill=8(104) imp:n=1
204 0 -204 -1 11 fill=7(105) imp:n=1
205 0 -205 -1 11 fill=7(106) imp:n=1
206 0 -206 -1 11 fill=7(107) imp:n=1
207 0 -207 -1 11 fill=8(108) imp:n=1
208 0 -208 -1 11 fill=7(109) imp:n=1
209 0 -209 -1 11 fill=8(110) imp:n=1
210 0 -210 -1 11 fill=7(111) imp:n=1
211 0 -211 -1 11 fill=7(112) imp:n=1
212 0 -212 -1 11 fill=7(113) imp:n=1
213 0 -213 -1 11 fill=8(114) imp:n=1
214 0 -214 -1 11 fill=7(115) imp:n=1
215 0 -215 -1 11 fill=7(116) imp:n=1
216 0 -216 -1 11 fill=7(117) imp:n=1
217 0 -217 -1 11 fill=8(118) imp:n=1
218 0 -218 -1 11 fill=8(119) imp:n=1
219 0 -219 -1 11 fill=7(120) imp:n=1
220 0 -220 -1 11 fill=7(121) imp:n=1
221 0 -221 -1 11 fill=7(122) imp:n=1
222 0 -222 -1 11 fill=8(123) imp:n=1
223 0 -223 -1 11 fill=7(124) imp:n=1
224 0 -224 -1 11 fill=7(125) imp:n=1
225 0 -225 -1 11 fill=7(126) imp:n=1
c
c %%%%%%%%%%%%%%%%%%%%%%%%%%%%%%
c Central Thimble
c %%%%%%%%%%%%%%%%%%%%%%%%%%%%%%
c
300 4 -7.86 300 -301 -302 11 imp:n=1
301 7 -1.0467e-3 -300 -302 1003 imp:n=1
c
c %%%%%%%%%%%%%%%%%%%%%%%%%%%%%%
c exp beam tube
c %%%%%%%%%%%%%%%%%%%%%%%%%%%%%%
c
c 310 4 -7.86 600 -601 -602 1001 imp:n=1
c 311 7 -1.0467e-3 -600 -604 603 imp:n=1
c 312 9 -11.34 -603 -600 1001 imp:n=1
c 313 7 -1.0467e-3 -600 604 -602 imp:n=1
c
c
c %%%%%%%%%%%%%%%%%%%%%%%%%%%%%%
c core shell/liner
c %%%%%%%%%%%%%%%%%%%%%%%%%%%%%%
c
 400 3 -2.7 410 -411 -2 11 imp:n=1
c
c %%%%%%%%%%%%%%%%%%%%%%%%%%%%%%
c reflector
c %%%%%%%%%%%%%%%%%%%%%%%%%%%%%%
```

```
c
410 3 -2.7 -315 422 -420 425 imp:n=1  $top edge of reflector covering
411 3 -2.7 -422 421 -420 423 imp:n=1  $outer edge of reflector covering
412 3 -2.7 423 -419 -421 411 imp:n=1  $bottom edge of reflector covering
c 413 3 -2.7 -424 427 425 -422 imp:n=1   $edge near lz
c 414 3 -2.7 411 -424 428 -427 imp:n=1  $edge under lz
415 15 -1.69786 (411 419 -421 -427):(425 -421 -422 427) imp:n=1   $graphite 0.085205
atom/cc = 1.69786 g/cc
c
c
c %%%%%%%%%%%%%%%%%%%%%%%%%%%%%
c Lazy susan
c %%%%%%%%%%%%%%%%%%%%%%%%%%%%%
c
c 420 7  -1.0467e-3 411 -425 -426 427 imp:n=1
c 420 13 -0.540837 411 -425 -426 427 imp:n=1
420 7 -1.0467e-3 -429 411 -312 428 imp:n=1   $ 1 inch air gap
421 3 -2.7 -310 429 -2 428 imp:n=1  $ inner wall
322 3 -2.7 -428 427 411 -425 imp:n=1  $ bottom wall
323 3 -2.7 311 -314 428 -425 imp:n=1  $ outer wall
324 3 -2.7 (-314 2 411 -311):(-313 312 -311 310):
      (313 -311 310 -2) imp:n=1  $ upper wall/aluminum block for air
325 7 -1.0467e-3 310 -311 -312 428 imp:n=1  $ air in lazy susan
326 3 -2.7 (-2 312 -429 411) imp:n=1  $ aluminum block on top of air gap and aluminum
above air in lazy susan
c
c
c %%%%%%%%%%%%%%%%%%%%%%%%%%%%%
c CT can for flux foils
c %%%%%%%%%%%%%%%%%%%%%%%%%%%%%
c
c
c 430 7 -1.0467E-3 -510 -512 514 imp:n=1 $air
c 430 14 0.000932439 -510 -512 514 imp:n=1 $ Ho-155
c 431 3 -2.7 (-511 512 -513):(-511 -514 515):
c      (-511 510 -512 514) imp:n=1  $al
c
c
c %%%%%%%%%%%%%%%%%%%%%%%%%%%%%
c control rods
c %%%%%%%%%%%%%%%%%%%%%%%%%%%%%
c
c shim 2
448 12 -1 462:-452:(451 452 -462) u=10 imp:n=1  $ water
c 449 1 -1  -452 u=10 imp:n=1
450 4 -7.86 -462 461 -450 u=10 imp:n=1  $stainless steel
451 2 -1.75 -461 460 -450 u=10 imp:n=1  $ Graphite
452 4 -7.86 -460 459 -450 u=10 imp:n=1  $ stainless steel spacer
453 6 -1.72066 -474 458 -473 u=10 imp:n=1 $ poison
700 6 -1.72066 -475 474 -483 u=10 imp:n=1
701 6 -1.72066 -476 475 -484 u=10 imp:n=1
702 6 -1.72066 -459 476 -485 u=10 imp:n=1
454 4 -7.86 -458 457 -450 u=10 imp:n=1  $ stainless steel spacer
455 5 -5.8 -15 -457 456 u=10 imp:n=1  $zr plug
456 109 0.0974388 15 -457 456 -450 u=10 imp:n=1 $ fuel
457 4 -7.86 -456 455 -450 u=10 imp:n=1  $ stainless steel spacer
458 2 -1.75 -455 454 -450 u=10 imp:n=1  $ graphite
459 4 -7.86 -454 -450 452 u=10 imp:n=1  $ stainless steel spacer
460 4 -7.86 450 -462 452 -451 u=10 imp:n=1  $Stainless steel
4061 2 -1.75 -450 -459 458 #453 #700 #701 #702 u=10 imp:n=1 $ graphite around poison
c
c shim 1
446 12 -1 462:-452:(451 452 -462) u=11 imp:n=1
```

```
c 447 1 -1 -452 u=11 imp:n=1
461 4 -7.86 -462 461 -450 u=11 imp:n=1
462 2 -1.75 -461 460 -450 u=11 imp:n=1    $ graphite
463 4 -7.86 -460 459 -450 u=11 imp:n=1
464 6 -1.72066 -474 458 -472 u=11 imp:n=1   $ Poison
703 6 -1.72066 -475 474 -480 u=11 imp:n=1
704 6 -1.72066 -476 475 -481 u=11 imp:n=1
705 6 -1.72066 -459 476 -482 u=11 imp:n=1  $ End Poison
465 4 -7.86 -458 457 -450 u=11 imp:n=1
466 5 -5.8 -15 -457 456 u=11 imp:n=1
467 108 0.0973729 15 -457 456 -450 u=11 imp:n=1
468 4 -7.86 -456 455 -450 u=11 imp:n=1
469 2 -1.75 -455 454 -450 u=11 imp:n=1    $ graphite
470 4 -7.86 -454 -450 452 u=11 imp:n=1
471 4 -7.86 450 -462 452 -451 u=11 imp:n=1
4072 2 -1.75 -459 458 -450 #464 #703 #704 #705  u=11 imp:n=1 $ graphite around
c
c reg rod
444 12 -1 462:-452:(451 452 -462) u=12 imp:n=1
c 445 1 -1 -452 u=12 imp:n=1
472 4 -7.86 -462 461 -450 u=12 imp:n=1
473 2 -1.75 -461 460 -450 u=12 imp:n=1  $graphite
474 4 -7.86 -460 459 -450 u=12 imp:n=1
475 6 -1.72066 -474 458 -453 u=12 imp:n=1  $poison
706 6 -1.72066 -475 474 -453 u=12 imp:n=1
707 6 -1.72066 -476 475 -453 u=12 imp:n=1
708 6 -1.72066 -459 476 -453 u=12 imp:n=1 $ End Poison
476 4 -7.86 -458 457 -450 u=12 imp:n=1
477 5 -5.8 -15 -457 456 u=12 imp:n=1
478 107 0.0973809 15 -457 456 -450 u=12 imp:n=1
479 4 -7.86 -456 455 -450 u=12 imp:n=1
480 2 -1.75 -455 454 -450 u=12 imp:n=1   $grahite
481 4 -7.86 -454 -450 452 u=12 imp:n=1
482 4 -7.86 450 -462 452 -451 u=12 imp:n=1
4083 2 -1.75 453 -450 -459 458 u=12 imp:n=1 $ graphite around poison
c
c transcient rod
483 3 -2.7 -462 468 -470 u=13 imp:n=1
484 2 -1.75 -468 467 -470 u=13 imp:n=1  $graphite
485 3 -2.7 -467 466 -470 u=13 imp:n=1
486 6 -1.72066 -477 465 -471 u=13 imp:n=1   $ Poison
709 6 -1.72066 -478 477 -486 u=13 imp:n=1
710 6 -1.72066 -479 478 -487 u=13 imp:n=1
711 6 -1.72066 -466 479 -488 u=13 imp:n=1 $End Poison
487 3 -2.7 -465 464 -470 u=13 imp:n=1
488 7  -1.0467e-3 -464 454 -470 u=13 imp:n=1
489 3 -2.7 -454 -470 452 u=13 imp:n=1
490 3 -2.7 -469 470 -462 452 u=13 imp:n=1
491 12 -1 462:-452:(469 -462 452) u=13 imp:n=1
4092 2 -1.75 -470 465 -466 #486 #709 #710 #711 u=13 imp:n=1  $ graphite around poison
c 492 1 -1 -452 u=13 imp:n=1
c
c %%%%%%%%%%%%%%%%%%%%%%%%%%%%
c water
c %%%%%%%%%%%%%%%%%%%%%%%%%%%%
c
c water in core
500 1 -1 (-410 501 -500
      301 $ central thimble
      105 104 103 102 101 100 $b-ring
      106 107 108 109 110 111 112 113 114 115  $ c-ring  450 474 462 486
      116 119 118 117 120 121 122 123 124 125 126 127 128 129 130
      131 132 133 134 135 $ d-ring
```

```
      136 137 138 139 140 141 142 143 144 145 146 147 148 149
      150 151 152 153 154 155 156 157 158 159 $e ring
      160 161 162 163 164 165 166 167 168 169 170 171
      172 173 174 175 176 177 178 179 180 181 182 183
      184 185 186 187 188 189 $ f ring
      190 191 192 193 194 195 196 197 198 199 200 201 202
      203 204 205 206 207 208 209 210 211 212 213 214 215 216
      217 218 219 220 221 222 223 224 225) $ g ring
      imp:n=1
c
c water out side core
501 12 -1
      (-411 -1 2 $2
      301 $ central thimble
      105 104 103 102 101 100 $b-ring
      106 107 108 109 110 111 112 113 114 115   $ c-ring   450 474 462 486
      116 119 118 117 120 121 122 123 124 125 126 127
      128 129 130 131 132 133 134 135 $ d-ring
      136 137 138 139 140 141 142 143 144 145 146 147 148 149
      150 151 152 153 154 155 156 157 158 159 $e ring
      160 161 162 163 164 165 166 167 168 169 170 171
      172 173 174 175 176 177 178 179 180 181 182 183
      184 185 186 187 188 189 $ f ring
      190 191 192 193 194 195 196 197 198 199 200 201 202
      203 204 205 206 207 208 209 210 211 212 213 214 215 216
      217 218 219 220 221 222 223 224 225): $ g ring
      (-119 -431 1001):(-118 -431 1001):  $shim 1 and shim 2
      (-117 -431 1001):(-116 -431 1001):  $reg and pulse rods
      (-411 -1003 1 301 116 117 118 119): $water in the control area to compensate for
movement
      (-425 314 -1003 411):  $water above lazy susan
      (-116 430 -1003):
      (-119 430 -1003):(-118 430 -1003):(-117 430 -1003): $water in control rod area
for movement
      (11 -423 411 -420): $water below reflector
c  This next part has the exp beam tube added to it as surface 601
c take out 601 if you want to remove the exp beam tube
      (-1000 425 315 -1003):(-1000 420 -2 11):
      (452 -431 1001 -1000):(-11 -1000 1001 116 117 118 119) $ below core
      imp:n=1
c
c water in ct
502 1 -1 (-1003 11 -300) $ 511) :
c      ( -511 -515 11) : (-511 513 -1003)  $ CT can in CT for flux foils
      imp:n=1
c
c %%%%%%%%%%%%%%%%%%%%%%%%%%%%
c gridplates
c %%%%%%%%%%%%%%%%%%%%%%%%%%%%
c upper gridplate
600 3 -2.7 -410 -2 500
      301 $ central thimble
      105 104 103 102 101 100 $b-ring
      106 107 108 109 110 111 112 113 114 115   $ c-ring   450 474 462 486
      116 119 118 117 120 121 122 123 124 125 126 127
      128 129 130 131 132 133 134 135 $ d-ring
      136 137 138 139 140 141 142 143 144 145 146 147 148 149
      150 151 152 153 154 155 156 157 158 159 $e ring
      160 161 162 163 164 165 166 167 168 169 170 171
      172 173 174 175 176 177 178 179 180 181 182 183
      184 185 186 187 188 189 $ f ring
      190 191 192 193 194 195 196 197 198 199 200 201 202
      203 204 205 206 207 208 209 210 211 212 213 214 215 216
```

```
      217 218 219 220 221 222 223 224 225 $ g ring
      imp:n=1
c
c lower gridplate
601 3 -2.7 -410 11 -501
      301 $ central thimble
      105 104 103 102 101 100 $b-ring
      106 107 108 109 110 111 112 113 114 115   $ c-ring   450 474 462 486
      116 119 118 117 120 121 122 123 124 125 126 127
      128 129 130 131 132 133 134 135 $ d-ring
      136 137 138 139 140 141 142 143 144 145 146 147 148 149
      150 151 152 153 154 155 156 157 158 159 $e ring
      160 161 162 163 164 165 166 167 168 169 170 171
      172 173 174 175 176 177 178 179 180 181 182 183
      184 185 186 187 188 189 $ f ring
      190 191 192 193 194 195 196 197 198 199 200 201 202
      203 204 205 206 207 208 209 210 211 212 213 214 215 216
      217 218 219 220 221 222 223 224 225 $ g ring
      imp:n=1
c
c %%%%%%%%%%%%%%%%%%%%%%%%%%%%%
c air above water
c %%%%%%%%%%%%%%%%%%%%%%%%%%%%%
c
900 7 -1.0467e-3 (1003 -302 -1000 301):
     (-601 -302 602) imp:n=1
c 601 is the outer surface of the exp beam tube
c
c %%%%%%%%%%%%%%%%%%%%%%%%%%%%%
c void
c %%%%%%%%%%%%%%%%%%%%%%%%%%%%%
1000 0 302:-1001:1000  imp:n=0

c ********************************************************************
c                              Surfaces
c ********************************************************************
c
c %%%%%%%%%%%%%%%%%%%%%%%%%%%%%
c  Stainless steel fuel rod
c %%%%%%%%%%%%%%%%%%%%%%%%%%%%%
c
c horizontal surfaces starting with the top fuel pin and working down
c 1  pz  37.7698      $top surface for pin
c 2  pz  34.18          $bottom surface for pin
c 3  pz  30.6324      $top surface of cladding
c 4  pz  30.5816      $inner surface of top cladding
c 5  pz  29.3624      $upper surface of graphite
c 6  pz  20.5486      $upper surface of fuel
c 7  pz -17.5514     $lower surface of fuel
c 8  pz -26.3652     $lower surface of bottom graphite
c 9  pz -27.6352     $inner surface of bottom cladding
c 10  pz -27.686     $outer surface of bottom cladding
c 11  pz -34.18       $bottom surface of lower pin
c
c
 1  pz  36.3812     $top surface for pin
 2  pz  33.2189     $bottom surface for upper pin 32.6814
 3  pz  29.1338     $top surface of cladding
 4  pz  29.083      $inner surface of top cladding
 5  pz  27.8638     $upper surface of graphite
 6  pz  19.05       $upper surface of fuel
 7  pz -19.05       $lower surface of fuel
 8  pz -27.8638     $lower surface of bottom graphite
```

```
 9  pz -29.1338      $inner surface of bottom cladding
10  pz -29.1846      $outer surface of bottom cladding
11  pz -35.6786      $bottom surface of lower pin
c
c vertical surfaces
12  cz 0.7874        $top and bottom pins
13  cz 0.92          $spacer
c 14  cz 1.85325       $inner surface for cladding
14  cz 1.8161        $ inner surface cladding
15  cz 0.3175        $ zr plug
31  cz 1.8669        $ ss outer surface
c
c %%%%%%%%%%%%%%%%%%%%%%%%%%%%
c  Aluminum fuel rod
c %%%%%%%%%%%%%%%%%%%%%%%%%%%%
c
c horizontal surfaces
16 pz 29.21 $ upper pin
c 17 pz 29.1338
18 pz 27.9392 $ lower
19 pz 17.78
20 pz -17.78
23 pz 17.907
24 pz -17.907
c 21 pz -27.8638
c
c vertical surfaces
c 22 cz 1.83642 $inner surface cladding
22 cz 1.8034 $ inner surface cladding
32 cz 1.8796 $ outter surface of cladding
c
c vertical surface for water to replace fuel elements
30 cz 2.1
c
c
c %%%%%%%%%%%%%%%%%%%%%%%%%%%%
c  grid positions
c %%%%%%%%%%%%%%%%%%%%%%%%%%%%
c
c
c b ring
100 c/z  1.0465 3.9141 1.91135
101 c/z  3.9141 1.0465 1.91135
102 c/z  -2.8677 2.8677 1.91135
103 c/z  -1.0465 -3.9141 1.91135
104 c/z  -3.9141 -1.0465 1.91135
105 c/z  2.8677 -2.8677 1.91135
c
c c ring
106 c/z 7.98068 0  1.91135
107 c/z 6.91134 3.99034 1.91135
108 c/z -6.91134 3.99034 1.91135
109 c/z -6.91134 -3.99034 1.91135
110 c/z 6.91134 -3.99034 1.91135
111 c/z 3.99034 6.91134 1.91135
112 c/z 3.99034 -6.91134 1.91135
113 c/z -3.99034 6.91134  1.91135
114 c/z -3.99034 -6.91134 1.91135
115 c/z -7.98068 0  1.91135
116 c/z 0.0 -7.98068 1.91135
c 116 c/z 0.0 -7.98068 1.74625
117 c/z 0.0 7.98068 1.91135
c 117 c/z 0.0 7.98068 1.74625
```

```
c
c d ring
118 c/z 11.9456 0.0 1.91135
c 118 c/z 11.9456 0.0 1.74625
119 c/z -11.9456 0.0 1.91135
c 119 c/z -11.9456 0.0 1.74625
120 c/z  11.2243 4.0843 1.91135
121 c/z  -11.2243 -4.0843 1.91135
122 c/z  -11.2243 4.0843 1.91135
123 c/z  11.2243 -4.0843 1.91135
124 c/z 9.1516 7.6784 1.91135
125 c/z -9.1516 -7.6784 1.91135
126 c/z -9.1516 7.6784 1.91135
127 c/z 9.1516 -7.6784 1.91135
128 c/z 5.9741 10.3454 1.91135
129 c/z -5.9741 -10.3454 1.91135
130 c/z -5.9741 10.3454 1.91135
131 c/z 5.9741 -10.3454 1.91135
132 c/z -2.0726 -11.3030 1.91135
133 c/z 2.0726 11.3030 1.91135
134 c/z 2.2225 -11.7653 1.91135 $D-5 (triflut)
135 c/z -2.2225 11.7653 1.91135 $D-14 (triflut)
c
c e ring
136 c/z 15.9156 0 1.91135
137 c/z -15.9156 0 1.91135
138 c/z 15.3721 4.1199 1.91135
139 c/z -15.3721 4.1199 1.91135
140 c/z 15.3721 -4.1199 1.91135
141 c/z -15.3721 -4.1199 1.91135
142 c/z 13.7820 7.9578 1.91135
143 c/z -13.7820 7.9578 1.91135
144 c/z 13.7820 -7.9578 1.91135
145 c/z -13.7820 -7.9578 1.91135
146 c/z 11.2547 11.2547 1.91135
147 c/z -11.2547 11.2547 1.91135
148 c/z 11.2547 -11.2547 1.91135
149 c/z -11.2547 -11.2547 1.91135
150 c/z 7.9578 13.7820 1.91135
151 c/z -7.9578 13.7820 1.91135
152 c/z 7.9578 -13.7820 1.91135
153 c/z -7.9578 -13.7820 1.91135
154 c/z 4.1199 15.3721 1.91135
155 c/z -4.1199 -15.3721 1.91135
156 c/z -0.2413 15.2019 1.91135 $E-7 (triflut)
157 c/z 0.2413 -15.2019 1.91135 $E-19 (triflut)
158 c/z 4.2062 -15.2019 1.91135 $E-18 (triflut)
159 c/z -4.2062 15.2019 1.91135 $E-6 (triflut)
c
c f ring
160 c/z 19.8882 0 1.91135
161 c/z 19.4539 4.1351 1.91135
162 c/z 18.1686 8.0899 1.91135
163 c/z 16.0909 11.6916 1.91135
164 c/z 13.3071 14.77803 1.91135
165 c/z 9.9441 17.2237 1.91135
166 c/z 6.1468 18.9154 1.91135
167 c/z 2.0777 19.7790 1.91135
168 c/z -19.8882 0 1.91135
169 c/z -19.4539 4.1351 1.91135
170 c/z -18.1686 8.0899 1.91135
171 c/z -16.0909 11.6916 1.91135
172 c/z -13.3071 14.77803 1.91135
```

```
173 c/z -9.9441 17.2237 1.91135
174 c/z -6.1468 18.9154 1.91135
175 c/z -2.0777 19.7790 1.91135
176 c/z 19.4539 -4.1351 1.91135
177 c/z 18.1686 -8.0899 1.91135
178 c/z 16.0909 -11.6916 1.91135
179 c/z 13.3071 -14.77803 1.91135
180 c/z 9.9441 -17.2237 1.91135
181 c/z 6.1468 -18.9154 1.91135
182 c/z 2.0777 -19.7790 1.91135
183 c/z -19.4539 -4.1351 1.91135
184 c/z -18.1686 -8.0899 1.91135
185 c/z -16.0909 -11.6916 1.91135
186 c/z -13.3071 -14.77803 1.91135
187 c/z -9.9441 -17.2237 1.91135
188 c/z -6.1468 -18.9154 1.91135
189 c/z -2.0777 -19.7790 1.91135
c
c g ring
190 c/z 23.8608 0 1.91135
191 c/z 23.4975 4.1427 1.91135
192 c/z 22.4206 8.1610 1.91135
193 c/z 20.6654 11.9304 1.91135
194 c/z 18.2778 15.3365 1.91135
195 c/z 15.3365 18.2778 1.91135
196 c/z 11.9304 20.6654 1.91135
197 c/z 8.1610 22.4206 1.91135
198 c/z 4.1427 23.4975 1.91135
199 c/z 0 23.8608 1.91135
200 c/z -23.8608 0 1.91135
201 c/z -23.4975 4.1427 1.91135
202 c/z -22.4206 8.1610 1.91135
203 c/z -20.6654 11.9304 1.91135
204 c/z -18.2778 15.3365 1.91135
205 c/z -15.3365 18.2778 1.91135
206 c/z -11.9304 20.6654 1.91135
207 c/z -8.1610 22.4206 1.91135
208 c/z -4.1427 23.4975 1.91135
209 c/z 23.4975 -4.1427 1.91135
210 c/z 22.4206 -8.1610 1.91135
211 c/z 20.6654 -11.9304 1.91135
212 c/z 18.2778 -15.3365 1.91135
213 c/z 15.3365 -18.2778 1.91135
214 c/z 11.9304 -20.6654 1.91135
215 c/z 8.1610 -22.4206 1.91135
216 c/z 4.1427 -23.4975 1.91135
217 c/z 0 -23.8608 1.91135
218 c/z -23.4975 -4.1427 1.91135
219 c/z -22.4206 -8.1610 1.91135
220 c/z -20.6654 -11.9304 1.91135
221 c/z -18.2778 -15.3365 1.91135
222 c/z -15.3365 -18.2778 1.91135
223 c/z -11.9304 -20.6654 1.91135
224 c/z -8.1610 -22.4206 1.91135
225 c/z -4.1427 -23.4975 1.91135
c
c %%%%%%%%%%%%%%%%%%%%%%%%%%%%%
c Central Thimble
c %%%%%%%%%%%%%%%%%%%%%%%%%%%%%
c
300 cz 1.7526
301 cz 1.905
302 pz 750  $ top of ct
```

```
c
c
c %%%%%%%%%%%%%%%%%%%%%%%%%%%%
c tank liner
c %%%%%%%%%%%%%%%%%%%%%%%%%%%%
c
c 410 cz 26.51125
410 cz 26.67 $ inner surface
c 411 cz 27.72833
411 cz 27.305 $ outer surface
c
c %%%%%%%%%%%%%%%%%%%%%%%%%%%%
c reflector
c %%%%%%%%%%%%%%%%%%%%%%%%%%%%
c
419 pz -27.5824
420 cz 56.03775
421 cz 54.2915
422 pz 28.2977
423 pz -29.3286
c 424 cz 33.17975
315 pz 30.0439 $ top surface of top cladding
c 316 pz
c
c %%%%%%%%%%%%%%%%%%%%%%%%%%%%
c Lazy susan
c %%%%%%%%%%%%%%%%%%%%%%%%%%%%
c
425 cz 37.465  $outer surface of outer wall
c 426 pz 31.9489 $ top of air portion of lazy susan
427 pz 4.6439 $ lower surface of bottom surface
428 pz 5.2789 $ upper surface of bottom surface
429 cz 29.845  $ outer surface of inner wall
310 cz 30.48   $ inner suface of inner wall
311 cz 36.83   $ inner surface of outer wall
312 pz 26.416  $ upper surface of 1 in gap
313 pz 31.3139 $ inner surface of top of air portion
314 pz 41.4739 $ very top of lazy susan
c
c %%%%%%%%%%%%%%%%%%%%%%%%%%%%
c control rods
c %%%%%%%%%%%%%%%%%%%%%%%%%%%%
c
430 pz 72.1136 $59.5406 $ upper move limit on control rods
431 pz -77.061 $-51.4828 $lower move limit on control rods
c
c 430 pz 76.945 $ upper move limit on control rods
c 431 pz -76.948 $lower move limit on control rods
c
c shim I, II, and reg rod
450 cz 1.69545 $ inner surface of cladding
c 451 cz 1.69545
c 451 cz 1.85325
451 cz 1.74625 $ outer surface of cladding
452 pz -77.0606
453 cz 1.69544 $ poison surface for reg rod
472 cz 0.68872 $ Poison for shim 1 Region 1
480 cz 1.22925 $ Region 2
481 cz 1.50638 $ Region 3
482 cz 1.64914 $ Region 4
473 cz 1.47259 $ Poison for shim 2
483 cz 1.57542 $ Region 2
484 cz 1.64335 $ Region 3
```

```
485 cz 1.68246 $ Region 4
454 pz -75.7398 $ bottome surface of bottom graphite
455 pz -61.7696 $ bottom surface of stainless steel spacer
456 pz -59.2298 $ bottom surface of fuel
457 pz -21.1298 $ bottom surface of stainless steel spacer
458 pz -19.8598 $ bottom surface of poison
459 pz 18.2402 $ top surface of poison
460 pz 19.5102 $ bottom surface of top graphite
461 pz 28.7622 $ top surface of  top graphite
462 pz 34.0136
c 463 pz 34.0644
c
c Boron Seperation Layers not transient rod
474 pz -10.3348
475 pz -0.8098
476 pz 8.7152
c
c transcient
464 pz -20.4948 $bottom surface of al spacer
465 pz -19.2248 $ bottom surface of poison
466 pz 18.8752 $ top surface of poison
467 pz 20.1452 $ bottom surface of graphite
468 pz 29.6702 $ top surface of graphite
469 cz 1.5875 $ outer surface of cladding
c 470 cz 1.5494 $ inner surface of cladding
470 cz 1.42875 $ cladding inner surface
471 cz 1.13556 $ poison for Region 1
486 cz 1.28442 $ poison for Region 2
487 cz 1.36849 $ poison for Region 3
488 cz 1.25724 $ Poison for Region 4
c
c Boron Seperation layers: Transient Rod
c
477 pz -9.6998
478 pz -0.1748
479 pz 9.3502
c
c %%%%%%%%%%%%%%%%%%%%%%%%%%%%%
c  gridplate horizontal lines
c %%%%%%%%%%%%%%%%%%%%%%%%%%%%%
c
c 500 pz 31.0939
500 pz 31.3139 $bottom surface of top grid
501 pz -33.7736 $top surface of bottom grid
c
c
c %%%%%%%%%%%%%%%%%%%%%%%%%%%%%
c  tube around flux foils in CT
c %%%%%%%%%%%%%%%%%%%%%%%%%%%%%
c
510 cz 1.27
511 cz 1.42875
c
c 8 inch can
c 512 pz 9.81
c 513 pz 11.1
c 514 pz -10.51
c 515 pz -11.78
c
c 12 inch can
512 pz 13.97
513 pz 15.24
514 pz -13.97
```

```
515 pz -15.24
c
c
c %%%%%%%%%%%%%%%%%%%%%%%%%%%%
c  experiment tube
c %%%%%%%%%%%%%%%%%%%%%%%%%%%%
c
 600 c/z 66 0 8.89  $tube with inner radius of 4 inches
 601 c/z 66 0 10.16  $outer radius of tube, 1 / 4 in thick
 602 pz 687.07  $top of tube (length of tube in cm 782.32)
 603 pz -30.5 $ surface for lead
 604 pz  60 $ surface for f2 tally for new source def
 605 c/z 66 0 .5
 606 c/z 66 0 1
 607 c/z 66 0 1.5
 608 c/z 66 0 2
 609 c/z 66 0 2.5
 610 c/z 66 0 3
 611 c/z 66 0 3.5
 612 c/z 66 0 4
 613 c/z 66 0 4.5
 614 c/z 66 0 5
 615 c/z 66 0 5.5
 616 c/z 66 0 6
 617 c/z 66 0 6.5
 618 c/z 66 0 7
 619 c/z 66 0 7.5
 620 c/z 66 0 8
 621 px 66
c
c
c
c %%%%%%%%%%%%%%%%%%%%%%%%%%%%
c tank boundry
c %%%%%%%%%%%%%%%%%%%%%%%%%%%%
1000 cz 115.57 $231.14
1001 pz -96.7486
c 1002 pz 672.8714
c water boundery
1003 pz 652.5514
c

c ***************************************************************************
c                                 Data
c ***************************************************************************
c
c %%%%%%%%%%%%%%%%%%%%%%%%%%%%
c transforms for fuel rods
c %%%%%%%%%%%%%%%%%%%%%%%%%%%%
c        x      y        z
c b ring
tr1 1.0465 3.9141 0
tr2 3.9141 1.0465 0
tr3 -2.8677 2.8677 0
tr4 -1.0465 -3.9141 0
tr5 -3.9141 -1.0465 0
tr6 2.8677 -2.8677 0
c c ring
c 7-18
tr7 7.98068 0  0
tr8 6.91134 3.99034 0
tr9 -6.91134 3.99034 0
tr10 -6.91134 -3.99034 0
```

```
tr11 6.91134 -3.99034 0
tr12 3.99034 6.91134 0
tr13 3.99034 -6.91134 0
tr14 -3.99034 6.91134 0
tr15 -3.99034 -6.91134 0
tr16 -7.98068 0  0
c tr17 0.0 -7.98068 0
c tr18 0.0 7.98068 0
c
c d ring
c tr19 11.9456 0 0
c tr20 -11.9456 0 0
tr21 11.2243 4.0843 0
tr22 -11.2243 -4.0843 0
tr23 -11.2243 4.0843 0
tr24 11.2243 -4.0843 0
tr25 9.1516 7.6784 0
tr26 -9.1516 -7.6784 0
tr27 -9.1516 7.6784 0
tr28 9.1516 -7.6784 0
tr29 5.9741 10.3454 0
tr30 -5.9741 -10.3454 0
tr31 -5.9741 10.3454 0
tr32 5.9741 -10.3454 0
tr33 -2.0726 -11.3030 0
tr34 2.0726 11.3030 0
tr35 2.2225 -11.7653 0
tr36 -2.2225 11.7653 0
c
c e ring
tr37 15.9156 0 0
tr38 -15.9156 0 0
tr39 15.3721 4.1199 0
tr40 -15.3721 4.1199 0
tr41 15.3721 -4.1199 0
tr42 -15.3721 -4.1199 0
tr43 13.7820 7.9578 0
tr44 -13.7820 7.9578 0
tr45 13.7820 -7.9578 0
tr46 -13.7820 -7.9578 0
tr47 11.2547 11.2547 0
tr48 -11.2547 11.2547 0
tr49 11.2547 -11.2547 0
tr50 -11.2547 -11.2547 0
tr51 7.9578 13.7820 0
tr52 -7.9578 13.7820 0
tr53 7.9578 -13.7820 0
tr54 -7.9578 -13.7820 0
tr55 4.1199 15.3721 0
tr56 -4.1199 -15.3721 0
tr57 -0.2413 15.2019 0
tr58 0.2413 -15.2019 0
tr59 4.2062 -15.2019 0
tr60 -4.2062 15.2019 0
c
c f ring
tr61 19.8882 0 0
tr62 19.4539 4.1351 0
tr63 18.1686 8.0899 0
tr64 16.0909 11.6916 0
tr65 13.3071 14.77803 0
tr66 9.9441 17.2237 0
tr67 6.1468 18.9154 0
```

```
tr68 2.0777 19.7790 0
tr69 -19.8882 0 0
tr70 -19.4539 4.1351 0
tr71 -18.1686 8.0899 0
tr72 -16.0909 11.6916 0
tr73 -13.3071 14.77803 0
tr74 -9.9441 17.2237 0
tr75 -6.1468 18.9154 0
tr76 -2.0777 19.7790 0
tr77 19.4539 -4.1351 0
tr78 18.1686 -8.0899 0
tr79 16.0909 -11.6916 0
tr80 13.3071 -14.77803 0
tr81 9.9441 -17.2237 0
tr82 6.1468 -18.9154 0
tr83 2.0777 -19.7790 0
tr84 -19.4539 -4.1351 0
tr85 -18.1686 -8.0899 0
tr86 -16.0909 -11.6916 0
tr87 -13.3071 -14.77803 0
tr88 -9.9441 -17.2237 0
tr89 -6.1468 -18.9154 0
tr90 -2.0777 -19.7790 0
c
c g ring
tr91 23.8608 0 0
tr92 23.4975 4.1427 0
tr93 22.4206 8.1610 0
tr94 20.6654 11.9304 0
tr95 18.2778 15.3365 0
tr96 15.3365 18.2778 0
tr97 11.9304 20.6654 0
tr98 8.1610 22.4206 0
tr99 4.1427 23.4975 0
tr100 0 23.8608 0
tr101 -23.8608 0 0
tr102 -23.4975 4.1427 0
tr103 -22.4206 8.1610 0
tr104 -20.6654 11.9304 0
tr105 -18.2778 15.3365 0
tr106 -15.3365 18.2778 0
tr107 -11.9304 20.6654 0
tr108 -8.1610 22.4206 0
tr109 -4.1427 23.4975 0
tr110 23.4975 -4.1427 0
tr111 22.4206 -8.1610 0
tr112 20.6654 -11.9304 0
tr113 18.2778 -15.3365 0
tr114 15.3365 -18.2778 0
tr115 11.9304 -20.6654 0
tr116 8.1610 -22.4206 0
tr117 4.1427 -23.4975 0
tr118 0 -23.8608 0
tr119 -23.4975 -4.1427 0
tr120 -22.4206 -8.1610 0
tr121 -20.6654 -11.9304 0
tr122 -18.2778 -15.3365 0
tr123 -15.3365 -18.2778 0
tr124 -11.9304 -20.6654 0
tr125 -8.1610 -22.4206 0
tr126 -4.1427 -23.4975 0
c
c control rod up and down movement
```

```
c to move to control rods up and down
c change the number in the z column.
c 25.527 is 670 units up
c 17.526 is 460 units up
c
c 26.289 is 690 units up
c 18.669 is 490 units up
c to change to position to a specific postion z: z=(units/1000)*15*2.54
c tr x    y    z    ---------------------
tr201 11.9456 0 18.669 $ shim 1
tr202 -11.9456 0.0 18.669 $ shim 2
tr203 0.0 -7.98068 18.669 $ trans
tr204 0.0 7.98068 18.669 $ reg
c
c Material
c ****************************************************************************
m1    1001.70c  .666  $ water
      8016.70c  .333
c
c ****************************************************************************
m2    6000.70c                1  $ graphite
c
c ****************************************************************************
c
m3    13027.70c        -0.967  $Al 0.9670
      26054.70c     -0.000316
      26056.70c     -0.005147
      26057.70c     -0.000121
      26058.70c     -1.6e-005
      14028.70c      -0.00735
      14029.70c     -0.000387
      14030.70c     -0.000263
      12024.70c   -0.00086889
      12025.70c     -.00011
      12026.70c    -.00012111
      24050.70c     -8.4e-005
      24052.70c     -0.001674
      24053.70c     -0.000193
      24054.70c     -4.9e-005
      25055.70c       -0.0013
      22046.70c     -0.000056
      22047.70c     -.0000511
      22048.70c     -.0005166
      22049.70c     -.0000385
      22050.70c     -.0000378
      28058.70c     -0.000269
      30000.70c        -0.001
      28060.70c     -0.000107
      28061.70c       -5e-006
      28062.70c     -1.5e-005
      28064.70c       -4e-006
      29063.70c     -0.002055
      29065.70c     -0.000945
c
c ****************************************************************************
c 304L stainless steel
m4    6000.70c         -0.00031519   $ carbon at .03%
      24050.70c        -0.0082555    $ chromium at 19.00%
      24052.70c        -0.1591991
      24053.70c        -0.0180519
      24054.70c        -0.0044935
      26054.70c        -0.0409413    $ Iron at 70.045%
      26056.70c        -0.6426909
```

```
      26057.70c        -0.0148425
      26058.70c        -0.0019753
      28058.70c        -0.0544616  $ Nickel at 8%
      28060.70c        -0.0209784
      28061.70c        -0.000912
      28062.70c        -0.0029072
      28064.70c        -0.0007408
      25055.70c        -.020       $ Manganese at 2%
      14028.70c        -0.00691722  $ silicon at .75%
      14029.70c        -3.5124E-4
      14030.70c        -2.3154E-4
       7014.70c        -9.9632E-4   $ Nitrogen at .1%
       7015.70c        -3.68E-6
      15031.70c        -.00045      $ Phosphorus at .045 %
      16032.70c        -2.8479E-4   $ Sulfur at .03$
      16033.70c        -2.28E-6
      16034.70c        -1.287E-5
      16036.70c        -6.0E-8
c
c
c ******************************************************************************
m5    40090.70c   0.5145
      40091.70c   0.1122
      40092.70c   0.1715
      40094.70c   0.1738
      40096.70c   0.028
c 40000.58c             -1  $ zr
c
c
c  *************************** UZr-H 8 wt% w/ burnup **************
c
c burn up @ 3.0% Sm-149 and Ba-134 and Mo-95 calc
c *************** F ring ***************
m101 40090.70c      2.5295E-01
      40091.70c     5.5163E-02
      40092.70c     8.4317E-02
      40094.70c     8.5448E-02
      40096.70c     1.3766E-02
      1001.70c      4.9165E-01
      92238.70c     1.3293E-02
      92235.70c     3.2103E-03
      42095.70c     1.0836E-05
      40094.70c     1.0786E-05
      40093.70c     1.0586E-05
      40096.70c     1.0569E-05
      42100.70c     1.0486E-05
      43099.70c     1.0186E-05
      40092.70c     1.0036E-05
      42097.70c     1.0036E-05
      40091.70c     9.7191E-06
      38090.70c     9.6357E-06
      54134.70c     1.1318E-05
      56138.70c     9.7833E-06
      55133.70c     9.6829E-06
      55135.70c     9.4534E-06
      57139.70c     9.2669E-06
      54136.70c     9.1235E-06
      58140.70c     8.9944E-06
      55137.70c     8.9514E-06
      60143.70c     8.6214E-06
      59141.70c     8.4637E-06
      58142.70c     8.4637E-06
      62149.70c     7.2026E-07
```

```
c
c burn up @ 1.2% Sm-149 and Ba-134 and Mo-95 calc
c *************** G ring **************
m106 40090.70c      2.5297E-01
      40091.70c     5.5166E-02
      40092.70c     8.4322E-02
      40094.70c     8.5453E-02
      40096.70c     1.3767E-02
      1001.70c      4.9168E-01
      92238.70c     1.3293E-02
      92235.70c     3.2723E-03
      42095.70c     4.3347E-06
      40094.70c     4.3147E-06
      40093.70c     4.2346E-06
      40096.70c     4.2280E-06
      42100.70c     4.1946E-06
      43099.70c     4.0746E-06
      40092.70c     4.0146E-06
      42097.70c     4.0146E-06
      40091.70c     3.8879E-06
      38090.70c     3.8545E-06
      54134.70c     4.5275E-06
      56138.70c     3.9136E-06
      55133.70c     3.8734E-06
      55135.70c     3.7816E-06
      57139.70c     3.7070E-06
      54136.70c     3.6496E-06
      58140.70c     3.5980E-06
      55137.70c     3.5808E-06
      60143.70c     3.4488E-06
      59141.70c     3.3857E-06
      58142.70c     3.3857E-06
      62149.70c     6.1970E-07
c
c  *************************** UZr-H 8.5 wt% w/ burnup **************
c  the fuel is 19.75% enriched fuel at 8.5 weight percent
c
c burn up @ 15.4% sm-149 and Ba-134 and Mo-99 Calc
c  ******** B RING ***************
m100  40090.70c     1.8794E-01
      40091.70c     4.0986E-02
      40092.70c     6.2648E-02
      40094.70c     6.3488E-02
      40096.70c     1.0228E-02
      1001.70c      6.2100E-01
      92238.70c     1.0632E-02
      92235.70c     2.2276E-03
      42095.70c     4.4490E-05
      40094.70c     4.4285E-05
      40093.70c     4.3463E-05
      40096.70c     4.3395E-05
      42100.70c     4.3053E-05
      43099.70c     4.1821E-05
      40092.70c     4.1205E-05
      42097.70c     4.1205E-05
      40091.70c     3.9904E-05
      38090.70c     3.9562E-05
      54134.70c     4.6470E-05
      56138.70c     4.0168E-05
      55133.70c     3.9756E-05
      55135.70c     3.8813E-05
      57139.70c     3.8048E-05
      54136.70c     3.7459E-05
```

```
      58140.70c     3.6929E-05
      55137.70c     3.6752E-05
      60143.70c     3.5398E-05
      59141.70c     3.4750E-05
      58142.70c     3.4750E-05
      62149.70c     5.7608E-07
c
c burn up @ 17.2% sm-149 and Ba-134 and Mo-99 Calc
c ********** C RING **************
m102  40090.70c     1.8794E-01
      40091.70c     4.0984E-02
      40092.70c     6.2645E-02
      40094.70c     6.3485E-02
      40096.70c     1.0228E-02
      1001.70c      6.2097E-01
      92238.70c     1.0631E-02
      92235.70c     2.1781E-03
      42095.70c     4.9688E-05
      40094.70c     4.9458E-05
      40093.70c     4.8541E-05
      40096.70c     4.8465E-05
      42100.70c     4.8082E-05
      43099.70c     4.6706E-05
      40092.70c     4.6018E-05
      42097.70c     4.6018E-05
      40091.70c     4.4566E-05
      38090.70c     4.4184E-05
      54134.70c     5.1898E-05
      56138.70c     4.4861E-05
      55133.70c     4.4400E-05
      55135.70c     4.3348E-05
      57139.70c     4.2493E-05
      54136.70c     4.1835E-05
      58140.70c     4.1243E-05
      55137.70c     4.1046E-05
      60143.70c     3.9533E-05
      59141.70c     3.8810E-05
      58142.70c     3.8810E-05
      62149.70c     5.7605E-07
c
c burn up @ 21.9% sm-149 and Ba-134 and Mo-99 Calc
c ********** D RING **************
m103  40090.70c     1.8791E-01
      40091.70c     4.0979E-02
      40092.70c     6.2637E-02
      40094.70c     6.3477E-02
      40096.70c     1.0226E-02
      1001.70c      6.2089E-01
      92238.70c     1.0630E-02
      92235.70c     2.0490E-03
      42095.70c     6.3257E-05
      40094.70c     6.2965E-05
      40093.70c     6.1797E-05
      40096.70c     6.1700E-05
      42100.70c     6.1213E-05
      43099.70c     5.9462E-05
      40092.70c     5.8586E-05
      42097.70c     5.8586E-05
      40091.70c     5.6737E-05
      38090.70c     5.6250E-05
      54134.70c     6.6072E-05
      56138.70c     5.7112E-05
      55133.70c     5.6526E-05
```

```
      55135.70c     5.5186E-05
      57139.70c     5.4097E-05
      54136.70c     5.3260E-05
      58140.70c     5.2506E-05
      55137.70c     5.2255E-05
      60143.70c     5.0329E-05
      59141.70c     4.9408E-05
      58142.70c     4.9408E-05
      62149.70c     5.7598E-07
c
c burn up @ 24.1% sm-149 and Ba-134 and Mo-99 Calc
c ********** E RING **************
m104  40090.70c     1.8790E-01
      40091.70c     4.0976E-02
      40092.70c     6.2633E-02
      40094.70c     6.3473E-02
      40096.70c     1.0226E-02
      1001.70c      6.2086E-01
      92238.70c     1.0629E-02
      92235.70c     1.9885E-03
      42095.70c     6.9608E-05
      40094.70c     6.9286E-05
      40093.70c     6.8001E-05
      40096.70c     6.7894E-05
      42100.70c     6.7359E-05
      43099.70c     6.5431E-05
      40092.70c     6.4467E-05
      42097.70c     6.4467E-05
      40091.70c     6.2433E-05
      38090.70c     6.1897E-05
      54134.70c     7.2705E-05
      56138.70c     6.2845E-05
      55133.70c     6.2200E-05
      55135.70c     6.0726E-05
      57139.70c     5.9528E-05
      54136.70c     5.8607E-05
      58140.70c     5.7778E-05
      55137.70c     5.7501E-05
      60143.70c     5.5382E-05
      59141.70c     5.4368E-05
      58142.70c     5.4368E-05
      62149.70c     5.7594E-07
c
c burn up @ 32.6% sm-149 and Ba-134 and Mo-99 Calc
c ********** G RING **************
m105  40090.70c     1.8786E-01
      40091.70c     4.0967E-02
      40092.70c     6.2619E-02
      40094.70c     6.3459E-02
      40096.70c     1.0223E-02
      1001.70c      6.2071E-01
      92238.70c     1.0627E-02
      92235.70c     1.7550E-03
      42095.70c     9.4136E-05
      40094.70c     9.3702E-05
      40093.70c     9.1964E-05
      40096.70c     9.1819E-05
      42100.70c     9.1095E-05
      43099.70c     8.8488E-05
      40092.70c     8.7185E-05
      42097.70c     8.7185E-05
      40091.70c     8.4433E-05
      38090.70c     8.3709E-05
```

```
      54134.70c     9.8325E-05
      56138.70c     8.4991E-05
      55133.70c     8.4119E-05
      55135.70c     8.2125E-05
      57139.70c     8.0505E-05
      54136.70c     7.9259E-05
      58140.70c     7.8137E-05
      55137.70c     7.7764E-05
      60143.70c     7.4898E-05
      59141.70c     7.3527E-05
      58142.70c     7.3527E-05
      62149.70c     5.7581E-07
c
c  ************************** UZr-H 12 wt% w/ burnup *****************
c burn up at 8.6% Sm-149 and Ba-134 and Mo-95 from calc
m90   40090.70c     1.8680E-01
      40091.70c     4.0736E-02
      40092.70c     6.2266E-02
      40094.70c     6.3101E-02
      40096.70c     1.0166E-02
      1001.70c      6.1721E-01
      92238.70c     1.5511E-02
      92235.70c     3.5221E-03
      42095.70c     3.6248E-05
      40094.70c     3.6081E-05
      40093.70c     3.5411E-05
      40096.70c     3.5356E-05
      42100.70c     3.5077E-05
      43099.70c     3.4073E-05
      40092.70c     3.3571E-05
      42097.70c     3.3571E-05
      40091.70c     3.2512E-05
      38090.70c     3.2233E-05
      54134.70c     3.7861E-05
      56138.70c     3.2727E-05
      55133.70c     3.2391E-05
      55135.70c     3.1623E-05
      57139.70c     3.0999E-05
      54136.70c     3.0519E-05
      58140.70c     3.0087E-05
      55137.70c     2.9944E-05
      60143.70c     2.8840E-05
      59141.70c     2.8312E-05
      58142.70c     2.8312E-05
      62149.70c     8.4047E-07
c
c
c burn up @ 1.0% sm-149 and Ba-134 and Mo-99 Calc
c ********** Reg rod **************
m107  40090.70c     1.8802E-01
      40091.70c     4.1002E-02
      40092.70c     6.2673E-02
      40094.70c     6.3513E-02
      40096.70c     1.0232E-02
      1001.70c      6.2125E-01
      92238.70c     1.0616E-02
      92235.70c     2.6445E-03
      42095.70c     2.8136E-06
      40094.70c     2.8006E-06
      40093.70c     2.7486E-06
      40096.70c     2.7443E-06
      43099.70c     2.6448E-06
      40092.70c     2.6058E-06
```

```
      40091.70c     2.5236E-06
      38090.70c     2.5019E-06
      54134.70c     2.9388E-06
      56138.70c     2.5402E-06
      55133.70c     2.5142E-06
      55135.70c     2.4546E-06
      57139.70c     2.4062E-06
      54136.70c     2.3689E-06
      58140.70c     2.3354E-06
      55137.70c     2.3242E-06
      60143.70c     2.2386E-06
      59141.70c     2.1976E-06
      58142.70c     2.1976E-06
      62149.70c     4.0224E-07
      42100.70c     2.72E-006
      42097.70c     2.61E-006
c
c
c burn up @ 18.0% sm-149 and Ba-134 and Mo-99 Calc
c ********** Shim 1 **************
m108  40090.70c     1.8793E-01
      40091.70c     4.0984E-02
      40092.70c     6.2645E-02
      40094.70c     6.3485E-02
      40096.70c     1.0228E-02
      1001.70c      6.2097E-01
      92238.70c     1.0611E-02
      92235.70c     2.1894E-03
      42095.70c     5.0622E-05
      40094.70c     5.0388E-05
      40093.70c     4.9453E-05
      40096.70c     4.9375E-05
      43099.70c     4.7584E-05
      40092.70c     4.6883E-05
      40091.70c     4.5404E-05
      38090.70c     4.5014E-05
      54134.70c     5.2874E-05
      56138.70c     4.5704E-05
      55133.70c     4.5235E-05
      55135.70c     4.4163E-05
      57139.70c     4.3291E-05
      54136.70c     4.2621E-05
      58140.70c     4.2018E-05
      55137.70c     4.1817E-05
      60143.70c     4.0276E-05
      59141.70c     3.9539E-05
      58142.70c     3.9539E-05
      62149.70c     5.8042E-07
      42100.70c     4.90E-005
      42097.70c     4.69E-005
c
c
c burn up @ 43.3% sm-149 and Ba-134 and Mo-99 Calc
c ********** Shim 2 **************
m109  40090.70c     1.8781E-01
      40091.70c     4.0956E-02
      40092.70c     6.2603E-02
      40094.70c     6.3442E-02
      40096.70c     1.0221E-02
      1001.70c      6.2055E-01
      92238.70c     1.0604E-02
      92235.70c     1.5129E-03
      42095.70c     1.2169E-04
```

```
      40094.70c     1.2113E-04
      40093.70c     1.1888E-04
      40096.70c     1.1870E-04
      43099.70c     1.1439E-04
      40092.70c     1.1270E-04
      40091.70c     1.0915E-04
      38090.70c     1.0821E-04
      54134.70c     1.2711E-04
      56138.70c     1.0987E-04
      55133.70c     1.0874E-04
      55135.70c     1.0616E-04
      57139.70c     1.0407E-04
      54136.70c     1.0246E-04
      58140.70c     1.0101E-04
      55137.70c     1.0053E-04
      60143.70c     9.6821E-05
      59141.70c     9.5049E-05
      58142.70c     9.5049E-05
      62149.70c     5.8003E-07
      42100.70c     1.18E-004
      42097.70c     1.13E-004
c
c
c  *************************** UZr-H 20% enriched U 12 w/ FRESH!!!! **************
c  the fuel is 20% enriched fuel at 12 weight percent
M110  $40000.58c      -0.8637902
      40090.70c   -0.44442
      40091.70c   -0.0969173
      40092.70c   -0.14814
      40094.70c   -0.150127
      40096.70c   -0.0241861
       1001.70c   -0.0162098
      92238.70c   -0.096
      92235.70c   -0.024
c
c  *************************** UZr-H 20% enriched U 8 w/ FRESH!!!! **************
c  the fuel is 20% enriched fuel at 8 weight percent
M111  40090.70c   0.2529777
      40091.70c   0.0551683
      40092.70c   0.0843259
      40094.70c   0.0854568
      40096.70c   0.0137675
       1001.70c   0.4916961
      92238.70c   0.0132690
      92235.70c   0.0033387
c
c ******************************************************************************
c     B4C poison (2.48 g/cc)
c M6    5010.70c     0.159936              $B10
c      5011.70c     0.64096               $B11
c      6000.70c     0.200                 $carbon
c
c      5010 0.0035454 5011 0.01427 6012 0.0686199 6013 0.0007702 $ 25% mass b4c and
Grapite 5% depleted
M6   5010.70c -0.03893
     5011.70c -0.15672
     6000.70c -0.80435
c
c ******************************************************************************
c    Air (density 1.0467e-3 g/cc at STP)
M7    8016.70c   -0.23                $air
      7014.70c   -0.77
c
```

```
c ****************************************************************************
c   AmBe source
c M8    95241.70c     1
c           8016.70c    2
c           4009.70c    1
c
c ****************************************************************************
c   Lead (density 11.34 )
c M9     82207.70c         1
c
c ****************************************************************************
c    9.895 g of Al-Sm2O3 for each wafer  ref: INEL-96/0482
M10   62149.70c       -0.00854074
      8016.70c        -0.00145926
      13027.70c       -.99
c
c ****************************************************************************
c   Aluminum gold foils for flux measurements
c M11   79197.70c 1 $s.00155 $Gold
c      13027.70c .99845 $ Aluminum
c
c ****************************************************************************
m12   1001.70c  .666  $ water
      8016.70c  .333
c
c ****************************************************************************
c  rho=.540837g/cm^3   Lazy susan mix of 80% air and 20% Aluminum alloy
c m13   8016.70c       -0.0003561  7014.70c      -.00119216    $air
c      13027.70c        -0.965503               $Al
c      26054.70c     -0.000315511 26056.70c     -0.00513903
c      26057.70c     -0.000120813 26058.70c     -1.59752e-5
c      14028.70c      -0.00733862 14029.70c     -.000386401
c      14030.70c     -0.000262593 12000.70c     -.0011
c      24050.70c      -8.38699e-5 24052.70c     -.00167141
c      24053.70c     -0.000192701 24054.70c     -4.89241e-5
c      25055.70c      -0.00129799 22000.70c     -.0006
c      28058.70c     -0.000268584 28060.70c     -.000106834
c      28061.70c      -4.99226e-6 28062.70c     -1.49768e-5
c      28064.70c      -3.99381e-6 29063.70c     -.00205182
c      29065.70c     -0.000943537 30000.70c     -.000998452
c
c ****************************************************************************
c   Ho-155 for production measurements
c M14   67165.70c  1
c
c ****************************************************************************
c   graphite in reflector
M15  6000.70c  1
c
c
c ****************************************************************************
mt1      lwtr.10t $ water  salphabeta card
mt12      lwtr.10t $ water  salphabeta card
mt2      grph.10t $ graphite  salphabeta card
mt15     grph.10t $ graphite  salphabeta card
mt90    h/zr.10t zr/h.10t $ 5728-1  salphabeta card
mt100   h/zr.10t zr/h.10t $ 5728-1  salphabeta card
mt101   h/zr.10t zr/h.10t $ 5728-1  salphabeta card
mt102    h/zr.10t zr/h.10t $ 5728-1  salphabeta card
mt103   h/zr.10t zr/h.10t $ 5728-1  salphabeta card
mt104   h/zr.10t zr/h.10t $ 5728-1  salphabeta card
mt105   h/zr.10t zr/h.10t $ 5728-1  salphabeta card
mt106    h/zr.10t zr/h.10t $ 5728-1  salphabeta card
```

```
mt107   h/zr.10t zr/h.10t $ 5728-1  salphabeta card
mt108   h/zr.10t zr/h.10t $ 5728-1  salphabeta card
mt109    h/zr.10t zr/h.10t $ 5728-1  salphabeta card
mt110    h/zr.10t zr/h.10t $ 5728-1  salphabeta card
mt3     al27.12t $aluminum salphabeta card
mt6     grph.10t $ graphite  salphabeta card
c mt13    al27.12t $aluminium salphabeta card
c
c ********************** Source Definition ***********************************
c
kcode  50000 1.0 15 1015
c ksrc 9 0 0
c
c NPS 1000000
c
sdef pos=0 0 0 axs=0 0 1 rad=D1 ext=d2
si1 h 0 26
si2 h -19 19
c
c ****************** TALLIES ************************
c


END OF LINE
```

APPENDIX B
RELAP STEADY STATE MODEL

This appendix includes the RELAP steady-state model described in Chapter 4 used to analyze the hot rod under normal operating conditions of 1.1 MW. The model is set to run until steady-state conditions are meet. The initial conditions are the limiting conditions of the technical specifications of the GSTR Safety Analysis Report. The geometry of this model matches the geometry described in Chapter 4.

```
=GSTR Core SS 12 wt% Model
*m: SNAP:Symbolic Nuclear Analysis Package,  Version 2.2.2, January 02, 2013
*m: PLUGIN:RELAP Version 4.3.0
*m: CODE:RELAP5 Version 3.3
*m: DATE:3/31/13
******************************
*        Model Options       *
******************************
*            type         state
100           new       stdy-st
*          iunits        ounits
102            si            si
*    Noncondensable Gas Species
110      nitrogen
*     tend minstep maxstep copt pfreq majed rsrtf
201 1200.0  1.0e-7     1.0    3  1000  1000  3000
20500000          999
******************************
*       General Tables        *
******************************
*
*            type          trip
20210000    power             0
*               Time          Power
20210001         0.0     2.218142e4
20210002        20.0     2.218142e4
20210003        50.0     2.218142e4
20210004       100.0     2.218142e4
20210005       150.0     2.218142e4
20210006      5000.0     2.218142e4
*
*************************
*       Materials       *
*************************
*
*n: Zirconium
*                type         tflag         vflag
20100100      tbl/fctn             1             1
*                temp        thcond
20100101        200.15     25.202959
20100102        400.15     21.601646
20100103        600.15     20.698202
20100104        800.15     21.601646
20100105       1000.15     23.701373
20100106       1200.15     26.000481
20100107       1500.15     28.798041
```

```
*                 temp      capacity
20100151         200.15     1.73406e6
20100152         400.15    1.970523e6
20100153         600.15    2.115028e6
20100154         800.15    2.246396e6
20100155        1000.15    2.377764e6
20100156        1200.15    2.259533e6
20100157        1500.15    2.259533e6
*
*n: Fuel
*                 type         tflag         vflag
20100200       tbl/fctn             1             2
*               thcond
20100201      17.584624
*         lower    upper         a0        a1  a2  a3  a4  a5      c
20100251 273.15 5810.928 2.039509e6 4168.9847 0.0 0.0 0.0 0.0 273.15
*
*n: GAP
*                 type
20100300           gap
*
*n: S-STEEL
*                 type
20100400       s-steel
*
************************************
*       Hydraulic Components       *
************************************
*
*                name          type
1000000       "Source"       tmdpvol
*                area         length           vol
1000101   3.800013e-4    0.99999698           0.0
*             az-angle     inc-angle            dz
1000102           0.0           0.0           0.0
*              x-rough          x-hd         flags
1000103           0.0    0.01309996             0
*               cword
1000200               3
*                srch         press          temp
1000201            0.0     1.67188e5        333.15
1000202         5000.0     1.67188e5        333.15
*
*                name          type
1030000     "HotChann"          pipe
*              ncells
1030001              24
*              x-area         volid
1030101    5.85532e-4            24
*            x-length         volid
1030301       0.02125             1
1030302      0.132738             2
1030303       0.01905            22
1030304      0.132738            23
1030305       0.02125            24
*              volume         volid
1030401           0.0            24
*          azim-angle         volid
1030501           0.0            24
*          vert-angle         volid
1030601          90.0            24
*              x-elev         volid
1030701       0.02125             1
```

```
1030702      0.132738            2
1030703       0.01905           22
1030704      0.132738           23
1030705       0.02125           24
*             x-wall           xhd         volid
1030801     2.1336e-6       0.019967           24
*             x-flags          volid
1031001              0           24
*       ebt     press   temp none none none id
1031201 003 1.42951e5 322.15  0.0  0.0  0.0 24
*           fwd. loss      rev.loss        junid
1030901           2.26           0.0            1
1030902            0.0           0.0           22
1030903           0.63           0.0           23
*            jefvcahs       jun num
1031101      00000000            23
*         jun control
1031300               1
*                 mfl           mfv        unused        junid
1031301   0.045359229           0.0           0.0           23
*                  hd          corr           gas         slope         junid
1031401      0.019967           0.0           1.0           1.0            23
*
*                name          type
1040000         "Sink"       tmdpvol
*                area        length           vol
1040101   3.800013e-4    0.99999698           0.0
*             az-angle     inc-angle            dz
1040102            0.0           0.0           0.0
*             x-rough          x-hd         flags
1040103            0.0    0.01309996             0
*               cword
1040200             103
*                srch         press          temp
1040201             0.0     1.60443e5        333.15
1040202          5000.0     1.60443e5        333.15
*
*                name          type
2020000       "jun202"       sngljun
*                from            to          area
2020101     100010002     103010001           0.0
*           fwd. loss     rev. loss       efvcahs
2020102           2.26           0.0             0
*           discharge       thermal
2020103             1.0          0.14
*                flow           mfl           mfv        unused
2020201                1   0.045359229           0.0           0.0
*
*                name          type
2030000       "jun203"       sngljun
*                from            to          area
2030101     103240002     104010001           0.0
*           fwd. loss     rev. loss       efvcahs
2030102           0.63           0.0             0
*           discharge       thermal
2030103             1.0          0.14
*                flow           mfl           mfv        unused
2030201                1   0.045359229           0.0           0.0
*
*********************************
*       Heat Structures         *
*********************************
*
```

```
*          nh    np      geom      ssif     leftcoord reflood
13030000   20    24         2         0           0.0       0
*                 mesh        format
13030100             0             1
*           intervals        radius
13030101             1      3.175e-3
13030102             1     3.9193e-3
13030103             1     4.6636e-3
13030104             1     5.4079e-3
13030105             1     6.1522e-3
13030106             1     6.8965e-3
13030107             1     7.6408e-3
13030108             1     8.3851e-3
13030109             1     9.1294e-3
13030110             1     9.8737e-3
13030111             1      0.010618
13030112             1     0.0113623
13030113             1     0.0121066
13030114             1     0.0128509
13030115             1     0.0135952
13030116             1     0.0143395
13030117             1     0.0150838
13030118             1     0.0158281
13030119             1     0.0165724
13030120             1     0.0173167
13030121             1      0.018061
13030122             1      0.018161
13030123             1      0.018669
*            material      interval
13030201             1             1
13030202             2            21
13030203             3            22
13030204             4            23
*                 rpkf      interval
13030301           0.0             1
13030302      0.064437            21
13030303           0.0            23
*                 temp      interval
13030401         300.0            24
*   Left Boundary Condition Data
*           bound      incr      type      code        factor      node
13030501        0         0         0         1       0.01905         1
13030502        0         0         0         1       0.01905         2
13030503        0         0         0         1       0.01905         3
13030504        0         0         0         1       0.01905         4
13030505        0         0         0         1       0.01905         5
13030506        0         0         0         1       0.01905         6
13030507        0         0         0         1       0.01905         7
13030508        0         0         0         1       0.01905         8
13030509        0         0         0         1       0.01905         9
13030510        0         0         0         1       0.01905        10
13030511        0         0         0         1       0.01905        11
13030512        0         0         0         1       0.01905        12
13030513        0         0         0         1       0.01905        13
13030514        0         0         0         1       0.01905        14
13030515        0         0         0         1       0.01905        15
13030516        0         0         0         1       0.01905        16
13030517        0         0         0         1       0.01905        17
13030518        0         0         0         1       0.01905        18
13030519        0         0         0         1       0.01905        19
13030520        0         0         0         1       0.01905        20
*   Right Boundary Condition Data
*           bound      incr      type      code        factor      node
```

```
13030601 103030000          0        101          1        0.01905          1
13030602 103040000          0        101          1        0.01905          2
13030603 103050000          0        101          1        0.01905          3
13030604 103060000          0        101          1        0.01905          4
13030605 103070000          0        101          1        0.01905          5
13030606 103080000          0        101          1        0.01905          6
13030607 103090000          0        101          1        0.01905          7
13030608 103100000          0        101          1        0.01905          8
13030609 103110000          0        101          1        0.01905          9
13030610 103120000          0        101          1        0.01905         10
13030611 103130000          0        101          1        0.01905         11
13030612 103140000          0        101          1        0.01905         12
13030613 103150000          0        101          1        0.01905         13
13030614 103160000          0        101          1        0.01905         14
13030615 103170000          0        101          1        0.01905         15
13030616 103180000          0        101          1        0.01905         16
13030617 103190000          0        101          1        0.01905         17
13030618 103200000          0        101          1        0.01905         18
13030619 103210000          0        101          1        0.01905         19
13030620 103220000          0        101          1        0.01905         20
*               source          mult          dmhl          dmhr          num
13030701           100        0.0301           0.0           0.0            1
13030702           100        0.0343           0.0           0.0            2
13030703           100        0.0404           0.0           0.0            3
13030704           100        0.0464           0.0           0.0            4
13030705           100        0.0516           0.0           0.0            5
13030706           100        0.0561           0.0           0.0            6
13030707           100        0.0597           0.0           0.0            7
13030708           100        0.0625           0.0           0.0            8
13030709           100        0.0642           0.0           0.0            9
13030710           100         0.065           0.0           0.0           10
13030711           100        0.0648           0.0           0.0           11
13030712           100        0.0636           0.0           0.0           12
13030713           100        0.0616           0.0           0.0           13
13030714           100        0.0585           0.0           0.0           14
13030715           100        0.0544           0.0           0.0           15
13030716           100        0.0496           0.0           0.0           16
13030717           100         0.044           0.0           0.0           17
13030718           100        0.0377           0.0           0.0           18
13030719           100        0.0308           0.0           0.0           19
13030720           100        0.0247           0.0           0.0           20
*   Right Additional Boundary Condition Data
13030900             0
*        hthd   hlf   hlr gslf gslr glcf glcr lbf node
13030901  0.0 3.048 3.048  0.0  0.0  0.0  0.0 1.0   20
*
.
```

APPENDIX C
RELAP TRANSIENT MODEL

This appendix contains the transient RELAP model described in Chapter 3. This model is currently set to model a $1.50 reactivity insertion pulse out to 20 s, including 1 s of inactivity to ensure the model is not drifting significantly. This model can easily be reconfigured to any reactivity insertion pulse, or any other transient event through altering the General tables defining reactivity as a function of time, and the time step controls to ensure that the time of interest is adequately recorded. The model's initial conditions match the technical specification limits of operation at the GSTR to provide bounding results.

```
=GSTR Core SS Transient Model
*m: SNAP:Symbolic Nuclear Analysis Package,  Version 2.2.2, January 02, 2013
*m: PLUGIN:RELAP Version 4.3.0
*m: CODE:RELAP5 Version 3.3
*m: DATE:3/31/13
*****************************
*        Model Options       *
*****************************
*            type         state
100           new       transnt
*          iunits        ounits
102            si            si
*    Noncondensable Gas Species
110       nitrogen
*   tend minstep maxstep copt pfreq  majed rsrtf
201 0.95  1.0e-8    0.01    7     3 500000 50000
202  1.5  1.0e-8  1.0e-5    7    50 250000 50000
203  5.0  1.0e-8  1.0e-4    7   100 250000 50000
204 12.0  1.0e-8  2.0e-4    7    50 250000 50000
205 20.0  1.0e-8    0.01    7     1 250000 50000
*        variable     parameter
301        httemp     300001002
302        httemp     300001005
303        httemp     300001022
304        httemp     300001024
305        reactf             0
306        rkreac             0
307        rktpow             0
308         tempf     104120000
309         voidg     104120000
20500000           999
*****************************
*       General Tables        *
*****************************
*
*            type          trip
20210000    power             0
*                Time         Power
20210001         0.0       2.217e4
20210002        20.0       2.217e4
20210003        50.0       2.217e4
20210004       100.0       2.217e4
20210005       150.0       2.217e4
```

```
20210006        5000.0       2.217e4
*
*n: Pulse
*            type          trip
20220000    reac-t             0
*                Time    Reactivity
20220001          0.0           0.0
20220002          1.0           0.0
20220003          1.2           1.5
20220004          2.5           1.5
20220005          4.5           0.0
20220006         16.0           0.0
20220007         17.0          -5.0
20220008       3600.0          -5.0
*
*n: Reg Rod Withdrawl
*            type          trip
20220100    reac-t             0
*                Time    Reactivity
20220101          0.0           0.0
20220102          1.0           0.0
20220103          4.9          0.07
20220104         8.79          0.33
20220105        12.69          0.78
20220106        16.58          1.33
20220107        20.48          2.03
20220108        24.38          2.71
20220109        28.27          3.33
20220110        32.17           3.8
20220111        36.06          4.15
20220112        39.96          4.25
20220113         60.0          4.25
*
*n: Reg Rod SCRAM
*            type          trip
20220200    reac-t             0
*                Time    Reactivity
20220201          0.0           0.0
20220202          1.0           0.0
20220203          4.9          0.07
20220204         8.79          0.33
20220205        12.69          0.78
20220206        13.87          0.95
20220207        15.87         -5.57
20220208         60.0         -5.57
*
*************************
*       Materials       *
*************************
*
*n: Zirconium
*                type         tflag         vflag
20100100      tbl/fctn             1             1
*                temp        thcond
20100101        200.15     25.202959
20100102        400.15     21.601646
20100103        600.15     20.698202
20100104        800.15     21.601646
20100105       1000.15     23.701373
20100106       1200.15     26.000481
20100107       1500.15     28.798041
*                temp      capacity
20100151        200.15     1.73406e6
```

```
20100152        400.15    1.970523e6
20100153        600.15    2.115028e6
20100154        800.15    2.246396e6
20100155       1000.15    2.377764e6
20100156       1200.15    2.259533e6
20100157       1500.15    2.259533e6
*
*n: Fuel
*                type         tflag         vflag
20100200      tbl/fctn             1             2
*               thcond
20100201     17.584624
*         lower    upper         a0        a1  a2  a3  a4  a5      c
20100251 273.15 5810.928 2.039509e6 4168.9847 0.0 0.0 0.0 0.0 273.15
*
*n: GAP
*                type
20100300         gap
*
*n: S-STEEL
*                type
20100400      s-steel
*
************************************
*       Hydraulic Components       *
************************************
*
*               name          type
0010000       "Upjun"       mtpljun
*             num jun       IC flag
0010001             2             0
*               from            to          area          rfor          rrev
0010011     104240002     105010001           1.0           0.0           0.0
+*              jflag       dischrg         therm           off          finc
+            00000000           1.0          0.14           0.0      -1000000
+*               tinc        unused           lim
+                  0             0             2
*                 vl            vv           lim
0011011           0.0           0.0             2
*
*               name          type
1000000      "Source"       tmdpvol
*               area        length           vol
1000101     8.6148e-4           1.0           0.0
*            az-angle     inc-angle            dz
1000102           0.0           0.0           0.0
*            x-rough          x-hd         flags
1000103           0.0    0.01309996             0
*              cword
1000200               3
*               srch         press          temp
1000201           0.0     1.69117e5        333.15
1000202        5000.0     1.69117e5        333.15
*
*               name          type
1030000     "Average"          pipe
*             ncells
1030001              24
*             x-area         volid
1030101     8.6148e-4            24
*           x-length         volid
1030301       0.02125             1
1030302      0.132738             2
```

```
1030303       0.01905            22
1030304      0.132738            23
1030305       0.02125            24
*              volume          volid
1030401           0.0            24
*          azim-angle          volid
1030501           0.0            24
*          vert-angle          volid
1030601          90.0            24
*              x-elev          volid
1030701       0.02125             1
1030702      0.132738             2
1030703       0.01905            22
1030704      0.132738            23
1030705       0.02125            24
*              x-wall           xhd          volid
1030801     2.1336e-6       0.014261             24
*             x-flags          volid
1031001             0            24
*       ebt     press   temp none none none id
1031201 003 1.42951e5 333.15  0.0  0.0  0.0 24
*           fwd. loss       rev.loss         junid
1030901          2.26           0.63             1
1030902           0.0            0.0            22
1030903          0.63           2.26            23
*            jefvcahs       jun num
1031101      00000000            23
*         jun control
1031300             1
*                 mfl            mfv        unused         junid
1031301   0.045359229            0.0           0.0            23
*                  hd           corr            gas         slope         junid
1031401      0.029377            0.0            1.0           1.0            23
*
*               name           type
1040000    "HotChann"           pipe
*              ncells
1040001            24
*              x-area          volid
1040101     8.6148e-4             24
*            x-length          volid
1040301       0.02125             1
1040302      0.132738             2
1040303       0.01905            22
1040304      0.132738            23
1040305       0.02125            24
*              volume          volid
1040401           0.0            24
*          azim-angle          volid
1040501           0.0            24
*          vert-angle          volid
1040601          90.0            24
*              x-elev          volid
1040701       0.02125             1
1040702      0.132738             2
1040703       0.01905            22
1040704      0.132738            23
1040705       0.02125            24
*              x-wall           xhd          volid
1040801     2.1336e-6       0.014261             24
*             x-flags          volid
1041001             0            24
*       ebt     press   temp none none none id
```

```
1041201 003 1.42951e5 333.15  0.0  0.0  0.0 24
*          fwd. loss      rev.loss         junid
1040901         2.26          0.63             1
1040902          0.0           0.0            22
1040903         0.63          2.26            23
*           jefvcahs       jun num
1041101     00000000            23
*        jun control
1041300              1
*                mfl           mfv        unused         junid
1041301   0.045359229           0.0           0.0            23
*                 hd          corr            gas         slope         junid
1041401     0.029377           0.0           1.0           1.0            23
*
*               name          type
1050000     "UPlenum"          pipe
*             ncells
1050001              1
*             x-area         volid
1050101     8.614e-4             1
*           x-length         volid
1050301          0.1             1
*             volume         volid
1050401          0.0             1
*          azim-angle         volid
1050501          0.0             1
*          vert-angle         volid
1050601         90.0             1
*             x-wall           xhd         volid
1050801          0.0          1.57             1
*            x-flags         volid
1051001            0             1
*       ebt     press   temp none none none id
1051201 003 1.42951e5 333.15  0.0  0.0  0.0  1
*
*               name          type
1060000     "LPlenum"          pipe
*             ncells
1060001              1
*             x-area         volid
1060101     8.6148e-4             1
*           x-length         volid
1060301          0.1             1
*             volume         volid
1060401          0.0             1
*          azim-angle         volid
1060501          0.0             1
*          vert-angle         volid
1060601         90.0             1
*             x-wall           xhd         volid
1060801          0.0          1.57             1
*            x-flags         volid
1061001            0             1
*       ebt     press   temp none none none id
1061201 003 1.42951e5 333.15  0.0  0.0  0.0  1
*
*               name          type
1070000        "Sink"       tmdpvol
*               area         length           vol
1070101     8.6148e-4            1.0           0.0
*           az-angle     inc-angle            dz
1070102          0.0           0.0           0.0
*            x-rough          x-hd         flags
```

```
1070103           0.0    0.01309996             0
*               cword
1070200           103
*                srch         press          temp
1070201           0.0     1.58514e5        333.15
1070202        5000.0     1.58514e5        333.15
*
*                name          type
2020000     "bJunctio"      sngljun
*                from            to          area
2020101     100010002     106010001           0.0
*           fwd. loss     rev. loss       efvcahs
2020102           0.0           0.0             0
*           discharge       thermal
2020103           1.0          0.14
*                  hd         flood     intercept         slope
2020110     0.029377           0.0           1.0           1.0
*                flow           vl            vv        unused
2020201             0   0.045359229          0.08           0.0
*
*                name          type
2030000      "jun203"      sngljun
*                from            to          area
2030101     105010002     107010001           0.0
*           fwd. loss     rev. loss       efvcahs
2030102           0.0           0.0             0
*           discharge       thermal
2030103           1.0          0.14
*                  hd         flood     intercept         slope
2030110     0.029377           0.0           1.0           1.0
*                flow           mfl           mfv        unused
2030201             1   0.045359229          0.08           0.0
*
*                name          type
2050000      "LowJun"      mtpljun
*             num jun       IC flag
2050001             2             0
*                from            to          area          rfor          rrev
2050011     106010002     104010001           1.0           0.0           0.0
+*              jflag       dischrg         therm           off          finc
+            00000000           1.0          0.14           0.0             0
+*               tinc        unused           lim
+           -1000000             0             2
*                 vl            vv           lim
2051011          0.0           0.0             2
*
*******************************
*       Heat Structures       *
*******************************
*
*n: AvgRod
*          nh   np      geom      ssif     leftcoord reflood
13000000   20   24         2         0           0.0       0
*                mesh        format
13000100            0             1
*           intervals        radius
13000101            1     3.175e-3
13000102            1     3.9193e-3
13000103            1     4.6636e-3
13000104            1     5.4079e-3
13000105            1     6.1522e-3
13000106            1     6.8965e-3
13000107            1     7.6408e-3
```

```
13000108              1     8.3851e-3
13000109              1     9.1294e-3
13000110              1     9.8737e-3
13000111              1      0.010618
13000112              1     0.0113623
13000113              1     0.0121066
13000114              1     0.0128509
13000115              1     0.0135952
13000116              1     0.0143395
13000117              1     0.0150838
13000118              1     0.0158281
13000119              1     0.0165724
13000120              1     0.0173167
13000121              1      0.018061
13000122              1      0.018161
13000123              1      0.018669
*            material      interval
13000201              1             1
13000202              2            21
13000203              3            22
13000204              4            23
*                rpkf      interval
13000301            0.0             1
13000302       0.044078             2
13000303        0.04409             3
13000304       0.044272             4
13000305       0.044447             5
13000306       0.044752             6
13000307       0.045189             7
13000308       0.045605             8
13000309       0.046139             9
13000310       0.046729            10
13000311       0.047427            11
13000312       0.048257            12
13000313       0.049252            13
13000314       0.050295            14
13000315       0.051481            15
13000316       0.052888            16
13000317       0.054503            17
13000318        0.05639            18
13000319       0.058563            19
13000320       0.061206            20
13000321       0.064437            21
13000322            0.0            23
*                temp      interval
13000401          333.15            24
*   Left Boundary Condition Data
*            bound      incr      type      code        factor      node
13000501         0         0         0         1       0.01905         1
13000502         0         0         0         1       0.01905         2
13000503         0         0         0         1       0.01905         3
13000504         0         0         0         1       0.01905         4
13000505         0         0         0         1       0.01905         5
13000506         0         0         0         1       0.01905         6
13000507         0         0         0         1       0.01905         7
13000508         0         0         0         1       0.01905         8
13000509         0         0         0         1       0.01905         9
13000510         0         0         0         1       0.01905        10
13000511         0         0         0         1       0.01905        11
13000512         0         0         0         1       0.01905        12
13000513         0         0         0         1       0.01905        13
13000514         0         0         0         1       0.01905        14
13000515         0         0         0         1       0.01905        15
```

```
13000516          0          0          0          1        0.01905         16
13000517          0          0          0          1        0.01905         17
13000518          0          0          0          1        0.01905         18
13000519          0          0          0          1        0.01905         19
13000520          0          0          0          1        0.01905         20
*   Right Boundary Condition Data
*            bound       incr       type       code         factor       node
13000601 103030000          0        101          1        0.01905          1
13000602 103040000          0        101          1        0.01905          2
13000603 103050000          0        101          1        0.01905          3
13000604 103060000          0        101          1        0.01905          4
13000605 103070000          0        101          1        0.01905          5
13000606 103080000          0        101          1        0.01905          6
13000607 103090000          0        101          1        0.01905          7
13000608 103100000          0        101          1        0.01905          8
13000609 103110000          0        101          1        0.01905          9
13000610 103120000          0        101          1        0.01905         10
13000611 103130000          0        101          1        0.01905         11
13000612 103140000          0        101          1        0.01905         12
13000613 103150000          0        101          1        0.01905         13
13000614 103160000          0        101          1        0.01905         14
13000615 103170000          0        101          1        0.01905         15
13000616 103180000          0        101          1        0.01905         16
13000617 103190000          0        101          1        0.01905         17
13000618 103200000          0        101          1        0.01905         18
13000619 103210000          0        101          1        0.01905         19
13000620 103220000          0        101          1        0.01905         20
*               source          mult          dmhl          dmhr           num
13000701          1000       3.63e-4           0.0           0.0             1
13000702          1000      3.328e-4           0.0           0.0             2
13000703          1000      3.684e-4           0.0           0.0             3
13000704          1000      4.085e-4           0.0           0.0             4
13000705          1000      4.532e-4           0.0           0.0             5
13000706          1000      4.879e-4           0.0           0.0             6
13000707          1000      5.132e-4           0.0           0.0             7
13000708          1000      5.255e-4           0.0           0.0             8
13000709          1000      5.433e-4           0.0           0.0             9
13000710          1000      5.468e-4           0.0           0.0            10
13000711          1000      5.401e-4           0.0           0.0            11
13000712          1000      5.326e-4           0.0           0.0            12
13000713          1000      5.183e-4           0.0           0.0            13
13000714          1000      4.921e-4           0.0           0.0            14
13000715          1000      4.613e-4           0.0           0.0            15
13000716          1000      4.277e-4           0.0           0.0            16
13000717          1000      3.894e-4           0.0           0.0            17
13000718          1000      3.464e-4           0.0           0.0            18
13000719          1000       3.01e-4           0.0           0.0            19
13000720          1000      2.982e-4           0.0           0.0            20
*   Right Additional Boundary Condition Data
13000900             0
*       hthd   hlf   hlr gslf gslr glcf glcr lbf node
13000901  0.0 3.048 3.048  0.0  0.0  0.0  0.0 1.0   20
*
*n: HotRod
*          nh   np      geom      ssif     leftcoord reflood
13001000   20   24         2         0           0.0       0
*               mesh       format
13001100           0            1
*          intervals       radius
13001101           1     3.175e-3
13001102           1    3.9193e-3
13001103           1    4.6636e-3
13001104           1    5.4079e-3
```

```
13001105              1      6.1522e-3
13001106              1      6.8965e-3
13001107              1      7.6408e-3
13001108              1      8.3851e-3
13001109              1      9.1294e-3
13001110              1      9.8737e-3
13001111              1       0.010618
13001112              1      0.0113623
13001113              1      0.0121066
13001114              1      0.0128509
13001115              1      0.0135952
13001116              1      0.0143395
13001117              1      0.0150838
13001118              1      0.0158281
13001119              1      0.0165724
13001120              1      0.0173167
13001121              1       0.018061
13001122              1       0.018161
13001123              1       0.018669
*            material       interval
13001201              1              1
13001202              2             21
13001203              3             22
13001204              4             23
*                rpkf       interval
13001301              0.0            1
13001302         0.044078            2
13001303          0.04409            3
13001304         0.044272            4
13001305         0.044447            5
13001306         0.044752            6
13001307         0.045189            7
13001308         0.045605            8
13001309         0.046139            9
13001310         0.046729           10
13001311         0.047427           11
13001312         0.048257           12
13001313         0.049252           13
13001314         0.050295           14
13001315         0.051481           15
13001316         0.052888           16
13001317         0.054503           17
13001318          0.05639           18
13001319         0.058563           19
13001320         0.061206           20
13001321         0.064437           21
13001322              0.0           23
*                 temp       interval
13001401           333.15           24
*   Left Boundary Condition Data
*            bound      incr      type      code        factor      node
13001501         0         0         0         1       0.01905         1
13001502         0         0         0         1       0.01905         2
13001503         0         0         0         1       0.01905         3
13001504         0         0         0         1       0.01905         4
13001505         0         0         0         1       0.01905         5
13001506         0         0         0         1       0.01905         6
13001507         0         0         0         1       0.01905         7
13001508         0         0         0         1       0.01905         8
13001509         0         0         0         1       0.01905         9
13001510         0         0         0         1       0.01905        10
13001511         0         0         0         1       0.01905        11
13001512         0         0         0         1       0.01905        12
```

```
13001513          0          0          0          1        0.01905         13
13001514          0          0          0          1        0.01905         14
13001515          0          0          0          1        0.01905         15
13001516          0          0          0          1        0.01905         16
13001517          0          0          0          1        0.01905         17
13001518          0          0          0          1        0.01905         18
13001519          0          0          0          1        0.01905         19
13001520          0          0          0          1        0.01905         20
*   Right Boundary Condition Data
*            bound      incr      type      code        factor      node
13001601 104030000         0       101         1        0.01905         1
13001602 104040000         0       101         1        0.01905         2
13001603 104050000         0       101         1        0.01905         3
13001604 104060000         0       101         1        0.01905         4
13001605 104070000         0       101         1        0.01905         5
13001606 104080000         0       101         1        0.01905         6
13001607 104090000         0       101         1        0.01905         7
13001608 104100000         0       101         1        0.01905         8
13001609 104110000         0       101         1        0.01905         9
13001610 104120000         0       101         1        0.01905        10
13001611 104130000         0       101         1        0.01905        11
13001612 104140000         0       101         1        0.01905        12
13001613 104150000         0       101         1        0.01905        13
13001614 104160000         0       101         1        0.01905        14
13001615 104170000         0       101         1        0.01905        15
13001616 104180000         0       101         1        0.01905        16
13001617 104190000         0       101         1        0.01905        17
13001618 104200000         0       101         1        0.01905        18
13001619 104210000         0       101         1        0.01905        19
13001620 104220000         0       101         1        0.01905        20
*               source          mult          dmhl          dmhr           num
13001701          1000      7.985e-4           0.0           0.0             1
13001702          1000      7.321e-4           0.0           0.0             2
13001703          1000      8.105e-4           0.0           0.0             3
13001704          1000      8.986e-4           0.0           0.0             4
13001705          1000      9.971e-4           0.0           0.0             5
13001706          1000      1.073e-3           0.0           0.0             6
13001707          1000      1.129e-3           0.0           0.0             7
13001708          1000      1.156e-3           0.0           0.0             8
13001709          1000      1.195e-3           0.0           0.0             9
13001710          1000      1.203e-3           0.0           0.0            10
13001711          1000      1.188e-3           0.0           0.0            11
13001712          1000      1.172e-3           0.0           0.0            12
13001713          1000       1.14e-3           0.0           0.0            13
13001714          1000      1.083e-3           0.0           0.0            14
13001715          1000      1.015e-3           0.0           0.0            15
13001716          1000      9.409e-4           0.0           0.0            16
13001717          1000      8.568e-4           0.0           0.0            17
13001718          1000       7.62e-4           0.0           0.0            18
13001719          1000      6.622e-4           0.0           0.0            19
13001720          1000      6.559e-4           0.0           0.0            20
*   Right Additional Boundary Condition Data
13001900             0
*        hthd   hlf   hlr gslf gslr glcf glcr lbf node
13001901  0.0 3.048 3.048  0.0  0.0  0.0  0.0 1.0   20
*
*****************************
*       Point Kinetics      *
*****************************
*d: Pulse Model
*                type      feedback
30000000         point      separabl
*                decay         power         react           dnf
```

```
30000001      no-gamma        1000.0           0.0       169.954
*               ratio      constant
30000101     0.0323075      0.012375
30000102      0.218462      0.301304
30000103      0.196923      0.111774
30000104      0.395385      0.307104
30000105      0.115385       1.13607
30000106     0.0415385       3.01304
*             control
30000011           200 * General Table 200 (Pulse)
*             density    reactivity
30000501        500.0         -5.04
30000502        550.0         -4.23
30000503        600.0         -3.45
30000504        650.0         -2.75
30000505        700.0         -2.16
30000506        750.0         -1.65
30000507        800.0         -1.18
30000508        850.0         -0.82
30000509        900.0         -0.44
30000510        950.0         -0.15
30000511       1000.0           0.0
*               temp    reactivity
30000601        293.6           0.0
30000602        400.0         -0.99
30000603        600.0         -4.34
30000604        800.0         -7.55
30000605       1200.0         -13.0
*              volume     increment        factor          coef
30000701    103010000             0           1.0          0.01
*               heat     increment        factor          coef
30000801     3000001              0           1.0           0.0
.
```

APPENDIX D
PARET MODEL

This appendix contains the PARET model described in Chapter 4. Like the RELAP model, the PARET model analyzes a reactivity insertion pulse out to 20 s for the GSTR. The model includes a single average channel to ensure that during pulse events the void fraction in the model does not exceed 0.2. Like the RELAP models, PARET is set with its initial conditions matching the technical specifications of the GSTR for pulse operations.

```
0                                                                                2
* GSTR PARET Analyses Test
! GSTR.test.v6.inp 6/25/2012
! radial node 1 is fuel
!       # channels #z    #r    Cyl   reac   subcooled
1001,      -1    20    24     1     1     1
1002,       0     0     6    -1     1    20
!            Power    Fuel Vol     Inlet P     Inlet T  Fuel Pin r Fuel Meat r
1003,        0.001     0.05622  142951.045       -60.0     0.01867     0.01806
!     Clad Inner r   0 for cyl   0 for cyl Fuel Length   Inlet/Exit non-fuel Length
1004,      0.01816         0.0         0.0       0.381       0.154       0.154
!              Beff      Lambda           g     Q water
1005,       0.00728    4.3035-5     9.80664         0.0
!          Sim Time
1006,          20.0
!                C2           n     mod den
1007,          0.80         1.0       998.0
!                G0          G1          G2          G3          G4           n
1008,           0.0     0.01393         0.0         0.0     -273.15         3.0
!              Physical Constants of the water
1009,         0.001         0.0       0.001       0.001        0.05        0.05
!                           delta           n
1010,          0.05         1.3        0.25
!  total flow area     flux weighting factor
1111,      0.098208         1.0
1112,       2     1     1     1     0
!1113,         -1.0       0.025       0.25         2.0      0.0         0.0
! set overpower trip at 50000 MW so it will not happen
1113,         -1.0        0.025    500000.0         2.0      0.0         0.0
1114,        2.0889      0.1889
!aaaaa1111111111112222222222223333333333334444444444455555555555566666666666
! Material: Fuel, simplified
2001,          0.0         0.0   17.584624         0.0         0.0
2002,          0.0     4.17E+3     2.04E+6         0.0     -273.15
! Material: Gap gas
2003,          0.0         0.0      0.1513         0.0         0.0
2004,          0.0         0.0     0.92746         0.0         0.0
! Material: Stainless Steel 304, simplified
2005,          0.0         0.0      7.7894         0.0         0.0
2006,      -1.7502      4723.4       2.E+6         0.0         0.0
! Radial Node Descriptions
3001,      3.175-3     2     1         0.0
3002,      7.443-4     3     1    0.881560
3003,      7.443-4     4     1    0.881800
3004,      7.443-4     5     1    0.885440
3005,      7.443-4     6     1    0.888940
```

```
3006,      7.443-4     7     1    0.895040
3007,      7.443-4     8     1    0.903780
3008,      7.443-4     9     1    0.912100
3009,      7.443-4    10     1    0.922780
3010,      7.443-4    11     1    0.934580
3011,      7.443-4    12     1    0.948540
3012,      7.443-4    13     1    0.965140
3013,      7.443-4    14     1    0.985040
3014,      7.443-4    15     1    1.005900
3015,      7.443-4    16     1    1.029620
3016,      7.443-4    17     1    1.057760
3017,      7.443-4    18     1    1.090060
3018,      7.443-4    19     1    1.127800
3019,      7.443-4    20     1    1.171260
3020,      7.443-4    21     1    1.224120
3021,      7.443-4    22     1    1.288740
3022,        1.0-4    23     2         0.0
3023,       5.08-4    24     3         0.0    2
! Axial Node Descriptions
4001,      0.01905    20
!aaaaa1111111111112222222222223333333333334444444444455555555555566666666666
! chose IFLOW=4 TO GET SOME NATURAL CONVECTION AUGMENTATION OF THE FLOW
!      IFLOW              DELP          RN          BM       ALOSCN       ALOSCX
5100,      4            6745.0      0.0217         1.0          0.5         0.55
! void and temp. coefs. are assumed by the code to be negative
!           SIGIN       SIGEX       DVOID        DTMP
5100,          1.00        1.00        0.06       -0.01
!          Inlet P    Outlet P  Inlet P HD Outlet P HD
5101,          0.1         0.1    2.9377-2    2.9377-2
5102,        0.669         1.0         1.0         1.0
5103,        0.788         1.0         1.0         1.0
5104,        0.908         1.0         1.0         1.0
5105,        1.006         1.0         1.0         1.0
5106,        1.094         1.0         1.0         1.0
5107,        1.164         1.0         1.0         1.0
5108,        1.218         1.0         1.0         1.0
5109,        1.252         1.0         1.0         1.0
5110,        1.268         1.0         1.0         1.0
5111,        1.263         1.0         1.0         1.0
5112,        1.241         1.0         1.0         1.0
5113,        1.201         1.0         1.0         1.0
5114,        1.140         1.0         1.0         1.0
5115,        1.106         1.0         1.0         1.0
5116,        1.062         1.0         1.0         1.0
5117,        0.967         1.0         1.0         1.0
5118,        0.859         1.0         1.0         1.0
5119,        0.735         1.0         1.0         1.0
5120,        0.600         1.0         1.0         1.0
5121,        0.481         1.0         1.0         1.0
!aaaaa1111111111112222222222223333333333334444444444455555555555566666666666
! Delayed Neutron Information:
! revised beta(4) so beta's sum to 1.00000
6001,     0.032308    0.012375    0.218462     0.03013   0.196923     0.111774
6002,     0.395384    0.301304    0.115385    1.136066   0.041538     3.013043
! Reactivity Insertion Table with Time
9000,      8
9001,          0.0         0.0
9002,          0.0         1.0
9003,          1.5         1.2
9004,          1.5         2.5
9005,          0.0         4.5
9006,          0.0        16.0
9007,         -5.0        17.0
```

```
9008,          -5.0       500.0
! Inlet Mass velocity with time
10000,      2
!10001,        236.0         0.0       236.0       500.0
! increase mass flow rate at time zero
10001,         50.0          0.0         50.0       500.0
!aaaaa1111111111112222222222223333333333334444444444445555555555556666666666666
! Clad Thermal Expansion vs. Temperature
11000,      2
11001,       17.0-6       300.0       17.0-6      1500.0
! Pressure Drop vs. Time
12000,      2
12001,       6745.0         0.0      3737.61       500.0
! Time Increment vs. Time
14000,      5
14001,         0.01         0.0        1.0-4        0.95
14002,        1.0-4         1.6        1.0-3         5.0
14003,         0.01        16.0
! Print Frequency vs. Time
16000,      5
!     Major Output   Inter. Output     Time
!aaaaa1111111111112222222222223333333333334444444444445555555555556666666666666
16001,         0.01       10000          0.0
16002,        0.001      100000          1.0
16003,          0.1       50000          3.0
16004,          1.0       10000          5.0
16005,          5.0       10000        500.0
! Pump mass velocity fraction vs. time (1 for natural convection)
17000,      2
17001,          1.0         0.0        1.000      3600.0
! Rod Worth Vs. Rod Location or Time
18000,      2
!        Worth ($)     Position (m)
18001,          0.0         0.0
18002,          0.1       0.381
```